Incorporation of different antimicrobial agents into a poly (ethylene-*co*-vinyl alcohol) matrix

By

Nelisa Assistance Dyayiya

Thesis presented in partial fulfilment of the requirements for the degree of Master of Science in the Faculty of Science (Polymer Science) at Stellenbosch University

Department of Chemistry and Polymer Science,

Stellenbosch University

Supervisor: Dr. Marietjie Lutz

March 2018

Declaration

By submitting this thesis/dissertation electronically, I declare that the entirety of the work contained therein is my own, original work, that I am the sole author thereof (save to the extent explicitly otherwise stated), that reproduction and publication thereof by Stellenbosch University will not infringe any third party rights and that I have not previously in its entirety or in part submitted it for obtaining any qualification.

Nelisa Assistance Dyayiya March 2018

Abstract

With the increase in microbial resistance to existing antimicrobial therapies, there is a need for the development of new and more effective ways to fight against microbes. This increase in resistance is a problem in many fields, which include the food packaging, water treatment and pharmaceutical industries. This research investigates the combination and characterization of different antimicrobial agents within a certain matrix in order to maximize the antimicrobial efficacy of the matrix.

Three different organic and inorganic antimicrobial agents were produced and isolated during this study, namely chitosan-reduced silver nanoparticles, silver impregnated microcrystalline cellulose and chitin nanowhiskers. Ultraviolet-visible spectroscopy and Fourier transform infrared spectroscopy confirmed the successful formation of these antimicrobial agents. Transmission electron microscopy and confocal fluorescence microscopy confirmed the formation of chitosan-reduced silver nanoparticles with an average diameter of 10 nm and variable shapes while chitin nanowhiskers were produced as small rod-like whiskers with an average length of 250 nm and 6 nm in width. The progressive formation of silver nanoparticles on the surface of the microcrystalline cellulose was monitored using ultraviolet-visible spectroscopy and transmission electron microscopy showed these nanoparticles were less than 10 nm in diameter and had variable shapes.

The three individual antimicrobial agents as well as different combinations and concentrations thereof were incorporated into a poly (ethylene-*co*-vinyl alcohol) (EVOH) matrix via two different methods, namely, electrospinning and solvent casting to obtain nanocomposite nanofibre mats and nanocomposite films, respectively. The distribution of these antimicrobial agents within the EVOH matrix was investigated using correlative light electron microscopy (CLEM). This technique gave an in-depth analysis of the arrangement and dispersion of multiple agents loaded simultaneously into the same polymer matrix. The nanocomposite films and fibres were dip-coated in a Gramicidin S solution and the successful attachment of the peptide to the surface of the films and fibre mats was shown by field emission scanning electron microscopy (FESEM). The peptide indicated a tendency to attach more to nanocomposite films and fibres containing higher loadings of antimicrobial agents but a complete disruption in the nanofibre morphology was observed with the 10 wt% loading.

The antimicrobial tests showed that these nanocomposites have high antimicrobial activity against the Gram-positive bacteria, *Micrococcus Luteus*. For both films and fibres, the concentration of the antimicrobial agent in the nanocomposite sample seem to have no effect on the activity and the antimicrobial activity was found to be slightly higher for neat composites compared to the peptide attached nanocomposites.

Opsomming

Met die toename in mikrobiese weerstand teen bestaande antibakteriële behandeling, het daar ’n aanvraag ontwikkel vir nuwe en meer effektiewe maniere om bakterieë te beveg. Hierdie toename in weerstandigheid is ’n probleem in baie velde, insluitend voedselverpakking, watersuiwering en die farmaseutiese industrieë. Hierdie navorsing behels die kombinasie en karakterisering van verskeie antimikrobiese stowwe in ’n polimeer matriks met die doel om die antimikrobiese aktiwiteit van die matriks te verhoog.

Drie verskillende organiese en anorganiese antimikrobiese middels is geproduseer en geïsoleer tydens hierdie studie, naamlik chitosan-gebaseerde silwer nanopartikels, silwer geïmpregneerde mikrokristallyne sellulose en chitien nanovesels. Ultraviolet-sigbare spektroskopie en Fourier transform infrarooi spektroskopie het die suksesvolle vorming van hierdie antimikrobiese agente bevestig. Transmissie elektron mikroskopie en konfokale mikroskopie het getoon dat chitien-gebaseerde silwer nanopartikels met ’n gemiddelde deursnit van 10 nm en wisselende vorms gevorm het terwyl die gevormde chitien nanovesels klein staafagtige vesels met ’n gemiddelde lengte van 250 nm en breedte van 6 nm opgelewer het. Die progressiewe vorming van silwer nanopartikels op die oppervlakte van die mikrokristallyne sellulose is gemonitor deur gebruik te maak van ultraviolet-sigbare spektroskopie en transmissie elektron mikroskopie het aangedui dat hierdie nanopartikels se deursnit kleiner as 10 nm was en uit wisselende vorms bestaan het.

Die drie individueel geproduseerde antimikrobiese middels sowel as verskillende kombinasies en konsentrasies daarvan was in ’n poli(etileen-*ko*-viniel alkohol) (EVOH) matriks geïnkorporeer deur middel van elektrospin en oplosmiddel gieting om nanosaamgestelde nanovesel matte en nanosaamgestelde films respektiewelik, te vorm. Die verspreiding van hierdie antimikrobiese middels in die EVOH matriks was geanaliseer deur middel van korrelatiewe lig elektron mikroskopie (KLEM). Hierdie tegniek het ’n in-diepte analise van die rangskikking en verspreiding van verskeie middels, wat gelaai is in dieselfde polimeer matriks, gegee. Die nanosaamgestelde films en vesels was gedoop in ’n oplossing van Gramisidien S en die suksesvolle hegting van die peptied aan die oppervlak van die films en matte was bevestig deur middel van veld emissie skandering elektron mikroskopie (FESEM). Die peptied het ’n neiging getoon om meer aan nanosaamgestelde films en vesels te bind wat hoër ladings van antimikrobiese middels bevat, maar ’n algehele ontwrigting van die nanovesel morfologie was waargeneem teen 10 massa% lading.

Die antimikrobiese toets het getoon dat hierdie nanosamestellings hoë antimikrobiese aktiwiteit toon teen Gram-positiewe bakterieë naamlik *Micrococcus Luteus*. In beide die films en vesels wou dit voorkom asof die konsentrasie van die antimikrobiese middel in die nanosaamgestelde monster geen effek gehad het op aktiwiteit nie, en dit was gevind dat die aktiwiteit effens hoër was vir die onbehandelde samestellings in vergelyking met die nanosamestellings waaraan die peptiede geheg was.

Dedication

"To my parents, Mzawupheli David Dyayiya and Nothembile Gloria Dyayiya, this Master's degree is yours"

Acknowledgements

If it was not for God's love and grace over my life, the strength and courage he gave me to be strong in stressful situations, this work would not have been successful.

I thank my mom, my dad and the rest of the Dyayiya family for their love and constant support. To my sister Noluvuyo Olivia Dyayiya, thank you for always being there for me.

I am forever grateful to my supervisor Dr. Marietjie Lutz for giving a chance, for supporting me academically, financially and otherwise throughout my MSc.

I thank Prof. Marina Rautenbach and the BIOPEP group for providing the antimicrobial peptide and for their help with the antimicrobial tests. To Wilma van Rensburg, I am grateful for all the time and effort you made for the antimicrobial tests and thank you for your patience.

I thank Prof. A.J Van Reenen and the rest of the Polyolefins group, for welcoming me into your family and allowing me to work in your lab. Special thanks to Marehette le Grange, Divaan Robertson, Sifiso Magagula and Ben Krige for their great advice and assistance.

To the rest of the Polymer Science department, thank you to everyone who might have helped me during my MSc. To Siyasanga Mbizana and Sithandile Ngxangxa and Anthony Ndiphiro thank you so much for everything.

Thank you to the CAF Stellenbosch staff for their help and advice regarding microscopy analysis for my MSc. Ms Madelaine Frazenburg, Dr A Laurie and Ms Lize Engelbrecht thank you for your help and patience. Ms Dumi Lumkwana and Ms Rozanne Adams thank you for your help with confocal fluorescence microscopy.

To the **National Research Foundation**, thank you for the bursary. If it was not for your funding, I would not have been able to complete my Master's degree.

Table of contents

List of figures

List of tables

Chapter 1: Introduction and objectives

1.1 Introduction

The fabrication of polymeric nanocomposite materials with antimicrobial activity received much attention in the past few years. These materials have a wide variety of applications, which include food packaging, medical device technology and water purification applications[1–4]. Incorporation of different antimicrobial agents into polymers provides versatile and beneficial properties which makes these nanocomposite materials excellent candidates to help fight against resistant microorganisms that mutate rapidly and are difficult to eliminate[5,6]. Combinations of different antimicrobial agents and good distribution thereof in a specific matrix may lead to even better antimicrobial properties.

Antimicrobial agents can be immobilized onto the surface of a variety of polymers where they retain their ability to bind and kill microorganisms. Some of the antimicrobial agents frequently used are metallic nanoparticles like silver nanoparticles and gold nanoparticles. These nanoparticles have good antimicrobial properties. Polysaccharide nanomaterials such as chitin nanowhiskers have previously also shown antimicrobial activity when used for their biodegradability, biocompatibility, very low toxicity and because of their large surface area, they are furthermore used to enhance the mechanical properties of some polymers[7–10].

Antimicrobial peptides (AMPs) have the ability to hinder the growth of potential microbial pathogens. AMPs are low molecular weight proteins that are cationic in nature and have a hydrophobic and hydrophilic side, a property that allows AMPs to be soluble in aqueous environments yet also enter lipid rich membranes[11,12]. With an increase in the resistance of antibiotics, there is an urgent need to look at other novel therapeutic approaches. AMPs are excellent candidates for this because they can be used to fight against more resistant pathogens without conferring unacceptable toxicity[11–16]. A few researchers have published some results of antimicrobial peptides incorporated into polymeric matrices mostly for wound healing and wound care applications[5].

In this study, chitin nanowhiskers (ChNWs) were isolated from chitin, chitosan-reduced silver nanoparticles (CTSAgNPs) and silver impregnated microcrystalline cellulose (AgMCC) were produced and the chemistry and morphology of these three antimicrobial agents were characterized using techniques such as transmission electron microscopy (TEM) and Fourier transform infrared spectroscopy. Research has shown evidence that polymers such as poly

(ethylene-co-vinyl alcohol) (EVOH) are often used as compatibilizers between hydrophobic and hydrophilic matrices, especially in the packaging industry[17,18]. EVOH was therefore chosen as the appropriate matrix for the incorporation and characterization of the individual antimicrobial agents as well as combinations of the AMPs (Gramicidin S), AgNPs and ChNWs. The proper distribution of the antimicrobial agents throughout the matrix is very important and was investigated using microscopy techniques such as correlative light electron microscopy (CLEM).

1.2 Aim

The main aim of this study was to investigate the antimicrobial effect of a combination of antimicrobial nanocomposites with different properties using organic and inorganic antimicrobial agents within a specific polymer matrix. This was done by incorporating CTSAgNPs, AgMCC and ChNWs into poly (ethylene-*co*-vinyl alcohol) (EVOH) as a polymer matrix. The antimicrobial agents were incorporated individually and in different combinations into the EVOH matrix. The CTSAgNPs were generated directly from a chitosan solution using a chemical reduction method and ChNWs were isolated by way of acid hydrolysis using hydrochloric acid. The chitosan-produced silver nanoparticles were then also impregnated on the surface of the microcrystalline cellulose. Solvent casting and electrospinning were utilized to obtain EVOH nanocomposite films and fibres fibre mats, respectively. The nanocomposites were treated with an antimicrobial peptide, Gramicidin S, in order to attach the peptide to the nanocomposite matrices and hereby aim to enhance the antimicrobial efficacy even more.

1.3 Objectives

1. Synthesis, isolation and characterization of organic and inorganic antimicrobial agents.
2. Incorporation of the antimicrobial agents, individually, into an EVOH polymer matrix in concentrations varying between 1 wt% and 10 wt% via solvent casting and electrospinning.
3. Incorporation of combinations of antimicrobial agents into an EVOH polymer matrix in concentrations varying between 1 wt% and 10 wt% via solvent casting and electrospinning
4. Gramicidin S treatment of the different EVOH nanocomposite films and fibres.
5. Characterization of nanocomposite films and fibres mats in terms of chemical character, thermal stability, morphology and antimicrobial activity. The emphasis was on the development of characterization methods necessary to investigate the distribution of

the combined antimicrobial agents within the polymer matrix. Investigation of antimicrobial activity was therefore limited to the Gram-positive bacteria, *Micrococcus Luteus*.

1.4 Thesis layout

Chapter 1: A brief introduction, aim and objectives of this study are discussed in this chapter.

Chapter 2: This chapter provides a literature review of the work done on active packaging, the use of EVOH in the packaging industry, EVOH nanocomposites and antimicrobial agents. It also gives a brief background on the techniques used to fabricate these nanocomposites.

Chapter 3: This chapter discusses the production and characterization of the different antimicrobial agents used in this study. It also provides a discussion of the results obtained from characterization of the antimicrobial agents.

Chapter 4: In this chapter, antimicrobial agents are individually incorporated into an EVOH matrix to produce nanocomposite fibres and films. The results for the chemical, morphological and thermal characterization of the nanocomposites are also presented.

Chapter 5: Combinations of antimicrobial agents were furthermore incorporated into an EVOH matrix and the results obtained from the characterization of these nanocomposites are discussed in this chapter.

Chapter 6: The successful attachment of the antimicrobial peptides to the surface of the nanocomposites and the antimicrobial activities of these peptide-attached nanocomposites, as well as the nanocomposites without any Gramicidin S attached, are evaluated in this chapter.

Chapter 7: This last chapter comprises of the conclusions drawn from this research study and presents recommendations for future research.

1.5 References

1. Chiono, V. Chiono, V., Mozetic, P., Boffito, M., Sartori, S., Gioffredi, E., Silvestri, A., Rainer, A., Giannitelli, S.M., Trombetta, M., Nurzynska, D. Polyurethane-based scaffolds for myocardial tissue engineering. *Interface Focus* **4,** 1–11 (2013).

2. Hosseini Pour, S. A., Pourabbas, B. & Salami Hosseini, M. Electrical and rheological properties of PMMA/LDPE blends filled with carbon black. *Mater. Chem. Phys.* **143,** 830–837 (2014).

3. Katsogiannis, K. A. G., Vladisavljević, G. T. & Georgiadou, S. Porous electrospun polycaprolactone (PCL) fibres by phase separation. *Eur. Polym. J.* **69,** 284–295 (2015).

4. Osterman, M. Tin whiskers remain a concern. *Transactions of the Institute of Metal Finishing* **30,** (2015)

5. Sobczak, M., Debek, C., Oledzka, E. & Kozłowski, R. Polymeric systems of antimicrobial peptides-strategies and potential applications. *Molecules* **18,** 14122–14137 (2013).

6. Gallo, R. L., Murakami, M., Ohtake, T. & Zaiou, M. Biology and clinical relevance of naturally occurring antimicrobial peptides. *J. Allergy Clin. Immunol.* **110,** 823–831 (2002).

7. Govindan, S., Nivethaa, E. K., Saravanan, R., Narayanan, V. & Stephen, a. Synthesis and characterization of chitosan–silver nanocomposite. *Appl. Nanosci.* **2,** 299–303 (2012).

8. Marie Arockianathan, P., Sekar, S., Sankar, S., Kumaran, B. & Sastry, T. P. Evaluation of biocomposite films containing alginate and sago starch impregnated with silver nano particles. *Carbohydr. Polym.* **90,** 717–724 (2012).

9. Wei, D., Sun, W., Qian, W., Ye, Y. & Ma, X. The synthesis of chitosan-based silver nanoparticles and their antibacterial activity. *Carbohydr. Res.* **344,** 2375–2382 (2009).

10. Wang, B., Xu, C., Xu, F. & Lu, T. Electrospinning of poly(ethylene-co-vinyl alcohol) nanofibres encapsulated with Ag nanoparticles for skin wound healing. *J. Nanomater.* **2011,** (2011).

11. Izadpanah, A. & Gallo, R. L. Antimicrobial peptides. *Dermatology J. Am. Acad.* **52,** 381–390 (2005).

12. Abraham, T., Prenner, E. J., Lewis, R. N. A. H., Mant, C. T., Keller, S., Hodges, R. S. & McElhaney, R. N. Structure-activity relationships of the antimicrobial peptide gramicidin S and its analogs: Aqueous solubility, self-association, conformation, antimicrobial activity and interaction with model lipid membranes. *Biochim. Biophys. Acta - Biomembr.* **1838,** 1420–1429 (2014).

13. Bahar, A. & Ren, D. Antimicrobial Peptides. *Pharmaceuticals* **6,** 1543–1575 (2013)

14. Grotenbreg, G. M. Witte, M.D, Van Hooft P. A. V., Spalburg, E., Reiß P, Noort, D., de Neeling, A. J., Koert, U.,van der Marel, G. A., Overkleeft, H. S. & Overhand, M.

Synthesis and biological evaluation of gramicidin S dimers. *Org. Biomol. Chem.* **3,** 233–238 (2005).

15. Malmsten, M. Antimicrobial peptides. *Ups. J. Med. Sci.* **119,** 199–204 (2014).

16. Ashrafuzzaman, M., Andersen, O. S. & McElhaney, R. N. The antimicrobial peptide gramicidin S permeabilizes phospholipid bilayer membranes without forming discrete ion channels. *Biochim. Biophys. Acta - Biomembr.* **1778,** 2814–2822 (2008).

17. Nel, A. *Investigation of the effect of chitin nanowhiskers distribution on structural and physical properties of high impact polypropylene / chitin nanocomposites.*(2014).

18. du Toit, M. L. *Incorporation of polysaccharide nanowhiskers into a poly (ethylene-co-vinyl alcohol) matrix.* (2013).

Chapter 2: Literature review

2.1 Introduction

The market is trending more and more toward easily prepared, minimally processed and "fresh" ready-to-eat food products containing a minimum of chemical additives[1–4]. The processes involved to produce these types of foods make use of technologies such as high-pressure, lower temperatures, electric pulse treatments or UV irradiation, which might allow the survival and propagation of the bacteria[1,5,6]. The globalization of the food trade, the distribution of food from centralized processing areas as well as recent foodborne microbial outbreaks lead to an on-going search for innovative ways to prevent microbial growth within foods while maintaining its freshness and quality[4,6,7]. A combination of the mentioned developing technologies with antimicrobial packaging technologies could allow for an extended shelf life of foods and could furthermore, help to support the prevention of recontamination with pathogens[8].

2.2 Active packaging

In active packaging, the packaging, the packed product and the environment interact together in order to solve specific problems encountered in the packaging industry[9]. Active packaging leads to an extension of the shelf life of packed food by actively changing the conditions of the food. This type of packaging largely improves the microbiological safety and/or sensory properties, while maintaining the quality of the food[10].

Materials that release (emitters) or absorb (scavengers) steam or gases can actively control the atmosphere inside a packaging. The goal of scavengers is to remove unwanted components from the atmosphere inside the packaging[11,12]. Scavengers are meant to improve the conditions inside the packaging but, there is no direct migration between the product and the scavenger, which extends the shelf life of the food. Scavengers are usually involved with processes whereby oxygen, moisture, ethylene, or carbon dioxide are adsorbed. The working of emitters on the other hand is based on the release of desirable substances that influence the packed food positively[2,3]. Packaging that contains emitters produce compounds that are able to migrate through the packaging and prevent unwanted processes. Emitters provide stable storage conditions in order to extend the shelf life. Emitters help to control the humidity inside packaging, inhibit the growth of harmful microorganisms, and prevents bacterial spoilage[3,10–12]. The following active packaging systems are generally used in the food packaging industry[10]:

- Oxygen, carbon dioxide, and ethylene scavengers;
- Carbon dioxide emitters;
- Odor emitters and absorbers;
- Relative humidity regulators (water content in the packaging atmosphere);
- Antioxidants;
- Antibacterial substances.

2.2.1 Antimicrobial packaging

Antimicrobial packaging is a form of active packaging[13]. In active packaging, there is an interaction with the food or the space between the packaging and the food in order to achieve the chosen outcome. The mechanism by which the antimicrobial agents acts allows for the migration of compounds which then have the ability to hinder or obstruct the development of microorganisms on the surface and inside the product[7,14]. Due to the migration of the antimicrobial agents as active compounds, the lag phase is longer and leads to a reduction in the growth speed of microorganisms[9]. Food packaging that is capable to slow down the growth of microorganisms or kill the microorganisms directly is utilized through addition of one or more antimicrobial compounds or by using a polymer with such desirable properties[1,15,16].

In this way, it is possible to prolong the shelf life of a product and ensure that it maintains its desirable microbiological condition for an extended period. There are different types of antimicrobial packaging and can be categorized accordingly[1,5,9,17]:

- Polymers that are naturally antimicrobial.
- Polymer surfaces coated with antimicrobials or antimicrobial agents adsorbed onto these polymer surfaces.
- Antimicrobial agents immobilized onto polymers by ion or covalent linkages.
- Packaging containing sachets/pads with volatile antimicrobial agents.
- Polymers that are directly loaded with volatile and non-volatile antimicrobial agents.

The utilization of polymers as carriers of antimicrobial agents allows for controlled release and reduces the amount required. This satisfies the consumer concerns and demands for lower quantities of additives[15,18]. Since microbial contamination occurs mainly at the surface of the

packaging material, the incorporation of the antimicrobial agents in a film or as a coating has several advantages due to the large exposure areas for the antimicrobial agents. Several compounds have been proposed for antimicrobial activity in food packaging, including essential enzymes, oils and organic acids[8,13].

The market offer of antimicrobial packaging material is however, still relatively small. This is most likely due to the hygienic regulations and constricting legislation in different countries combined with a lack of the welcoming approval from consumers for such relatively high cost solutions[10,19].

Many of the current commercially available antimicrobial packaging systems are based mainly on materials that contain silver. Zeomic®, one of the first inorganic packaging materials produced contains silver and controls growth of Gram-positive and Gram-negative bacteria as well as the growth of fungi[13]. This material displays good thermal resistance at elevated temperatures when compared to other organic antimicrobial materials. Other materials containing silver in zeolite operate in a similar way: Microban®, AgIon®, and Irgaguard®[7]. Table 1 presents some of the modern solutions for antimicrobial packaging in combination with their potential functions in the food retail trade[8,13].

Table 2.1 Selected applications of active packaging in the food industry[9,10,13,20].

Form	**Function**	**Applications**	**Commercial Product**
Antibacterial and antifungal sheets, labels and films	Inhibition of microorganism growth	Fresh fruits and vegetables	Biomaster®
Silver-based master batch	Extend shelf life	Meat products, cheese and bakery products	AgIon®
Silver-based trays and films	Reduce post-harvest decay	Maintain food quality	Irgaguard®
Antifungal coatings	Maintain storage quality	Inhibit microorganisms	Surfacine®

2.2.2 Poly (ethylene-*co*-vinyl alcohol) (EVOH) in the packaging industry

One of the best hydrophilic food-contact polymers widely used in industry for packaging purposes is poly (ethylene-*co*-vinyl alcohol) (EVOH). Ethylene-vinyl alcohol copolymers are a family of semi-crystalline random copolymers that are made with hydrophilic vinyl alcohol and hydrophobic ethylene segments[21,22]. These EVOH copolymers usually have a higher content of the vinyl alcohol co-monomer as compared to ethylene, which makes EVOH hydrophilic in nature[5,23]. The random sequencing of ethylene (ET) and vinyl alcohol (VA) monomeric units constructs EVOH chains. The chemical hydrolysis of ethylene-vinyl acetate (EVA) copolymerised units forms EVOH, as illustrated in Figure 2.1. The monomer arrangement renders the polymer properties that vary drastically depending on the copolymer composition[14]. EVOH copolymers are biocompatible, have high thermal resistance, good optical properties and good mechanical properties. This well-known moisture-sensitive random copolymer is widely used in the food packaging industry because of its outstanding gas barrier properties with regards to oxygen and organic compounds (solvents and food aromas). EVOH's use in antimicrobial food packaging is increasing because of its gas-barrier properties. In addition it has an ability to act as a carrier of bioactive agents in dry conditions and a dispenser of antimicrobial agents in humid conditions[17,24].

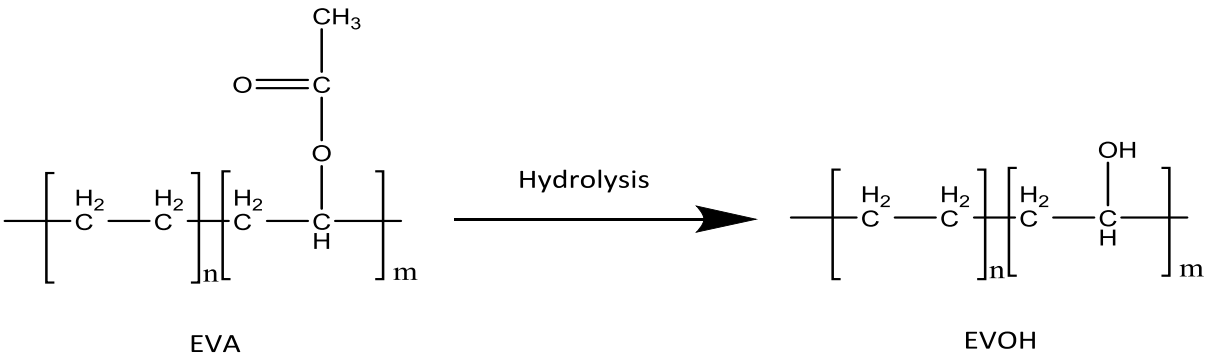

Figure 2.1 Hydrolysis of EVA to obtain EVOH.

In packaging, EVOH is mostly used in shelf-stable and refrigerated foods where the presence of oxygen decreases food quality and therefore, shelf-life[5]. These properties are the main reason EVOH copolymers and EVOH based nanocomposites have attracted a great deal of attention, especially for active and smart packaging applications.[25–27].

2.3 EVOH nanocomposites

Polymer nanocomposites are materials in which the filler or dispersed material has at least one dimension smaller than 100 nm[20,28,29]. These nanocomposites are prepared by dispersing a filler or nano-sized material in a polymer matrix. These nanocomposites can be either electrospun into nanofibre mats or solvent casted into films. Nanocomposites represent a new alternative to conventional technologies for improving polymer properties. Nanocomposites exhibit increased barrier properties, increased mechanical strength and improved heat resistance in comparison to their neat polymers and conventional composites[20]. EVOH/montmorillonite and EVOH/kaolinite nanocomposite films have been shown to have enhanced barrier properties to oxygen as well as increased thermal resistance as shown by Cabedo et al.[23]. In work published by Martínez-Abad et al., silver nanoparticles were incorporated into an EVOH matrix by solvent casting followed by characterizing the films for morphological, thermal and antimicrobial properties[7]. In a similar study, bacterial cellulose nanowhiskers were also added to EVOH and electrospun to form antimicrobial nanofibres. In both these cases, the nanostructured antimicrobial agents were used to improve the antimicrobial efficacy of EVOH without changing the polymer properties[30,31].

The characteristics of the polymer matrix such as its hydrophilicity and molecular weight have a great influence on the antimicrobial activity of the final nanocomposite. Therefore, it is very important to choose the polymer matrix wisely. López-de-Dicastillo et al. have used EVOH materials as matrices for the development of active packaging systems, where the EVOH protects the active agents during storage and triggers their activity on exposure to a humid environment caused by the food product[2,12,32].

2.4 Organic antimicrobial agents

Antimicrobial agents are compounds that kill microorganisms or prevent their growth[19,33]. These compounds can be categorized as organic and inorganic antimicrobial agents[34]. For the purpose of this research, the background of antimicrobial agents will only focus on those utilized in the present work i.e. chitin nanowhiskers and Gramicidin S. These antimicrobial agents exhibit high antimicrobial activity, low toxicity and biocompatibility[35,36]. These properties make them desirable for a wide variety of applications including food packaging.

Organic antimicrobial agents are available at low cost. They are nontoxic and due to their low density, they are easy to modify[37-39]. These are some of the advantages of organic antimicrobial

agents over inorganic agents. Chitin is one of the polysaccharides used to isolate nanomeric antimicrobial agents to obtain chitin nanowhiskers[37,40].

2.4.1 Chitin nanowhiskers

(β-(1→4)-N-acetyl-D-glucosamine) commonly known as chitin is a naturally occurring high molecular weight polysaccharide and second most abundant naturally occurring polymer after cellulose[41-43]. Chitin, in its native state, occurs as ordered crystalline microfibrils that form structural components in the cell walls of fungi, yeast or in the exoskeleton of arthropods[37,39,44]. Chitin has many valuable properties including physiological inertness, mechanical stability and antibacterial activity, which enable an extraordinarily broad range of applications[35,37,40,42,45]. Figure 2.2 shows the molecular structure of β-chitin.

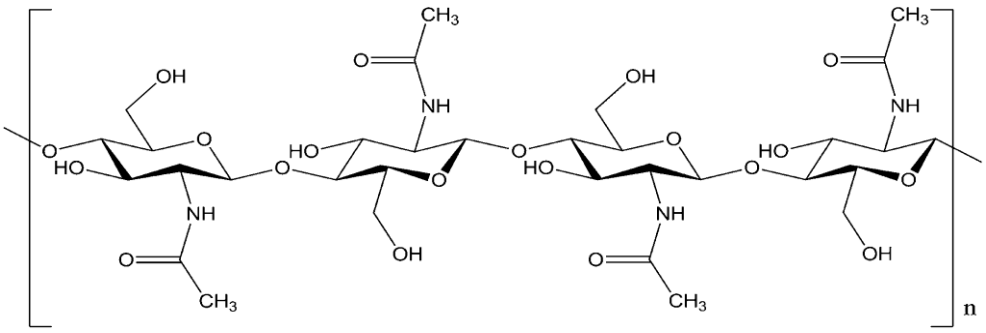

Figure 2.2 Schematic diagram of the molecular structure of chitin.

Since chitin is non-toxic, odourless, biocompatible with living tissue and has moisture retention properties, it can be utilized for biomedical applications, water purification, textile finishes, antimicrobial coatings and paper production[46-49]. Chitin's applications are limited by the relative rigid polysaccharide chains with significant interactions and by their significant hydrophilic character. These drawbacks can be overcome by blending chitin with thermoplastic polymers[41].

According to Mincea et al., nanowhiskers are crystalline nanofibrils that can be made from breaking down of crystalline materials into nanocrystalline entities with rod-like shapes, as shown in the transmission electron microscopy images in Figure 2.3[40]. Chitin nanowhiskers (ChNWs) occur in biological tissues with proteins and inorganic compounds. Various methods

have been used to prepare or isolate ChNWs from chitin. These methods include acid hydrolysis, TEMPO-mediated oxidation, ultra-sonication, electrospinning, mechanical treatment and gelation[37]. Due to the high surface area of ChNWs, they are used mostly as fillers to improve mechanical properties of some synthetic polymers[16,35]. This property has been taken into account in the present work to also improve the mechanical properties of the nanocomposites.

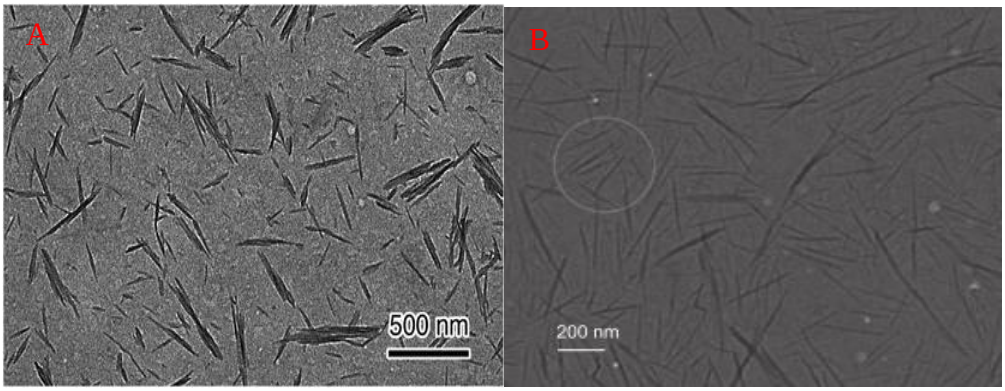

Figure 2.3 Transmission electron microscopy (TEM) images showing rod-like chitin nanowhiskers[40].

Villanueva et al. recently reported the use of ChNWs in controlled release studies. It has been reported that antimicrobial finishing provides a persistent and gradual antibiotic release from the surface into the surroundings[35]. ChNWs were used as carriers of methyl paraben in the preparation of durable antimicrobial cotton textiles. Villanueva et al. concluded that treated textiles show antimicrobial activity with laundering durability of up to 20 washing cycles. In addition the textile mechanical properties were not altered by the finishing[35].

2.4.2 Antimicrobial peptides - Gramicidin S

Antimicrobial peptides (AMPs) are a group of small proteins that are very diverse but, fall under the same classification due to their native antimicrobial activity[50]. AMPs have a varying number (5 – 100) of amino acids and a broad spectrum of targeted organisms ranging from viruses to parasites. These molecules were discovered in 1939 by Dubos when he extracted an antimicrobial agent from the Bacillus strain that showed antimicrobial activity in mice with pneumococci infection[51,52]. Bacterial membranes differ from the membranes of animals and plants that are mainly neutral. This is caused by the presence of negatively charged phospholipid groups on the outer sides. AMPs are very selective and prefer to interact with bacterial membranes without conferring any toxicity to animal and human cells[53-55]. Most

AMPs form α-helical or β–structures and they differ from various antibiotics by their universal mechanism of action on bacterial membranes[53].

The mode of action of AMPs depends on the kind of bacteria and the interaction between with the peptide. In Figure 2.4 (A) peptides insert themselves perpendicularly while in (B) small areas are coated with AMPs with hydrophobic sides facing inward, leaving pores behind. The model in (C) resembles the Barrel-stave model where the AMPs are always in contact with phospholipid head groups. The red colour represents the hydrophilic parts of the AMPs while the blue colour represents the hydrophobic parts[51].

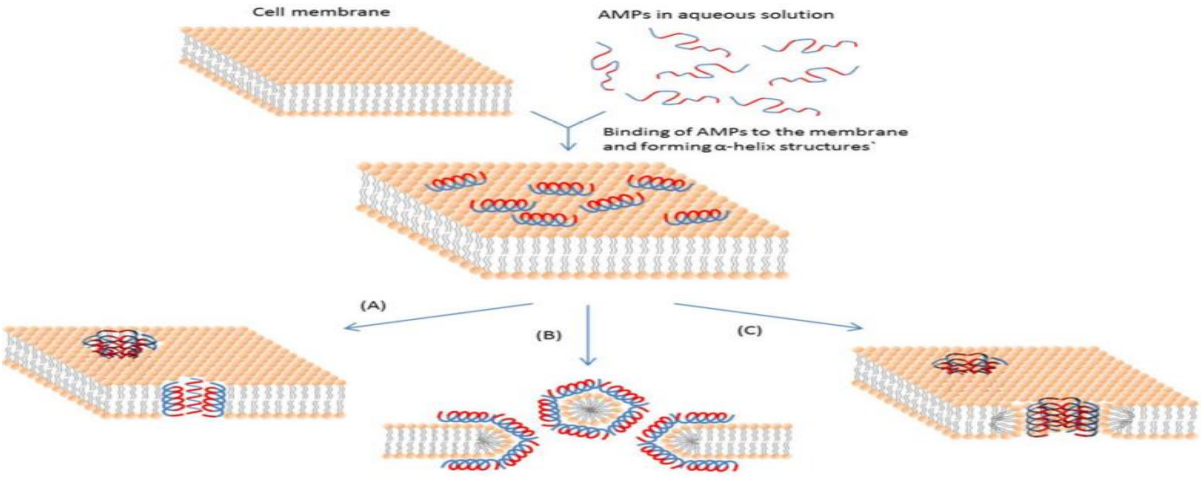

Figure 2.4 Schematic representation of some action mechanisms of membrane-active AMPs: (A) Barrel-Stave model, (B) Carpet model and (C) Toroidal pore model[51].

The antimicrobial peptide Gramicidin S (GS) is in a class of structurally diverse peptide-based compounds, usually called cationic antimicrobial peptides, as shown in Figure 2.5. These peptides are present abundantly in nature and are often important compounds of innate immune systems[51,56]. GS is a cyclic cationic decamer that was isolated from the Gram-positive bacterium Bacillus brevis. GS is an antibiotic that works against a broad range of Gram-positive and Gram-negative bacteria as well as several pathogenic fungi[57,58]. The peptide kills bacteria by disrupting the cell membrane; this is attributed to both the basic and amphiphilic nature of the rigid cyclic molecular structure[58].

Antimicrobial peptides can be immobilised on a variety of polymers to obtain polymeric antimicrobial systems[33]. The immobilisation can be done via absorption of the peptides to the surface of the polymer matrices. This can be achieved by using methods that include interfacial polymerization, solvent diffusion and solvent casting. Polyethylene is one of the polymers that

have been attached with a polycyclic antimicrobial peptide, nisin, to retard spoilage and increase food preservation times[33,51].

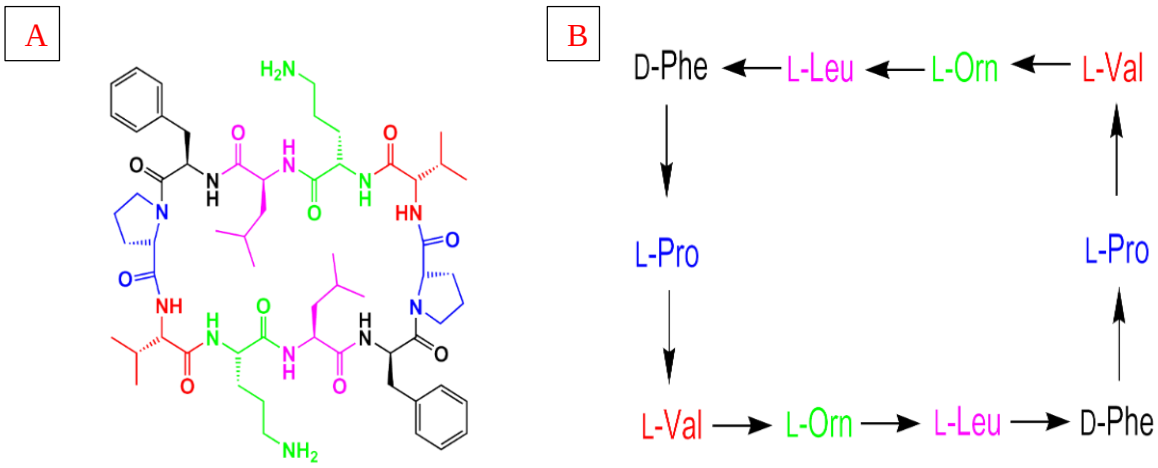

Figure 2.5 Gramicidin S (GS) antimicrobial peptide: (A) shows the molecular structure and (B) shows the arrangement of the four GS constituents.

2.5 Inorganic antimicrobial agents

The use of inorganic nanoparticles is becoming more prevalent as they possess defined chemical, optical and mechanical properties[59,62]. These nano-sized materials provide solutions to technological and environmental challenges in the areas of solar energy conversion, catalysis, medicine, and water treatment. Metallic nanoparticles are most promising as they show good antibacterial properties due to their large surface area-to-volume ratio[59]. Different types of metallic nanoparticles like copper, zinc, titanium, gold and silver have been studied but silver nanoparticles have proved to be most effective as they have good antimicrobial efficacy against bacteria, viruses and other micro-organisms[14,63,64] Inorganic silver nanoparticles were previously synthesized using an organic naturally occurring polymer to reduce and stabilize silver salts to silver nanoparticles. The process is a "green" technique that uses chitosan to synthesize nanoparticles with higher antimicrobial activity[65-67].

Silver nanoparticles have been incorporated into polymers with other antimicrobial agents to form nanocomposites with improved antimicrobial properties[29,34,68]. Chitin and chitosan are examples of polysaccharides that have been individually incorporated in silver containing nanocomposite matrices and in both cases, the nanocomposites containing combined antimicrobial agents showed more activity compared to the agents incorporated individually[69,70].

2.5.1 Chitosan-reduced silver nanoparticles (CTSAgNPs)

Silver and its salts has been used as an antimicrobial agent for centuries. The recent revival in interest in the element particularly focuses on the increasing threat of antibiotic resistance[63,71]. Several studies have been conducted in order to evaluate the efficiency of different methods for the synthesis of silver nanoparticles. Physical and chemical synthetic methods or combinations of both have been excessively explored. Among the physical methods, the most used are evaporation-condensation and laser ablation while in the chemical methods, chemical reduction to form colloidal dispersions of silver nanoparticles has been the most popular[34,69,72,73]. Researchers have been exploring "green" methods of producing silver nanoparticles, which is in conjunction with the global efforts to eliminate or decrease the use of toxic chemicals and to generate less hazardous waste[69,74,75]. These "green" chemicals and techniques should be in line with the principles of green chemistry such as chemical biodegradability and non-toxicity, reduced process derivatives and the use of systems or techniques that are energy efficient[63, 76].

It is recognized that silver nanoparticles may attach to the cell wall, thus disturbing cell-wall permeability and cellular respiration. Silver nanoparticles may also penetrate inside the cell-wall causing damage by interacting with phosphorus and sulphur-containing compounds such as protein and deoxyribonucleic acid (DNA)[69]. Chitosan has interesting properties that include antimicrobial properties, an inexpensive nature, biocompatibility and biodegradability. These properties make it very attractive for use as a "green" reducing and stabilizing agent allowing efficient production of silver nanoparticles. According to literature silver nanoparticles reduced using chitosan and other chemicals appear as small particles with variable shapes and sizes as shown in the TEM images shown in Figure 2.6[36,74-76].

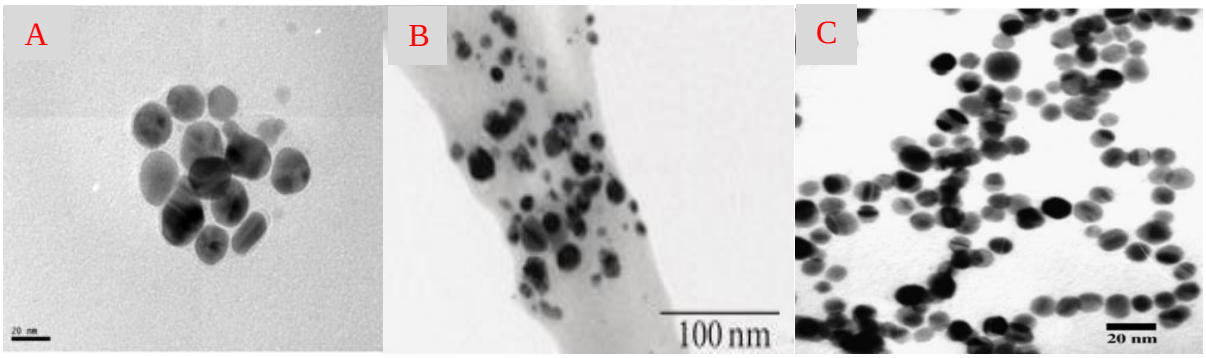

Figure 2.6 Sodium borohydride reduced (A), chitosan reduced (B) MCC impregnated and size controlled silver nanoparticles (C) [36,74-76]

2.5.2 Silver impregnated microcrystalline cellulose

In a study done by Vivekanandhan et al., silver nanoparticles were immobilised and grown on the surface of the microcrystalline cellulose using curry leaves (*Murraya koenigii*) as a reducing agent[78]. Silver impregnated surfaces have been investigated for their unique physico-chemical properties such as catalytic, electrical, optical and anti-microbial properties. Following the same method, other reducing agents like sodium borohydride and chitosan could be used to reduce silver nitrate powder to silver nanoparticles[73,78]. Figure 2.7 shows the shapes, sizes and distribution of these8silver nanoparticles on the microcrystalline cellulose. These silver nanoparticles show a tendency to agglomerate and form clusters on the surface of the MCC[80]. Different synthetic techniques and reducing agents have been explored in the process of embedding the "green" silver nanoparticles on the surface of the MCC[81-85].

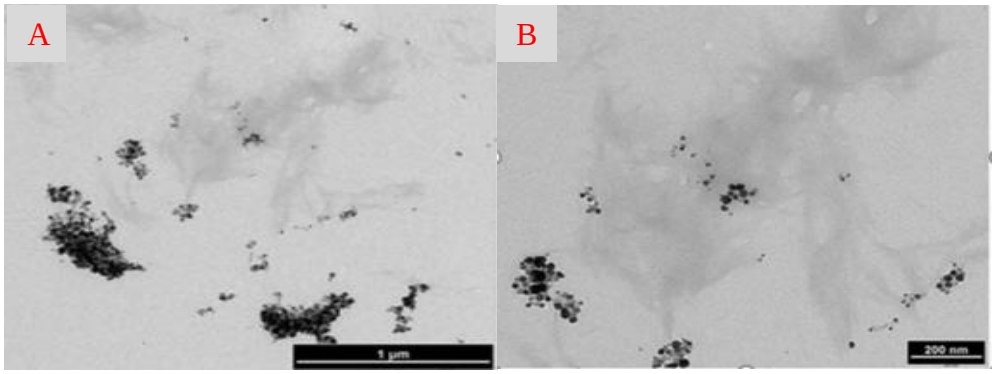

Figure 2.7 TEM images of silver nanoparticle impregnated microcrystalline cellulose at different magnifications[78].

2.6 Methods of nanocomposite synthesis

2.6.1 Solvent casting

In solvent casting/evaporation, a polymer is dissolved in an organic solvent and the mixture is cast onto a glass plate or a plastic petri dish to produce a membrane. When the solvent evaporates, it creates a composite film consisting of the particles dispersed within the polymer. The composite mixture is either air dried or oven dried to make sure all excess solvent is removed and film is completely dried[7,86].

2.6.2 Electrospinning

Electrospinning is a process used for generating extremely fine submicron fibres from a variety of materials that include polymers, composites and ceramics[87]. Figure 2.8 shows an electrospinning apparatus, which includes a high voltage power supply, a grounded collector, and a spinneret. Electrodes connect the collector to the spinneret, which completes a circuit to produce an electric field[88]. Electrostatic forces are used to generate polymer jets, which are gathered on a collector screen as fine fibre non-woven mats[89,90].

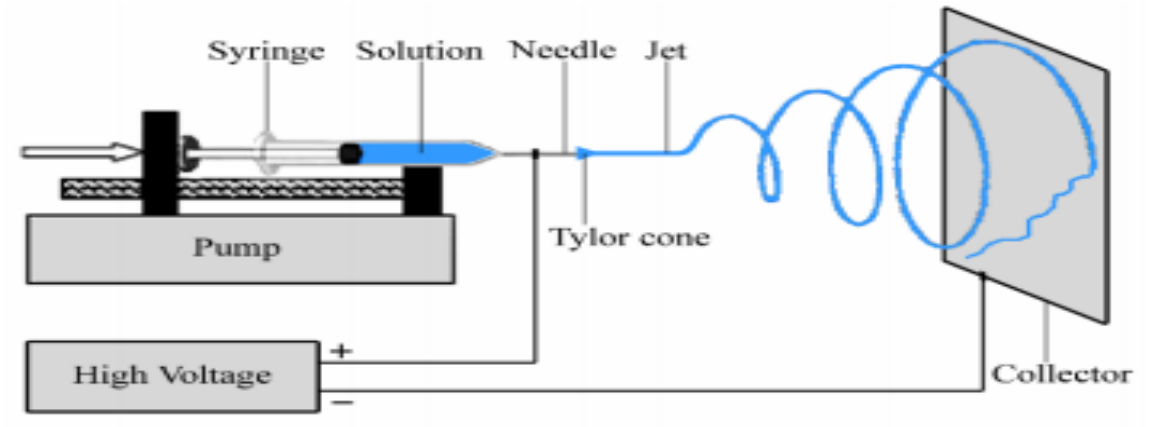

Figure 2.8 Electrospinning setup[88].

Regarding the processing conditions, it has been established that the volume charge density of any dissolution, which is directly related to its surface tension follows power laws dependencies with voltage, flow-rate, tip-to-collector distance, concentration, molecular weight and solvent content[88,89]. During the electrospinning process, the location of the antimicrobial agents can be controlled by doing blend, coaxial or emulsion electrospinning[87]. Figure 2.9 shows some of the typical fibre morphologies that are obtained after electrospinning different polymers as described in literature[38,91,92]. Scanning electron microscopy (SEM) is generally used to characterise the morphology of the formed nanofibre mat after electrospinning.

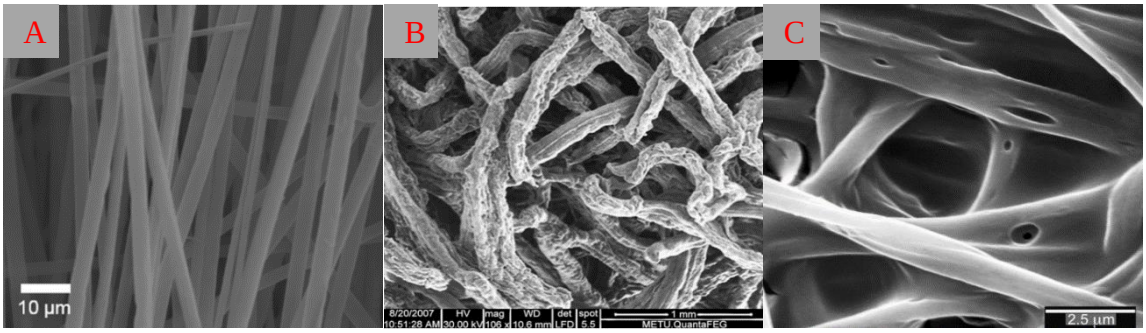

Figure 2.9 SEM images of nanofibres showing different morphologies of the fibres[38,91,92].

The parameters mentioned above determine how these nanofibres will look under the SEM microscope. The fibres could be individually aligned or form an entangled mat and they may also have different diameters as shown in Figure 2.9.

2.7 Conclusions

In this chapter, different types of antimicrobial polymers and as well as their synthesis have been discussed. Different antimicrobial agents incorporated into a wide range of polymers to render them antimicrobial have been mentioned and discussed. Highlights of some of the work done on these antimicrobial agents, antimicrobial polymers and a combination of both that results in nanocomposite mixtures with antimicrobial activity. With the advancement of antimicrobial technologies, which includes nanotechnology, there is a need for scientists to further explore the applications of nanotechnology in polymers.

Active packaging forms an excellent solution for a wide variety of applications in the food industry. Even though industries are still widely using the traditional technologies of food packaging, the future will be part of the innovation brought forward by active packaging characteristics of the 21st century. Antimicrobial packaging specifically offers the most important advantage, which is a decrease in the loss of food products when extending their shelf life. Antimicrobial packaging should therefore be designed in such a way that the components contained in them are released and interact with food in the most effective way.

The use of EVOH nanocomposites containing combinations of organic and inorganic antimicrobial agents that have high antimicrobial activity amongst other beneficial properties can form nanocomposites with high activity against a wide variety of microbes. The use of these antimicrobial agents in their nanometre form and in different combinations could even further improve the antimicrobial efficacy against a broader range of microbes.

2.8 References

1. Muriel-Galet, V., López-Carballo, G., Hernández-Muñoz, P. & Gavara, R. Characterization of ethylene-vinyl alcohol copolymer containing lauril arginate (LAE) as material for active antimicrobial food packaging. *Food Packag. Shelf Life* **1,** 10–18 (2014).

2. López-de-Dicastillo, C., Gallur, M., Catalá, R., Gavara, R. & Hernandez-Muñoz, P. Immobilization of β-cyclodextrin in ethylene-vinyl alcohol copolymer for active food packaging applications. *J. Memb. Sci.* **353,** 184–191 (2010).

3. Ozdemir, M. & Floros, J. D. Active Food Packaging Technologies. *Crit. Rev. Food Sci. Nutr.* **44,** 185–193 (2004).

4. Luo, Z., Wang, Y., Wang, H. & Feng, S. Impact of nano-CaCO3-LDPE packaging on quality of fresh-cut sugarcane. *J. Sci. Food Agric.* **94,** 3273–3280 (2014).

5. Mokwena, K. K. & Tang, J. Ethylene vinyl alcohol: a review of barrier properties for packaging shelf stable foods. *Crit. Rev. Food Sci. Nutr.* **52,** 640–50 (2012).

6. Muriel-Galet, V., Muriel-Galet, V., Cerisuelo, J. P., López-Carballo, G., Lara, M., Gavara, R. & Hernández-Muñoz, P. Development of antimicrobial films for microbiological control of packaged salad. *Int. J. Food Microbiol.* **157,** 195–201 (2012).

7. Martínez-Abad, A., Lagaron, J. M. & Ocio, M. J. Development and Characterization of Silver-Based Antimicrobial Ethylene−Vinyl Alcohol Copolymer (EVOH) Films for Food-Packaging Applications. *Am. Chem. Soc.* **60,** 5350−5359 (2012).

8. De Moura, M. R., Mattoso, L. H. C. & Zucolotto, V. Development of cellulose-based bactericidal nanocomposites containing silver nanoparticles and their use as active food packaging. *J. Food Eng.* **109,** 520–524 (2012).

9. Catalá, R., Cerisuelo, J. P., Domínguez, I., Carballo, G. L. Hernández-Muñoz, P. & Gavara, R. Antimicrobial Active Packaging Systems Based on EVOH Copolymers. *Antimicrobial food packaging.* **22**, 297–303 (2016).

10. Wyrwa, J., Barska A. Innovations in the food packaging market: active packaging. *Eur. Food Res. Technol*. 1–12 (2017).

11. López-De-Dicastillo, C., Catalá, R., Gavara, R. & Hernández-Munoz, P. Food applications of active packaging EVOH films containing cyclodextrins for the preferential scavenging of undesirable compounds. *J. Food Eng.* **104,** 380–386 (2011).

12. López-De-Dicastillo, C., Alonso, J. M., Catalá, R., Gavara, R. & Hernández-Munoz, P. Improving the antioxidant protection of packaged food by incorporating natural flavonoids into ethylene-vinyl alcohol copolymer (EVOH) films. *J. Agric. Food Chem.* **58,** 10958–10964 (2010).

13. Suppakul, P., Miltz, J., Sonneveld, K. & Bigger, S. W. Active Packaging Technologieswith an Emphasis on Antimicrobial Concise Reviews in Food Science. *J. Food Sci.* **68,** 408–420 (2003).

14. Martínez-Abad, A., Sanchez, G., Lagaron, J. M. & Ocio, M. J. Influence of speciation in the release profiles and antimicrobial performance of electrospun ethylene vinyl alcohol copolymer (EVOH) fibers containing ionic silver ions and silver nanoparticles. *Colloid Polym. Sci.* **291,** 1381–1392 (2013).

15. Uz, M. & Altinkaya, S. A. Development of mono and multilayer antimicrobial food packaging materials for controlled release of potassium sorbate. *LWT - Food Sci. Technol.* **44,** 2302–2309 (2011).

16. Tang, X. Z., Kumar, P., Alavi, S. & Sandeep, K. P. Recent Advances in Biopolymers and Biopolymer- Based Nanocomposites for Food Packaging Materials Recent Advances in Biopolymers and Biopolymer-Based Nanocomposites. *Crit. Rev. Food Sci. Nutr.* **52,** 526–442 (2012).

17. Muriel-Galet, V., López-Carballo, G., Gavara, R. & Hernández-Muñoz, P. Antimicrobial Properties of Ethylene Vinyl Alcohol/Epsilon-Polylysine Films and Their Application in Surimi Preservation. *Food Bioprocess Technol.* **7,** 3548–3559 (2014).

18. Muriel-galet, V., López-carballo, G., Gavara, R. & Hernández-muñoz, P. International Journal of Food Microbiology Antimicrobial food packaging fi lm based on the release of LAE from EVOH. *Int. J. Food Microbiol.* **157,** 239–244 (2012).

19. Cran, M. J., Rupika, L. A. S., Sonneveld, K., Miltz, J. & Bigger, S. W. Release of Naturally Derived Antimicrobial Agents from LDPE Films. *J. Food Sci.* **75,** 126–133 (2010).

20. Arora, A. & Padua, G. W. Review: Nanocomposites in food packaging. *J. Food Sci.* **75,** 43–49 (2010).

21. Cerisuelo, J. P. Muriel-Galet, V., Bermúdez, J. M., Aucejo, S., Catalá, R., Gavara, R. & Hernández-Muñoz, P. Mathematical model to describe the release of an antimicrobial agent from an active package constituted by carvacrol in a hydrophilic EVOH coating on a PP film. *J. Food Eng.* **110,** 26–37 (2012).

22. Franzoso, F., Tabasso, S., Antonioli, D., Montoneri, E., Persico, P., Laus, M., Mendichi, R & Negre M. Films made from poly(vinyl alcohol-co-ethylene) and soluble biopolymers isolated from postharvest tomato plant. *J. Appl. Polym. Sci.* **132,** 1–11 (2015).

23. Cabedo, L., Giménez, E., Lagaron, J. M., Gavara, R. & Saura, J. J. Development of EVOH-kaolinite nanocomposites. *Polymer (Guildf).* **45,** 5233–5238 (2004).

24. Martínez-Abad, A., Sanchez, G., Lagaron, J. M. & Ocio, M. J. Influence of speciation in the release profiles and antimicrobial performance of electrospun ethylene vinyl alcohol copolymer (EVOH) fibers containing ionic silver ions and silver nanoparticles. *Colloid Polym. Sci.* **291,** 1381–1392 (2013).

25. Takahashi, M., Tashiro, K. & Amiya, S. Crystal structure of ethylene-vinyl alcohol copolymers. *Macromolecules* **32,** 5860–5871 (1999).

26. Shang, M., Matsuyama, H., Maki, T., Teramoto, M. & Lloyd, D. R. Preparation and characterization of poly(ethylene-co-vinyl alcohol) membranes via thermally induced

liquid-liquid phase separation. *J. Appl. Polym. Sci*. **87,** 853–860 (2002).

27. Alipour, N.,Gedde, U. W., Hedenqvist, M. S., Yu, S., Roth, S., Bruning, K., Vieyres, A & Schneider, K. Structure and properties of polyethylene-based and EVOH-based multilayered films with layer thicknesses of 150 nm and greater. *Eur. Polym. J.* **64,** 36–51 (2015).

28. Arjmandi, R., Hassan, A., Haafiz, M. K. M. & Zakaria, Z. Effect of Microcrystalline Cellulose on Biodegradability , Tensile and Morphological Properties of Montmorillonite Reinforced Polylactic Acid Nanocomposites. **16,** 2284–2293 (2015).

29. Jing, S., Xing, S., Yu, L. & Zhao, C. Synthesis and characterization of Ag/polypyrrole nanocomposites based on silver nanoparticles colloid. *Mater. Lett.* **61,** 4528–4530 (2007).

30. Martínez-Sanz, M., Olsson, R. T., Lopez-Rubio, A. & Lagaron, J. M. Development of bacterial cellulose nanowhiskers reinforced EVOH composites by electrospinning. *J. Appl. Polym. Sci.* **124,** 1398–1408 (2012).

31. Barud, H. S., Hernane S. Barud, Regiani, T., Marques, R . F. T., Lustri, W. R., Messaddeq, Y & Ribeiro, S. J. L. Antimicrobial bacterial cellulose-silver nanoparticles composite membranes. *J. Nanomater.* **2011**, (2011).

32. López De Dicastillo, C., Nerín, C., Alfaro, P., Catalá, R. & Gavara, R. Development of new antioxidant active packaging films based on ethylene vinyl alcohol copolymer (EVOH) and green tea extract. *J. Agric. Food Chem.* **59,** 7832–7840 (2011).

33. Sobczak, M., Debek, C., Oledzka, E. & Kozłowski, R. Polymeric systems of antimicrobial peptides-strategies and potential applications. *Molecules* **18,** 14122–14137 (2013).

34. Aubert-Viard, Martin, A., Chai, F., Neut, C., Tabary, S., Martel, B & Blanchemain, N. Chitosan finishing nonwoven textiles loaded with silver and iodide for antibacterial wound dressing applications. *Biomed. Mater.* **10,** 015–023 (2015).

35. Villanueva, Emilia, M., Salinas, A., Díaz, L. E. & Copello, G. J. Chitin nanowhiskers as alternative antimicrobial controlled release carriers. *New J. Chem.* **39,** 614–620 (2015).

36. De Mesquita, J. P., Donnici, C. L. & Pereira, F. V. Biobased nanocomposites from layer-by-layer assembly of cellulose nanowhiskers with chitosan. *Biomacromolecules* **11,** 473–480 (2010).

37. Zeng, J. B., He, Y. S., Li, S. L. & Wang, Y. Z. Chitin whiskers: An overview. *Biomacromolecules* **13,** 1–11 (2012).

38. Geng, X., Kwon, O. H. & Jang, J. Electrospinning of chitosan dissolved in concentrated acetic acid solution. *Biomaterials* **26,** 5427–5432 (2005).

39. Rafiee, Z. & Keshavarz, V. Progress in Organic Coatings Synthesis and characterization of polyurethane / microcrystalline cellulose bionanocomposites. *Prog. Org. Coatings* **86,** 190–193 (2015).

40. Mincea, M., Negrulescu, A. & Ostafe, V. Preparation, modification, and applications

of chitin nanowhiskers: A review. *Rev. Adv. Mater. Sci.* **30,** 225–242 (2012).

41. Sugimoto, M., Morimoto, M., Sashiwa, H., Saimoto, H. & Shigemasa, Y. Preparation and characterization of water-soluble chitin and chitosan derivatives. *Carbohydr. Polym.* **36,** 49–59 (1998).

42 Younes, I. & Rinaudo, M. Chitin and chitosan preparation from marine sources. Structure, properties and applications. *Mar. Drugs* **13,** 1133–1174 (2015).

3. Pereira, A. G. B., Muniz, E. C. & Hsieh, Y. Lo. Chitosan-sheath and chitin-core nanowhiskers. *Carbohydr. Polym.* **107,** 158–166 (2014).

44. Kadokawa, J., Takegawa, A., Mine, S. & Prasad, K. Preparation of chitin nanowhiskers using an ionic liquid and their composite materials with poly(vinyl alcohol). *Carbohydr. Polym.* **84,** 1408–1412 (2011).

45. Kelnar, I. Kovářová, J., Tishchenko, G., Kaprálková. L., Pavlová, E., Carezzi, F., & Morganti, P. Chitosan/Chitin nanowhiskers composites: effect of plasticisers on the mechanical behaviour. *J. Polym. Res.* **22,** 5 (2015).

46. Rinaudo, M. & Ã, M. R. Chitin and chitosan: Properties and applications. *Prog. Polym. Sci.* **31,** 603–632 (2006).

47 Nakorn, P. N. A. Chitin Nanowhisker and Chitosan Nanoparticles in Protein Immobilization for Biosensor Applications. *J. Met. Mater. Miner.* **18,** 73–77 (2008).

48. Khoushab, F. & Yamabhai, M. Chitin research revisited. *Mar. Drugs* **8,** 1988–2012 (2010).

49. Ravi Kumar, M. N. A review of chitin and chitosan applications. *React. Funct. Polym.* **46,** 1–27 (2000).

50. Khrushchev, A I., Kashparov, I.A, Klimenko, L. V & Mitin, I. V. Branched antimicrobial peptides. *Russ. J. Bioorganic Chem.* **33,** 588–592 (2007).

51. Bahar, A. & Ren, D. Antimicrobial Peptides. *Pharmaceuticals* **6,** 1543–1575 (2013).

52. Spathelf, B. *Qualitative structure-activity relationships of the major tyrocidines , cyclic decapeptides from Bacillus aneurinolyticus*. PhD Thesis, Stellenbosch University, South Africa. (2013).

53. Malmsten, M. Antimicrobial peptides. *Ups. J. Med. Sci.* **119,** 199–204 (2014).

54. Zou, Y. Zhao, Q., Zhang, C., Wang, L., Li, W., Li, X., Wu, Q & Hu, H. Synthesis and antibacterial activities of novel tyrocidine A glycosylated derivatives towards multidrug- resistant pathogens. *J. Pept. Sci.* **21,** 586–592 (2015).

55. Guaní-Guerra, E., Santos-Mendoza, T., Lugo-Reyes, S. O. & Terán, L. M. Antimicrobial peptides: General overview and clinical implications in human health and disease. *Clin. Immunol.* **135,** 1–11 (2010).

56. Abraham, T., Prenner, E. J., Lewis, R. N. A. H., Mant, C. T., Keller, S., Hodges, R. S. & McElhaney, R. N. Structure-activity relationships of the antimicrobial peptide

gramicidin S and its analogs: Aqueous solubility, self-association, conformation, antimicrobial activity and interaction with model lipid membranes. *Biochim. Biophys. Acta - Biomembr.* **1838,** 1420–1429 (2014).

57. Kapoerchan, V. V., Spalburg, E. De Neeling, A. J., Mars-Groenendijk, R. H. Noort, D. Gramicidin S derivatives containing cis- and trans-morpholine amino acids (MAAS) as turn mimetics. *Chem. - A Eur. J.* **16,** 4259–4265 (2010).

58. Grotenbreg, G. M. Witte, M.D, Van Hooft P. A. V., Spalburg, E., Reiß P, Noort, D., de Neeling, A. J., Koert, U.,van der Marel, G. A., Overkleeft, H. S. & Overhand, M.Synthesis and biological evaluation of gramicidin S dimers. *Org. Biomol. Chem.* **3,** 233–238 (2005).

59. Abou El-Nour, K. M. M., Eftaiha, A., Al-Warthan, A. & Ammar, R. a a. Synthesis and applications of silver nanoparticles. *Arab. J. Chem.* **3,** 135–140 (2010).

60 Kim, J. S. Kim, J. S. Kuk, E., Yu, K. N., Kim, J. H., Park, S. J., Lee, H. J., Kim, S. H., Park, Y. K., Park, Y. H., Hwang, C. Y., Kim, Y. K., Lee, Y. S., Jeong, D. H & Cho, M. H. Antimicrobial effects of silver nanoparticles. Nanomedicine Nanotechnology, Biol. Med. **3,** 95–101 (2007).

61. Vega-baudrit, J., Alvarado-meza, R. & Solera-jiménez, F. Synthesis of silver nanoparticles using chitosan as a coating agent by sonochemical method. *Avances en Química.* **9,** 125–129 (2014).

62. Rai, M., Yadav, A. & Gade, A. Silver nanoparticles as a new generation of antimicrobials. *Biotechnol. Adv.* **27,** 76–83 (2009).

63. Sharma, V. K., Yngard, R. a. & Lin, Y. Silver nanoparticles: Green synthesis and their antimicrobial activities. *Adv. Colloid Interface Sci.* **145,** 83–96 (2009).

64. Uygur, B., Craig, G., Mason, M. D. & Ng, A. K. Cytotoxicity and genotoxicity of silver nanomaterials. *Tech. Proc. 2009 NSTI Nanotechnol. Conf. Expo, NSTI-Nanotech 2009* **2,** 383–386 (2009).

65. Vigneshwaran, N., Nachane, R. P., Balasubramanya, R. H. & Varadarajan, P. V. A novel one-pot 'green' synthesis of stable silver nanoparticles using soluble starch. *Carbohydr. Res.* **341,** 2012–2018 (2006).

66. Oluwafemi, O. S.Lucwaba, Y., Gura, A., Masabeya, M., Ncapayi, V., Olujimi, O.O & Songca. S. P. A facile completely 'green' size tunable synthesis of maltose-reduced silver nanoparticles without the use of any accelerator. *Colloids Surfaces B Biointerfaces* 102, 718–723 (2013).

67. Reiad, N. a., Abdel Salam, O. E., Abadir, E. F. & Harraz, F. a. Green synthesis of antibacterial chitosan films loaded with silver nanoparticles. *Chinese J. Polym. Sci.* **31,** 984–993 (2013).

68. Wan, C., Jiao, Y., Sun, Q & Li, J. Properties of Silver Nanoparticles Embedded into Cellulose Aerogels. **37,** 1137–1142 (2016).

69. Govindan, S., Nivethaa, E. a. K., Saravanan, R., Narayanan, V. & Stephen, A. Synthesis

and characterization of chitosan–silver nanocomposite. *Appl. Nanosci.* **2,** 299–303 (2012).

70. Prema, P. Chemical mediated synthesis of silver nanoparticles and its potential antibacterial application. *Intech Open* **6,** 152–166 (2011).

71. Long, D., Wu, G. & Chen, S. Preparation of oligochitosan stabilized silver nanoparticles by gamma irradiation. *Radiat. Phys. Chem.* **76,** 1126–1131 (2007).

72. Wei, D., Sun, W., Qian, W., Ye, Y. & Ma, X. The synthesis of chitosan-based silver nanoparticles and their antibacterial activity. *Carbohydr. Res.* **344,** 2375–2382 (2009).

73. Abou El-Nour, K. M. M., Eftaiha, A., Al-Warthan, A., Ammar, R. A. A. Preparation of silver nanoparticles with controlled particle size. *Spectrochim. Acta - Part A Mol. Biomol. Spectrosc.* **2,** 251–257 (2009).

74. Shameli, K. Ahmad, M.B., Jazayeri, S. D., Sedaghat, S., Shabanzadeh, P., Jahangirian, H., Mahdavi, M & Abdollahi, Y. Synthesis and characterization of polyethylene glycol mediated silver nanoparticles by the green method. *Int. J. Mol. Sci.* **13,** 6639–6650 (2012).

75. Hoskote Anand, K. K. & Mandal, B. K. Activity study of biogenic spherical silver nanoparticles towards microbes and oxidants. *Spectrochim. Acta - Part A Mol. Biomol. Spectrosc.* **135,** 639–645 (2015).

76. Anonymous. The 12 Principles of Green Chemistry. *Pharm. Technol.* **33,** 46 (2009).

77. Agasti, N. & Kaushik, N. K. One Pot Synthesis of Crystalline Silver Nanoparticles. *Am. J. Nanomater.* **2,** 4–7 (2014).

78. Vivekanandhan, S. Green Process for Impregnation of Silver Nanoparticles into Microcrystalline Cellulose and Their Antimicrobial Bionanocomposite Films. *J. Biomater. Nanobiotechnol.* **3,** 371–376 (2012).

79. Bindhu, M. R. & Umadevi, M. Antibacterial and catalytic activities of green synthesized silver nanoparticles. *Spectrochim. Acta - Part A Mol. Biomol. Spectrosc.* **135,** 373–378 (2015).

80. Cataldi, A., Dorigato, A., Deflorian, F., & Pegoretti, A. Innovative microcrystalline cellulose composites as lining adhesives for canvas. *Pol. Eng. Sci*, **55**, 1349-1354 (2015)

81. Jankauskaitė, V., Abzalbekuly, B., Lisauskaitė, A., Procyčevas, I., Fataraitė, E & Vitkauskienė, A. U. J. Silicone rubber and microcrystalline cellulose composites with antimicrobial properties. *Mater. Sci.* **20,** 42–49 (2014).

82. Fan, Y., Fukuzumi, H., Saito, T. & Isogai, A. Comparative characterization of aqueous dispersions and cast films of different chitin nanowhiskers/nanofibers. *Int. J. Biol. Macromol.* **50,** 69–76 (2012).

83. Wanasekara, N. D., Santos, R. P. O., Douch, C., Frollini, E. & Eichhorn, S. J. Orientation of cellulose nanocrystals in electrospun polymer fibres. *J. Mater. Sci.* **51,** 218–227 (2016).

84. Smiechowicz, E., Kulpinski, P., Niekraszewicz, B. & Bacciarelli, A. Cellulose fibers modified with silver nanoparticles. *Cellulose*. **18,** 975–985 (2011).

85. Yan, J., Abdelgawad, A. M., El-Naggar, M. E. & Rojas, O. J. Antibacterial activity of silver nanoparticles synthesized In-situ by solution spraying onto cellulose. *Carbohydr. Polym.* **147,** 500–508 (2016).

86. Marie Arockianathan, P., Sekar, S., Sankar, S., Kumaran, B. & Sastry, T. P. Evaluation of biocomposite films containing alginate and sago starch impregnated with silver nano particles. *Carbohydr. Polym.* **90,** 717–724 (2012).

87. Rieger, K. A., Birch, N. P. & Schi, J. D. Designing electrospun nanofiber mats to promote wound healing - a review wound healing. *Mater. Chem. B.* **1,** 4531–4541 (2013).

88. Li, D. & Xia, Y. Electrospinning of nanofibers: Reinventing the wheel? *Adv. Mater.* **16,** 1151–1170 (2004).

89. Jacobs, V., Patanaik, A., Anandjiwala, R. D. & Maaza, M. Optimization of Electrospinning Parameters for Chitosan Nanofibres. *Curr. Nanosci.* **7,** 396–401 (2011).

90. Zhuang, X., Cheng, B., Kang, W. & Xu, X. Electrospun chitosan/gelatin nanofibers containing silver nanoparticles. *Carbohydr. Polym.* **82,** 524–527 (2010).

91. Torres-Giner, S., Ocio, M. J. & Lagaron, J. M. Development of active antimicrobial fiber based chitosan polysaccharide nanostructures using electrospinning. *Eng. Life Sci.* **8,** 303–314 (2008).

92. Shalumon, K. T. Anulekha, K. H., Girish, C.M., Prasanth, R., Nair, S.V & Jayakumar R. Single step electrospinning of chitosan/poly(caprolactone) nanofibers using formic acid/acetone solvent mixture. *Carbohydr. Polym.* **80,** 414–420 (2010).

Chapter 3: Preparation and characterization of antimicrobial agents

3.1 Introduction

Reducing the size of a material to the nanoscale may improve the material's biocompatibility and can also lead to changes in the physical, chemical and biological properties of that material[1,2]. A variety of organic and inorganic nanometer-sized materials have been widely studied, which due to their high surface-to-volume ratios, are versatile and have a wide range of desirable properties[1,3,4]. Polysaccharide-based nanofibrils isolated from cellulose and chitin, known as nanowhiskers are examples of such organic nano-sized materials and have attracted attention in various fields. This attention is because of their properties, which include high absorptivity, nontoxicity and biodegradability. It is because of these properties that nanowhiskers are mostly used as fillers in nanocomposite synthesis for biomedical applications[5]. Silver nanoparticles are amongst those inorganic nano-sized materials that are continuously receiving attention, more specifically due to the versatility of this element with applications in the field of semiconductors, biological sensors, antiviral and antibacterial activity[1,6]. Furthermore, research has previously focused on the development of "green" techniques for the production of silver nanoparticles[7]. For this purpose, Wei et al. has used chitosan as a reducing and a stabilizing agent in order to produce silver nanoparticles with high antibacterial activity towards both Gram-positive and Gram-negative bacteria[8]. Silver nanoparticles tend to aggregate or form clusters at high concentrations, which is due to the high chemical activity of these particles and the effects of Van der Waals forces. This leads to the decrease in performance of these particles[9,10]. Wan et al. impregnated cellulose aerogels with silver nanoparticles while Vivekanandhan et al. used microcrystalline cellulose to attach silver nanoparticles. Both these studies have shown that these micro-nano structures effectively hinder agglomeration of silver nanoparticles within these cellulose matrices[10,11].

This chapter reports on the isolation and production of three antimicrobial agents that are of organic and inorganic origin. Isolated chitin nanowhiskers (ChNWs) present the organic antimicrobial agents and chitosan reduced silver nanoparticles (CTSAgNPs) as well as silver impregnated microcrystalline cellulose were produced as inorganic antimicrobial agents. These antimicrobial agents are then characterized using transmission electron microscopy (TEM), UV-Vis spectroscopy, confocal fluorescence microscopy (CFM) and Fourier transform infra-red spectroscopy (FTIR). The isolated chitin nanowhiskers and microcrystalline cellulose were labelled using fluorescent staining agents, Rhodamine B and fluorescein isothiocyanate, respectively. This fluorescent staining was done so it would be possible to view the distribution

of combined antimicrobial agents in the same polymer matrix. The results of the chemical and morphological analysis of these synthesized antimicrobial agents are discussed.

3.2 Experimental

3.2.1 Materials

Silver nitrate ($AgNO_3$) (purity/grade), chitosan (from crab shells), chitin, N-acetyl-1,4-ß-D-glucopyranosamine (from shrimp shells) and sodium hydroxide (pellets) were all purchased from Sigma Aldrich. Sulphuric acid (96 wt. %), acetic acid (100 wt. %) and hydrochloric acid (32 wt. %) were all supplied by Merck. JRS Pharma provided microcrystalline cellulose (MCC) under the product name VIVAPUR101. The 5(6)-fluorescein isothiocyanate mixed isomer (FITC) and N-[9-(ortho-carboxyphenyl)-6-(diethylamino)-3H-xanthen-3-ylidene] diethyl ammonium chloride, commonly known as Rhodamine B dye (95% dye content) were purchased from Sigma Aldrich. An Elga Purelab instrument produced deionized water in-house and Merck supplied the isopropanol used.

3.2.2 Production of antimicrobial agents

3.2.2.1 Isolation and fluorescent labelling of chitin nanowhiskers (ChNWs)

Chitin nanowhiskers were isolated by a four-step acid hydrolysis procedure as described by Mincea et al[3]. Acid hydrolysis was carried out using 3.0 g of chitin powder in 90 mL of 3.0 M hydrochloric acid. The reaction was stirred at 105 °C for 4 hours after which 90 mL of ice-cold deionized water was added to dilute the solution reaction mixture. This was followed by centrifugation, which was done for about six times per sample for five minutes each time and a rotation speed of 4450 rotations per minute was used. The purpose of this was to wash away the larger particles within the ChNWs solution. The solution was then decanted into dialysis tubes, which were placed in a large flask with deionized water for 7-10 days. After dialysis, the nanowhisker solution was freeze-dried to form white cotton-like nanowhisker crystals.

Rhodamine B (RhB) was used for labeling of the ChNWs to study their dispersion in EVOH by way of CFM. Freeze-dried ChNWs, 250 mg, were added to 15 mL of 0.1 N NaOH and the solution was sonicated for 10 min. The staining was done according to an experimental procedure described by Du Toit[12]. The ChNW suspension was then added to a 10 mL solution of RhB that was prepared by dissolving 10 mg of powdered RhB in deionized water. The mixtures were added together and sonicated for 5 minutes, then covered with foil and stirred

for 3 days in the dark. The mixture was then centrifuged and washed with 0.1 M NaOH and the excess NaOH was decanted off. The solution was then freeze dried to obtain the RhB labeled ChNWs.

3.2.2.2 Production of chitosan-reduced silver nanoparticles (CTSAgNPs)

Chitosan-reduced silver nanoparticles were prepared using a method described by Wei et al., where chitosan was used as a reducing and stabilizing agent[8]. Chitosan (692 mg) was dispersed in 100 mL of a 1% solution of acetic acid with vigorous stirring. A 52.0 mM solution of silver nitrate was prepared by dissolving 883.3 mg of silver nitrate in 100 mL deionised water to make a 52.0 mM solution. From these stock solutions, varying volumes of silver nitrate and chitosan were added together to prepare mixtures that contain different concentrations of both silver and chitosan, as described in Table 3.1. The three concentrations of silver and chitosan were chosen in order to prepare mixtures containing lower amounts (Sample 1 and Sample 2) and higher amounts (Sample 3) of silver nitrate with respect to chitosan, in the final mixtures. This was done to determine the optimum silver to chitosan ratio that forms nanoparticles with the smallest diameters, as various applications of silver nanoparticles require the nanoparticles to have small diameters. Each solution was stirred until homogeneous and transferred to a 12.5 × 2 cm^2 cuvette. Each solution was left to stand in the oven for 12 hours at 95 °C. The different solutions changed colour from colourless to light-yellow and finally to a yellowish-brown solution after hours 12 hours. The pH of the prepared nanoparticle solution was then adjusted from pH 4.0 to pH 11.7 using a 1 M solution of sodium hydroxide in order to investigate the optimal pH conditions.

Table 3.1: Preparation of chitosan-reduced silver nanoparticles.

Sample number	Silver nitrate concentration (mmol/mL)	Silver nitrate solution volume (mL)	Chitosan solution density (mg/mL)	Chitosan solution volume (mL)
1	15	8	5	20
2	22	12	4	16

3	30	16	3	12

3.2.2.3 Production of silver nanoparticle impregnated microcrystalline cellulose (AgMCC)

The process of impregnation of silver nanoparticles on the microcrystalline cellulose surface was using chitosan as reducing agent was carried out according to a combination of techniques described by Vivekanandhan et al. and Wei et al.[8,11]. A silver nitrate solution was prepared by dissolving 883.3 mg of silver nitrate powder in 100 mL deionised water to make a 52.0 mM solution. A chitosan solution was prepared by dispersing chitosan (692 mg) in 100 mL of a 1% solution of acetic acid with vigorous stirring. Microcrystalline cellulose (5.3 g) was dispersed in 12 mL of the prepared chitosan solution and sonicated for 10 minutes. The $AgNO_3$-MCC (12 mL) and chitosan (16 mL) solutions were added together, sonicated for a further 2 minutes, and stirred for 6 hours to allow for silver ion reduction to silver nanoparticles. The suspension was allowed to settle down and excess solvent was decanted. The mixture was then washed five times with deionized water and dried overnight in an oven at 95 °C. A film was obtained which was pulverized in order to obtain AgMCC in the form of a powder. A yellowish-brown powder was obtained and kept for further analysis.

Microcrystalline cellulose (MCC) was labelled with a fluorescent dye, fluorescein isothiocyanate (FITC). This staining was carried out by dispersing 250 mg MCC and 10.8 mg FITC in 25 mL of a 0.1 M sodium hydroxide solution. To ensure the attachment of FITC on the surface of MCC, the solution was stirred under reflux in the dark for 72 hours[13].

3.3 Analysis techniques

3.3.1 Ultraviolet-visible spectroscopy (UV-Vis)

Samples of the synthesized CTSAgNPs and AgMCC were diluted with deionized water (1:10 sample : water) and analyzed by UV-Vis spectrometry. A small glass cuvette was filled with the diluted nanoparticle samples and the UV measurements of the absorbance were taken at wavelengths between 300 nm and 800 nm.

3.3.2 Transmission electron microscopy (TEM)

Morphological characterization of the produced CTSAgNPs and isolated ChNWs was done using a LEO 912 EM TEM instrument. For the CTSAgNPs, sample preparation was done by depositing a drop of the silver nanoparticle solution on a carbon-coated grid. The silver nanoparticle containing grids were then air-dried and analysed. ChNWs were first dispersed in deionized water and sonicated. A drop of dilute chitin nanowhiskers (0.1 wt. % and 0.01 wt. %) was then deposited on a carbon coated grid, negatively stained with uranyl acetate and allowed to dry. This process was done twice to ensure successful staining and the grids were then air-dried before analysis.

3.3.3 Scanning transmission electron microscopy (STEM)

A Carl Zeiss MERLIN FE SEM in STEM-seg mode was used to image the AgMCC samples with images taken using the dark fields mode. AgMCC (0.01 wt %) was dispersed in deionized water and a drop of this mixture was deposited on carbon coated grids and allowed to dry. The AgMCC containing grids were subjected to STEM analysis at a working distance of 9.5 mm and EHT target 20 kV.

3.3.4 Attenuated total reflectance-Fourier transform infrared spectroscopy (ATR-FTIR)

FTIR data were recorded using a Thermo Fisher Nicolet iS10 instrument. All the spectra were recorded at a minimum number of 32 scans, taking background information before every sample scan. A resolution of 4 cm^{-1} was used. The synthesized silver nanoparticles and isolated ChNWs were analysed as thin films and solid whiskers, respectively.

3.3.5 Confocal fluorescence microscopy (CFM)

Successful labelling with RhB and FITC was studied using CFM. A 405 nm laser was used to excite the chitosan-reduced silver nanoparticles to auto fluoresce. In the case of RhB and FITC, 561 nm and 488 nm lasers were used to fluoresce the labelled chitin nanowhiskers and microcrystalline cellulose, respectively. For the FITC labelled MCC, a green fluorescent colour of the FITC dye appears around 510 nm while in the case of chitin nanowhiskers, a red fluorescent colour for RhB appears around 650 nm on the emission spectrum and that is what

the confocal microscope was set to detect. Image acquisition was performed on a Carl Zeiss Laser Scanning Microscope (LSM) 780. The setup for the experiment was as follows:

1. Lasers: 488 nm and 561 nm for FITC and RhB, respectively.

2. Beam splitters (used to direct light to the sample), MBS: 48 MBS InVis: Plate

3. FW1: None LSM

4. Master gain: 800

5. Thiopurine S-methyltransferase (TPMT) filter used

6. Objective used: alpha Plan-Apochromat 100 x magnification

7. The Images were acquired with a pixel dwell time of 3.15 µs

8. Zoom: 1.0

3.4 Results and discussion

3.4.1 Chitin nanowhiskers (ChNWs)

ChNWs were isolated from chitin as described in Section 3.2.2.1. Freeze dried ChNWs were dispersed in deionized water and sonicated in order to improve the ChNW dispersion and avoid agglomeration. Techniques such as TEM, FTIR and CFM were used to characterize the isolated nanowhiskers and the results are discussed below. TEM was done to confirm the successful isolation of ChNWs and to show the shape and size of the isolated whiskers. ChNW staining with RhB, a fluorescent dye, was done so that the ChNWs could fluoresce and thus be easily identifiable with CFM when dispersed within a non-fluorescent polymer matrix.

Figure 3.1 illustrates the TEM results of the freeze dried ChNWs dispersed in deionized water after sonication. The isolated ChNWs are slender and rod-like with sharp points with an average size of 160 nm in length and 27 nm in width. Uniformly dispersed single nanowhiskers can be seen in Figure 3.1 (A) while Figure 3.1 (B) shows chitin whiskers that have agglomerated nanowhiskers overlapping with each other. The shape and the size of the isolated chitin nanowhiskers are similar to those isolated in research done by Fan et.al[14]. However, the isolated ChNWs reported by Fan et al. appeared longer in length compared to the ChNWs shown below but similar to Figure 3.1 (B), they also assumed spindle-like morphologies.

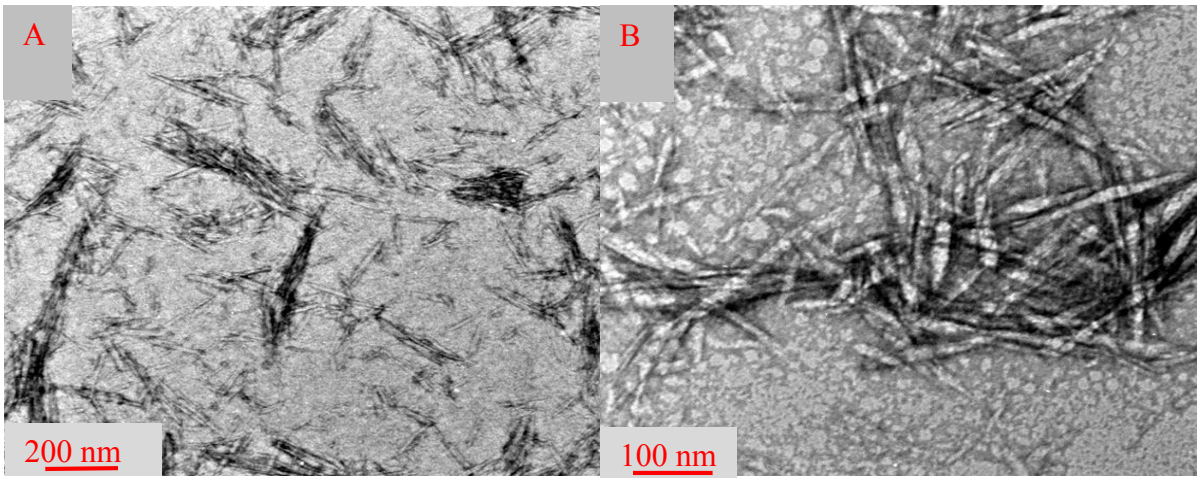

Figure 3.1 TEM micrographs of ChNWs isolated from chitin by acid hydrolysis, dispersed in deionized water and sonicated.

The CFM micrographs shown in Figure 3.2 illustrate the successful labelling of ChNWs with Rhodamine B (RhB). Figure 3.2 (A) presents RhB-labelled whisker bundles that showed fluorescent signals when excited with the 561 nm laser. Figure 3.2 (B) shows nanowhiskers on

a TPMT filter background. Figure 3.2 (C) is an overlay of (A) and (B). The nanowhiskers appear well dispersed though some clusters or agglomerates can be seen. The CFM micrographs support the TEM results shown in Figure 3.1 although it is not possible to observe the rod-like shape of individual whiskers with CFM, staining of the nanowhiskers was successful.

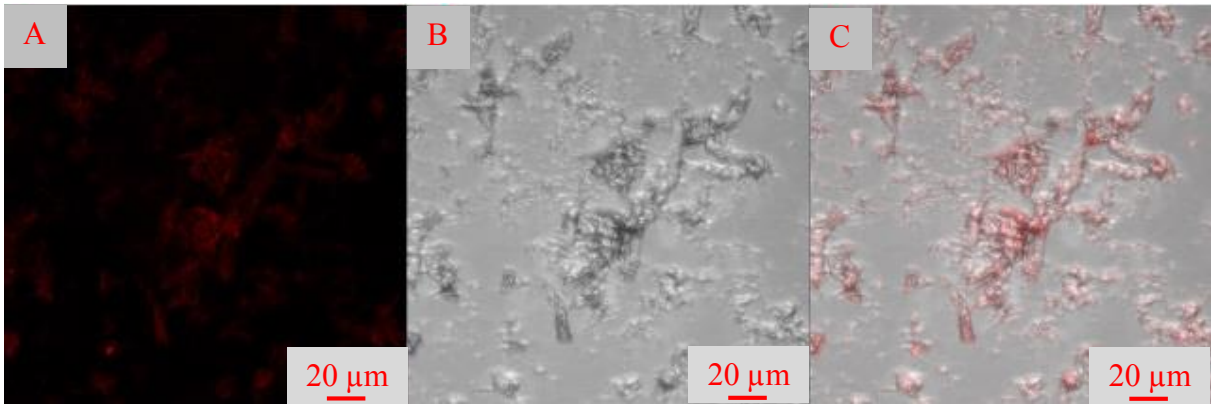

Figure 3.2 CFM micrographs of RhB labelled ChNWs redispersed in deionized water (A) 488 nm laser, (B) TPMT filter and (C) is an overlay of (A) and (B).

The agglomeration of ChNWs observed in both TEM and CFM could be attributed to the high specific surface area and hydrogen bonding that occurs between the ChNWs. During acid hydrolysis, the ChNWs acquire a negative charge. The negative charge causes the ChNWs to repel each other and this should allow good dispersion within a nanocomposite mixture, however, this is not always the case because in some instances, the effect of the hydrogen bonding between the chitin nanowhiskers is stronger than the effect of the repelling negative charges resulting in agglomeration[15].

FTIR analysis was carried out on the isolated ChNWs to evaluate the functional groups present in the whiskers. In Figure 3.3, the bands at 3257 cm^{-1} and 2926-2852 cm^{-1} correspond to O-H and C-H stretching vibrations of the ChNWs, respectively. The characteristic amide moieties of the ChNWs are also observed at 1556 cm^{-1}, 1626 cm^{-1} and 1653 cm^{-1}. This corresponds to the results reported by Du Toit et al [12] where these amide peaks were observed between 1500 -1660 cm^{-1}. The peak at 1073 cm^{-1} corresponds to the C-O bond of the chitin, with the double peak indicating the presence of either an ether or an alcohol C-O bond.

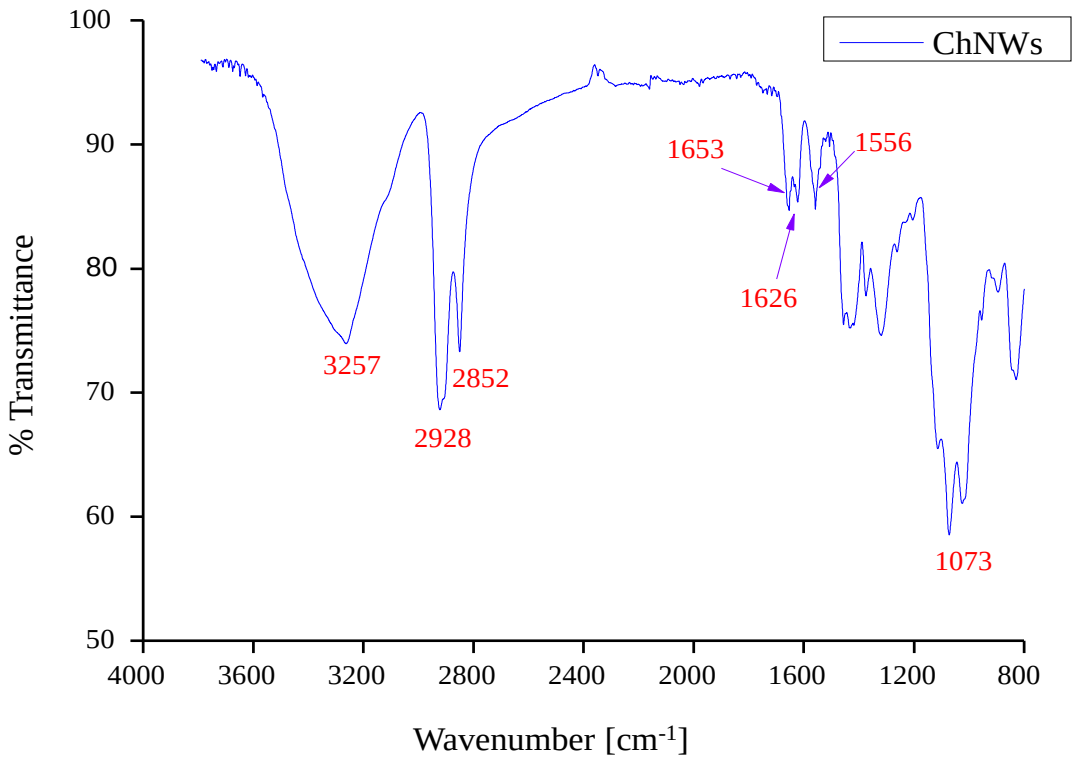

Figure 3.3 ATR-FTIR of the isolated ChNWs.

3.4.2 Chitosan-reduced silver nanoparticles (CTSAgNPs)

CTSAgNPs were produced from silver nitrate using chitosan as a reducing and stabilizing agent at a temperature of 95 °C[8]. Three solutions containing different concentrations of silver nitrate and chitosan were prepared as explained in Section 3.2.2.2. A progressive change in colour of the silver containing solutions from colourless to yellowish-brown was observed in all three solutions, which is indicative of the successful reduction of silver to silver nanoparticles[19, 20].

The formation of silver nanoparticles was also monitored by UV-Vis. The appearance of the surface plasmon resonance (SPR) band at a wavelength range of 380 nm - 460 nm indicates the presence of silver nanoparticles[8,19]. Figure 3.4 shows the UV-Vis spectra of the three samples containing 15 mM (Sample 1), 22 mM (Sample 2) and 30 Mm (Sample 3) concentrations of $AgNO_3$. One of the most notable observations is that even though a change in colour was observed in all $AgNO_3$ solutions, only Sample 2 showed an SPR peak at 448 nm, as shown in Figure 3.4. The reason for absence of the SPR bands in Samples 1 and 3 (regardless of the positive colour change indicating the formation of silver nanoparticles) is not clear. A possible explanation for the absence of the SPR band for Sample 1 in Figure 3.4 may be due to a too low concentration of silver nanoparticles. In the case of Sample 3, which was produced

using the highest concentration of silver nitrate of all three samples, the absence of the SPR band may possibly be due to the formation of a higher concentration of silver nanoparticles that produces clusters. These clusters may then be incorrectly characterized by the UV-Vis spectrometer as a decrease in the nanoparticle concentration and therefore causing a decrease in the SPR band intensity.

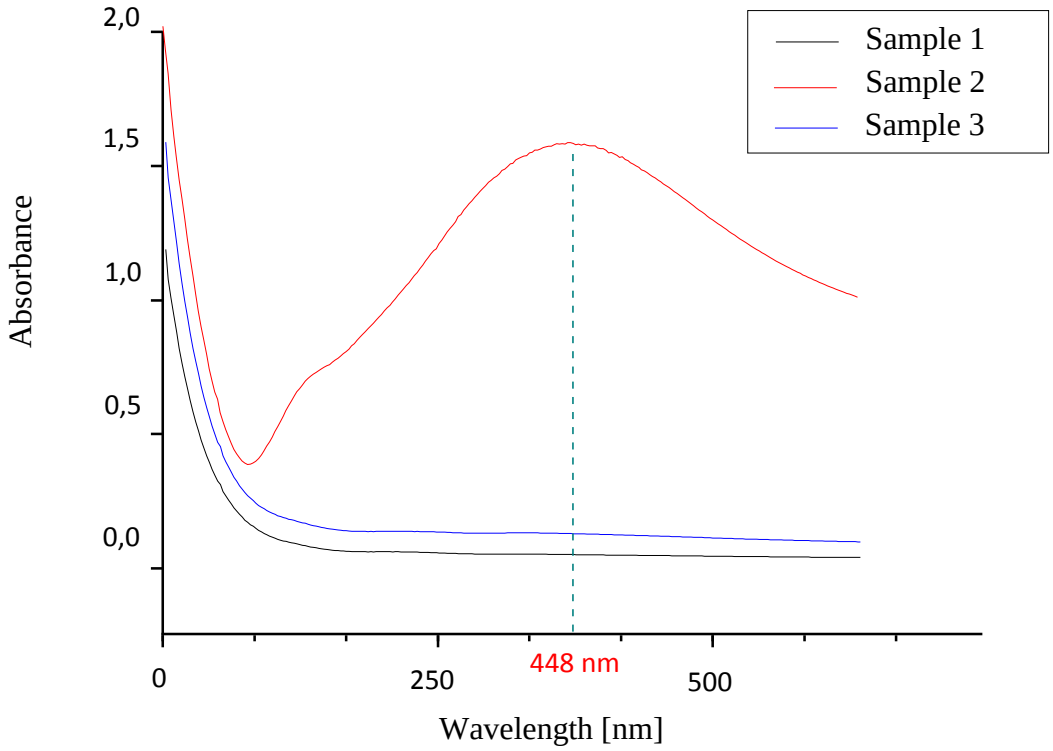

Figure 3.4 UV–Vis absorption spectra of chitosan-reduced CTSAgNPs produced using different $AgNO_3$ concentrations, reduced at 95 °C for 12 hours.

The absence of the SPR band in the case of Sample 1 and the Sample 3 suggest the unsuccessful formation of silver nanoparticles and this is in contradiction with the colour change that was positive for all three samples. Hence there was a need to use additional techniques to further investigate and confirm the successful reduction of silver to silver nanoparticles in all three samples. TEM was therefore used for this purpose. Figure 3.5 shows the TEM images and corresponding frequency distribution graphs for Sample 1 (A and B), Sample 2 (C and D) and Sample 3 (E and F) showing the sizes and shapes of the formed silver nanoparticles. Sample 1 is shown to have uniformly dispersed, spherically shaped nanoparticles that have an average diameter of 7.3 nm with a normal size distribution. The average dameter of nanoparticles

obtained in Sample 2 is 4.0 nm and the sizes of these nanoparticles assume a bimodal distribution. Sample 3 shows the formation of nanoparticles with an average diameter of 99 nm, which also revealed a normal size distribution. Sample 2 showed nanoparticles that are slightly smaller compared to those obtained from Sample 1 and significantly smaller than those for Sample 3. The size distribution is confirmed by the appearance of a definite SPR band which suggests that the nanoparticles have variable shapes. This is because the number of SPR bands depends on the symmetry of the nanoparticles formed[13]. According to Figure 3.5 (C), Sample 2 shows a tendency of the nanoparticles to agglomerate, which was even more so in the case of Sample 3 according to Figure 3.5 (D), but not for Sample 1 as seen in Figure 3.5 (C). As explained during the discussion of the UV-Vis results the clusters formed in the case of Sample 3 may possibly be characterized by the UV-Vis spectrometer as a low nanoparticle concentration and therefore cause an absence of the SPR band. The possible explanations for the absence in the SPR band in the case of Sample 1 and Sample 3 is unfortunately not certain, but the TEM results clearly show the formation of silver nanoparticles in the case of all three samples, which corresponds to the positive colour change during the production of these nanoparticles.

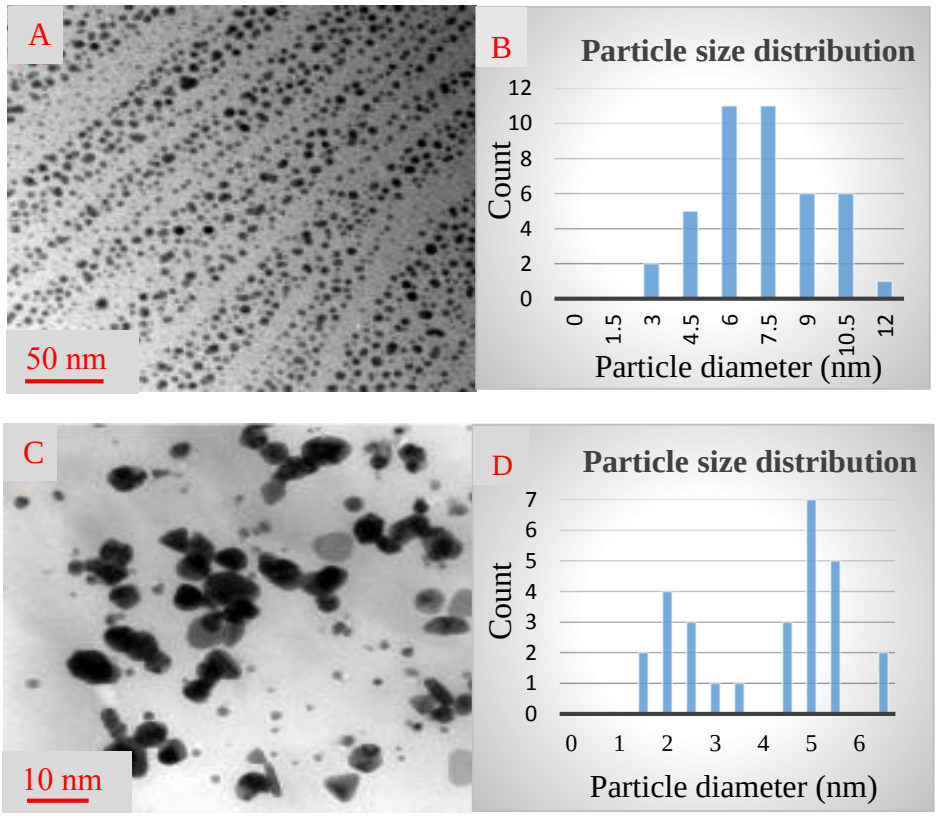

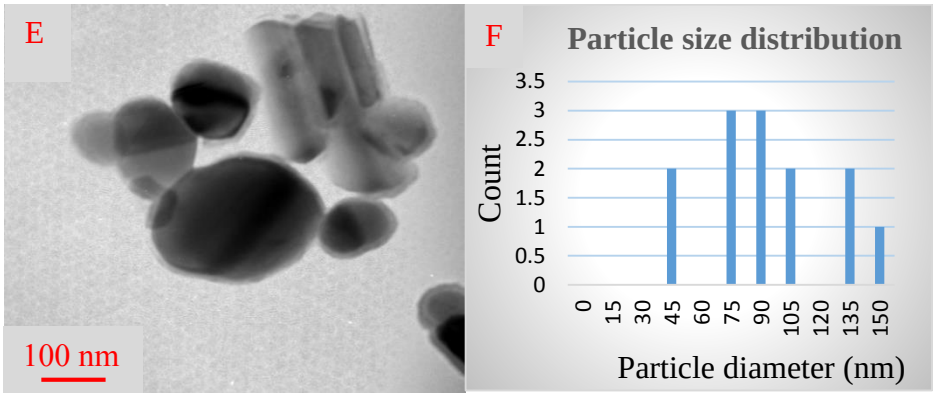

Figure 3.5 TEM micrographs of CTSAgNPs formed in the case of Sample 1 (A), Sample 2 (C) and Sample 3 (E) with corresponding frequency distribution graphs of the nanoparticles formed in the case of each sample.

The agglomeration of silver nanoparticles at higher silver nitrate concentrations could be attributed to the presence of larger particles that tend to form clusters, resulting in the polydispersion of the nanoparticles within the chitosan mixture. The silver nanoparticles formed in the case of Sample 2 revealed the smallest average particle size of the three samples with little to no agglomeration and therefore suggests that the silver nitrate-chitosan ratio used for the preparation of Sample 2 is the most suitable. Sample 2 was therefore used for the rest of the study.

In order to investigate the effect of pH on the formation of the chitosan-reduced silver nanoparticles, the pH of the Sample 2 was adjusted from pH = 1 to pH = 11 by gradually adding 1 M NaOH solution to the silver nanoparticle solution. This was done because for nanoparticles reduced and stabilized using an organic reducing agent, the stability and distribution ability of the nanoparticles depends on the pH and ionic strength of the silver nanoparticle solution[9]. Figure 3.6 presents UV-Vis results of the silver nanoparticles formed in the case of Sample 2 at different pH levels. At pH = 11, a shift was seen in the SPR band from around 448 nm to 425 nm. The band also becomes narrower, which indicates the formation of nanoparticles with a narrow size distribution. The different sizes and shapes of the formed nanoparticles shown in the TEM image in Figure 3.5 (C) is in agreement with the UV-Vis results; this is confirmed by the bimodal size distribution of the nanoparticles. This also shows that the size of silver nanoparticles can be controlled not only by chitosan parameters and the concentration of silver nitrate, but by the pH conditions in which the reduction process is carried out as well[7].

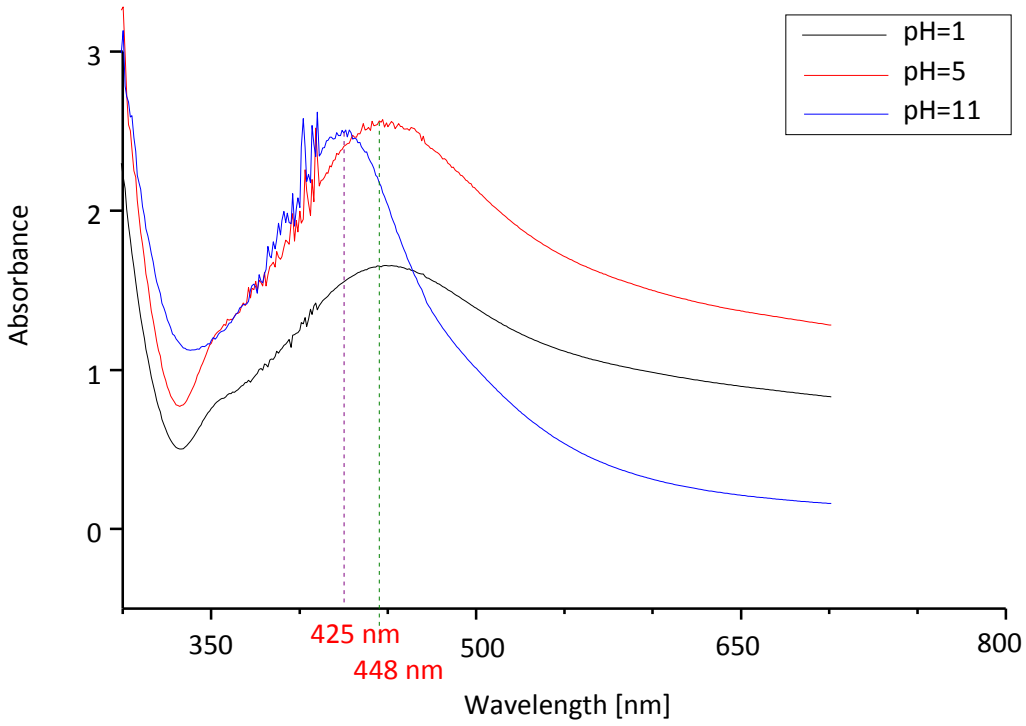

Figure 3.6 UV–Vis absorption spectra of CTSAgNPs prepared in the case of Sample 2 at different pH values, stabilized with 1 M sodium hydroxide.

Figure 3.7 presents the confocal fluorescence microscopy micrographs of silver nitrate and CTSAgNPs prepared in the case of Sample 2, which showed auto-fluorescence when excited with the 405 nm laser. Although silver nanoparticles have been used to enhance the fluorescence of some chromophores and metal complexes, as reported by Liu et al. and Suslov et al., the auto-fluorescence of chitosan-based silver nanoparticle has not yet been report[17,18].

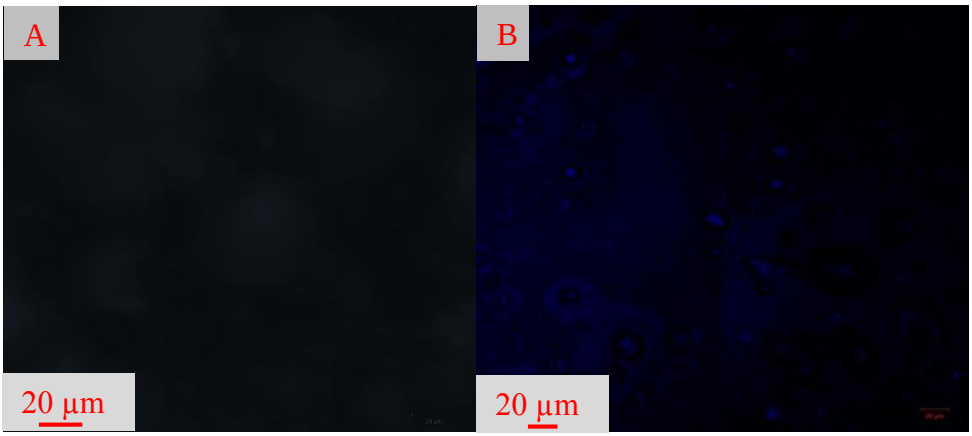

Figure 3.7 Silver nitrate CFM micrograph (A) and CFM micrograph showing the auto fluorescence of CTSAgNPs of Sample 2 (B).

Figure 3.7 (A) shows that silver nitrate does not fluoresce when excited with the 405 nm laser. The auto-fluorescence signal was relatively strong and brighter in certain areas of the sample indicating agglomeration of the CTSAgNPs, as seen in (B). These results are in agreement with the TEM results presented in Figure 3.5 which showed the formation of polydispersed chitosan-reduced silver nanoparticles which also had some agglomerated areas.

Figure 3.8 shows the FTIR spectra representing the characteristic peaks of functional groups present in powdered chitosan, silver nitrate and chitosan-reduced silver nanoparticles prepared from sample. The broad band at 3200-3500 cm^{-1} in Figure 3.8 is characteristic of an overlap between the N-H and O-H stretching vibrations while the band at 2850 cm^{-1} correspond to the C-H respectively for both the CTSAgNPs and CTS. The peaks at 1665 cm^{-1} and 1510 cm^{-1} correspond to the carbonyl bonds and the N-H bonds of the primary amines respectively for both the CTSAgNPs and CTS. The peak at 1260 cm^{-1} corresponds to the N=O bond of silver nitrate. The sharp peaks observed in the fingerprint region at 450 cm^{-1} and 510 cm^{-1} are indicative of the attachment of the silver nanoparticles to the hydroxyl groups of the chitosan, this shows the Van der Waals interactions between the chitosan backbone and the silver nanoparticles[9,10]. These results correspond to FTIR results in research done by Wei et. al. They reported the shift in the N–H bending vibration bands from about 1578.1 cm^{-1} to 1570.8 cm^{-1} along with a decrease in the intensity of the band. This band shift suggests an attachment of silver to nitrogen atoms that causes the vibration intensity of the N–H bond to decrease, which is attributed to the increase in molecular weight after silver attachement[8].

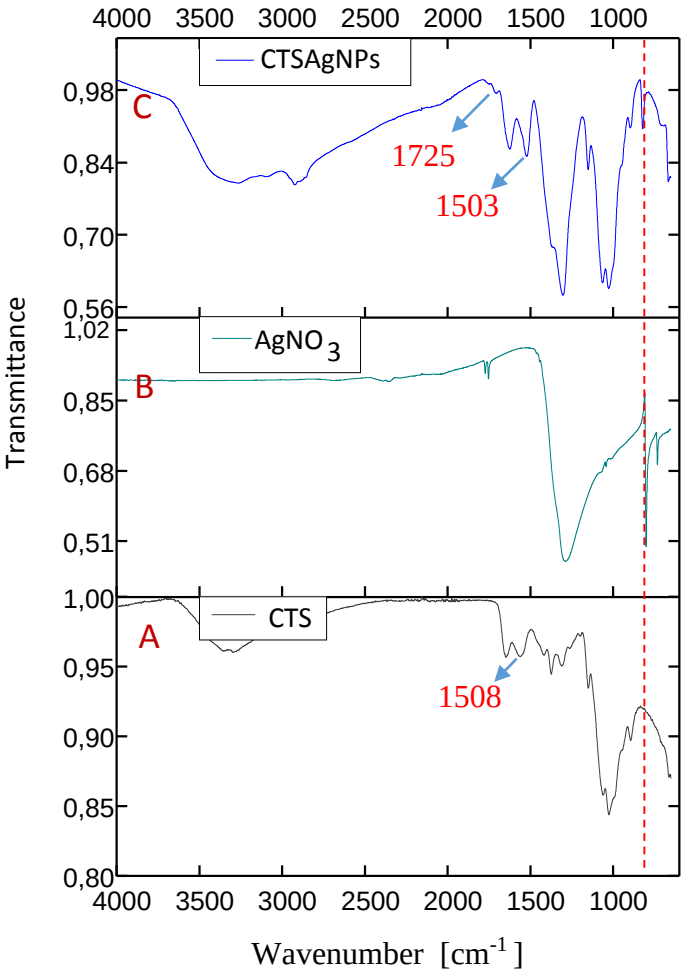

Figure 3.8 FTIR spectra of (A) chitosan (CTS), (B) silver nitrate ($AgNO_3$) and (C) chitosan-reduced silver nanoparticles (CTSAgNPs).

3.4.3 Silver nanoparticle impregnated microcrystalline cellulose (AgMCC)

The third antimicrobial agent that was produced during this study involved the use of microcrystalline cellulose (MCC) as a matrix to which CTSAgNPs can be attached, in order to produce silver nanoparticle impregnated microcrystalline cellulose (AgMCC). The method of attachment of the nanoparticles to the MCC is described in Section 3.2.2.3. This was done to explore a greener method of insitu impregnation of silver nanoparticles on a polysaccharide and also to attempt to hinder agglomeration of the silver nanoparticles and enhance the distribution of the silver nanoparticles. A drop of AgMCC suspension was placed on carbon coated copper grids and the solvent was allowed to evaporate prior to TEM analysis to investigate the successful formation and attachment of silver nanoparticles on MCC.

Fluorescein isothiocyanate (FITC) was used to label the microcrystalline cellulose prior to silver impregnation. Successful labelling was studied using confocal fluorescence microscopy where a 405 laser was used to excite the auto fluorescent silver nanoparticles and a 488 nm laser was then used to excite the FITC labelled microcrystalline cellulose[15].

The reaction mixture was monitored for 6 hours for the formation of the silver nanoparticles[11]. Figure 3.9 shows the UV-Vis spectra taken hourly up to 5 hours.

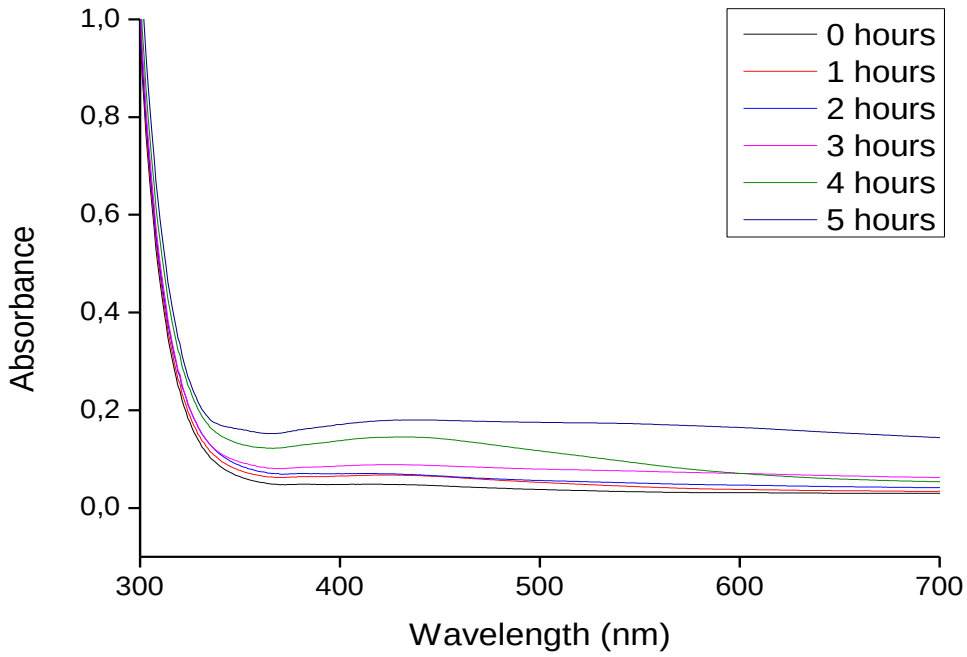

Figure 3.9 UV-Vis spectra of silver nanoparticle impregnated microcrystalline cellulose (AgMCC) reaction mixture, for 0-5 hours reaction time.

These results show that no nanoparticles formed during the first 3 hours of the reaction, but after the fourth hour an SPR band characteristic of the formation of silver nanoparticles started to appear at around 425 nm. A gradual increase in the absorbance was observed with the increase in the reaction time. At a six-hour reaction time the absorbance of the silver nanoparticles is seen to almost double when compared to the measurements taken at 5 hours of the reaction. The huge difference between the absorbance in the measurements taken at 5 hours and 6 hours provided a challenge to include the UV-Vis spectra for the 6 hours measurement into Figure 3.9 with regards to the scale. The UV-Vis spectrum for the 6 hours measurement is therefore illustrated in Figure 3.10. This figure shows a distinct peak at a wavelength of about

440 nm after 6 hours, which confirms the successful reduction of silver nitrate to silver nanoparticles in the MCC matrix using chitosan as a reducing agent.

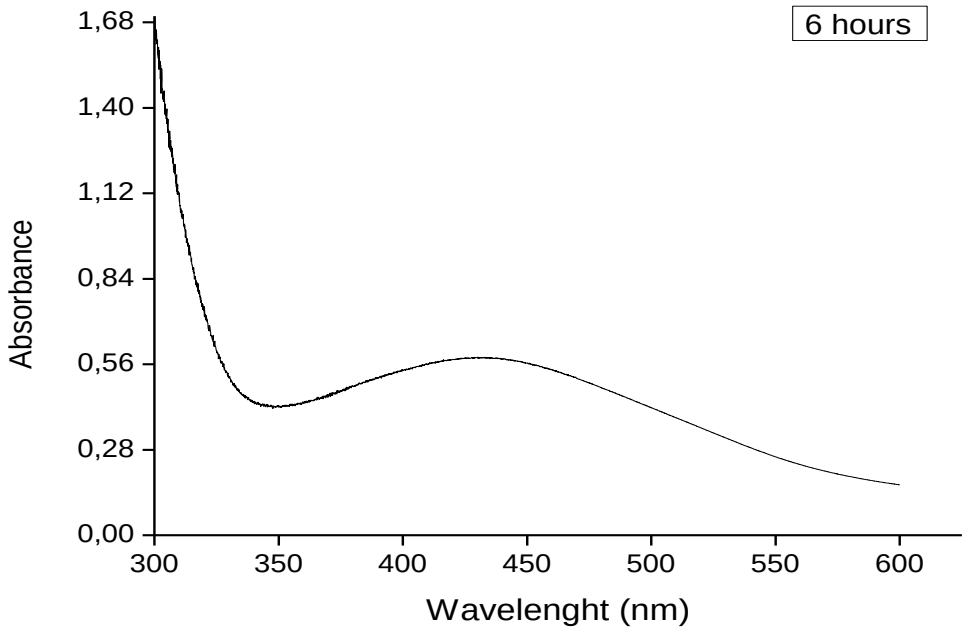

Figure 3.10 UV-vis spectra of a silver nanoparticle impregnated microcrystalline cellulose reaction mixture after 6 hours of reaction time.

The successful impregnation of the silver nanoparticles within the microcrystalline cellulose matrix was also confirmed by the progression of the white cellulose mixture to a brownish suspension as illustrated in Figure 3.11. This colour change in MCC powder is consistent with results observed in the work done by Vivekanandhan where curry leaf broth was used as a reducing agent. After 6 hours of stirring, the solution was dried and a brown coloured film was obtained which was then pulverized into fine powder, as shown in Figure 3.11 A and B, for further analysis[11].

Figure 3.11 Microcrystalline cellulose impregnated with silver nanoparticles (A) solvent cast film (B) pulverized film and (C) AgMCC and neat MCC.

The AgMCC powder shown in Figure 3.11 (C) was dispersed in deionized water and sonicated in order to increase the dispersion. A drop of the mixture was then placed on a carbon coated TEM grid and analyzed. The STEM images shown in Figure 3.12 confirm the successful formation of silver nanoparticles in the MCC matrix, showing polydispersed silver nanoparticles throughout the MCC. Figure 3.12 (A) shows silver nanoparticle agglomerates, which appear as small black spots on the surface of the larger MCC microfibrils as observed in (B).

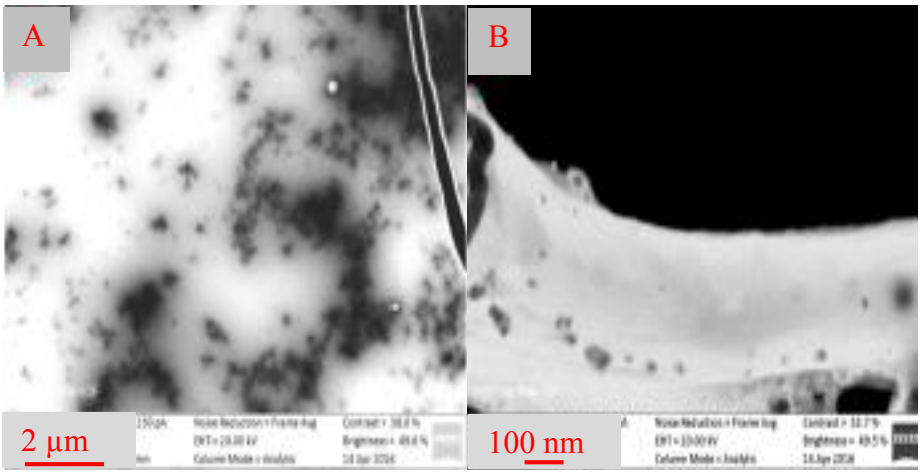

Figure 3.12 STEM micrographs of AgMCC showing silver impregnation on the surface of microcrystalline cellulose.

The average size of the nanoparticles formed was between 10 - 40 nm in diameter, spherically shaped and revealed a narrow size distribution (Figure 3, Addendum A). These diameters are similar to those of nanoparticles that were bio-produced using curry leaf as a reducing agent[11]. However, these curry leaf reduced nanoparticles were poorly dispersed within the MCC matrix, showing more agglomerated silver nanoparticles on the surface of MCC. The chitosan-reduced silver nanoparticles obtained in this study appear homogeneously dispersed in the MCC matrix and although agglomeration can be seen in Figure 3.12 (A) and (B) it is less than in the case when curry leaves were used as reducing agent. This suggests that chitosan is more effective as a reducing agent than curry leaf in forming homogeneously dispersed nanoparticles on the MCC surface.

Figure 3.13 shows the CFM micrographs of silver nanoparticle impregnated microcrystalline cellulose. These micrographs show auto-fluorescence of the silver nanoparticles and FITC induced MCC fluorescence.

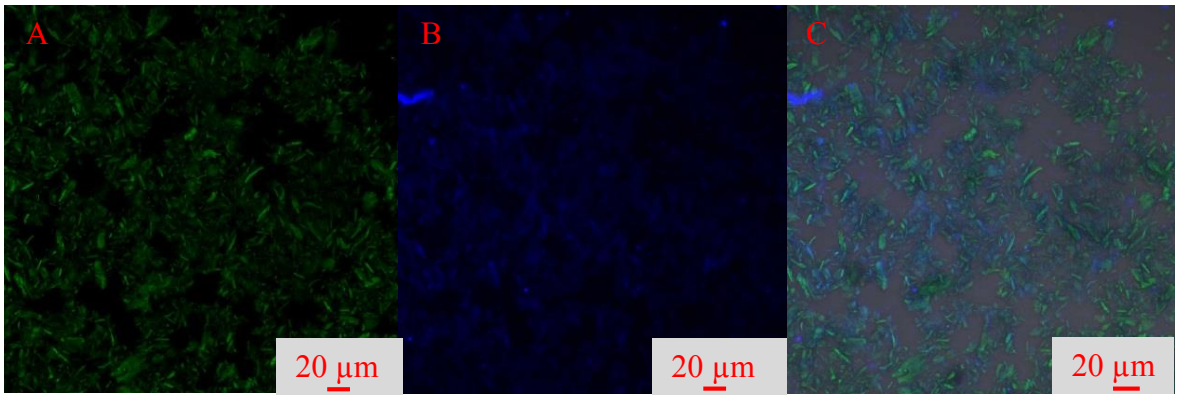

Figure 3.13 CFM micrographs of AgMCC. (A) 488 nm laser revealing fluorescence of FITC labelled MCC, (B) 405 nm laser showing auto fluorescence of silver nanoparticles and (C) an overlay of (A) and (B).

The CFM micrograph in Figure 3.13 (A) shows the homogeneous dispersion of the MCC while (B) shows some tendency of silver nanoparticle agglomeration, This is shown by the brighter blue spots of silver nanoparticle auto-fluorescence attached to the surface of the microcrystalline cellulose. These results agree with STEM results in Figure 3.12, which not only confirm the presence of the nanoparticles in the MCC matrix but also show the homogeneous dispersion of the silver nanoparticles within the MCC matrix.

3.5 Conclusions

The applications of the nanomaterials highly depend on the size and distribution of the produced materials. The surface area of the nanomaterials increases as the nanomaterials become smaller and this also makes them easy to disperse in different media. Three antimicrobial agents of organic and inorganic origin were successfully produced in this study. TEM and CFM were used to evaluate the shape and size of the antimicrobial agents as well as showing the arrangement and dispersion of the agents in an aqueous mixture. These two techniques revealed the tendency of the isolated ChNWs and produced CTSAgNPs to agglomerate in water but this could be overcome by proper sonication of the agents after dispersion in a matrix. In the case of silver nanoparticles, different concentrations of silver nitrate and chitosan were evaluated and the 22 mM silver nitrate concentration was found to be the optimum concentration for the production of nanoparticles with very small diameters. The sizes and shapes of the different produced antimicrobial agents are summarized in Table 3.2.

Table 3.2: Summary of antimicrobial agents.

Antimicrobial agent	Average size	Shape
Chitin nanowhiskers (ChNWs)	Length = 160 nm Diameter = 27 nm	Rod-like with sharp ends
Chitosan-reduced silver nanoparticles (CTSAgNPs)	Diameter = 4.0 nm	Mostly spherically shaped but other shapes were observed
Silver impregnated silver nanoparticles (AgMCC)	Diameter = 40 nm	Spherical

The FTIR spectra showed all the characteristic peaks of ChNWs and AgMCC indicating the successful isolation and impregnation of silver in microcrystalline cellulose. UV-Vis was used to confirm the successful reduction of the silver nanoparticles in both CTSAgNPs and AgMCC by revealing the silver characteristic SPR peak. The results of the formation of these antimicrobial agents agree with research published in literature. An enhanced technique to inpregnate silver nanoparticles on the surface of MCC using chitosan as a reducing agent was successfully done.

3.6 References

1. Abou El-Nour, K. M. M., Eftaiha, A., Al-Warthan, A. & Ammar, R. a a. Synthesis and applications of silver nanoparticles. *Arab. J. Chem.* **3,** 135–140 (2010).
2. Raheman, F., Deshmukh, S., Ingle, A., Gade, A. & Rai, M. Silver nanoparticles : Novel antimicrobial agent synthesized from an endophytic fungus Pestalotia sp . isolated from leaves of Syzygium cumini (L). *Nano. Biomed Eng.* **3,** 174–178 (2011).
3. Mincea, M., Negrulescu, A. & Ostafe, V. Preparation, modification, and applications of chitin nanowhiskers: A review. *Rev. Adv. Mater. Sci.* **30,** 225–242 (2012).
4. Kadokawa, J., Takegawa, A., Mine, S. & Prasad, K. Preparation of chitin nanowhiskers using an ionic liquid and their composite materials with poly(vinyl alcohol). *Carbohydr. Polym.* **84,** 1408–1412 (2011).
5. Villanueva, Emilia, M., Salinas, A., Díaz, L. E. & Copello, G. J. Chitin nanowhiskers as alternative antimicrobial controlled release carriers. *New J. Chem.* **39,** 614–620 (2015).
6. Agasti, N. & Kaushik, N. K. One Pot Synthesis of Crystalline Silver Nanoparticles. *Am. J. Nanomater.* **2,** 4–7 (2014).
7. Sharma, V. K., Yngard, R. a. & Lin, Y. Silver nanoparticles: Green synthesis and their antimicrobial activities. *Adv. Colloid Interface Sci.* **145,** 83–96 (2009).
8. Wei, D., Sun, W., Qian, W., Ye, Y. & Ma, X. The synthesis of chitosan-based silver nanoparticles and their antibacterial activity. *Carbohydr. Res.* **344,** 2375–2382 (2009).
9. Shameli, K., Ahmad, M.B., Jazayeri, S. D., Sedaghat, S., Shabanzadeh, P., Jahangirian, H., Mahdavi, M & Abdollahi, Y. Synthesis and characterization of polyethylene glycol mediated silver nanoparticles by the green method. *Int. J. Mol. Sci.* **13,** 6639–6650 (2012).
10. Wan, C., Jiao, Y., Sun, Q & Li, J. Properties of Silver Nanoparticles Embedded into Cellulose Aerogels. *Pol. Comp*. **37,** 1137–1142 (2016).
11. Vivekanandhan, S., Christensen, L., Misra, M., Mohanty, AK. Green Process for Impregnation of Silver Nanoparticles into Microcrystalline Cellulose and Their Antimicrobial Bionanocomposite Films. *J. Biomater. Nanobiotechnol.* **3,** 371–376 (2012).
12. Du Toit, M. L. *Incorporation of polysaccharide nanowhiskers into a poly (ethylene-co-vinyl alcohol) matrix.* MSc Thesis, Stellenbosch University, South Africa, (2013).
13. Vega-baudrit, J., Alvarado-meza, R. & Solera-jiménez, F. Synthesis of silver nanoparticles using chitosan as a coating agent by sonochemical method. *Avances en*

Química. **9,** 125–129 (2014).

14. Fan, Y., Fukuzumi, H., Saito, T. & Isogai, A. Comparative characterization of aqueous dispersions and cast films of different chitin nanowhiskers/nanofibers. *Int. J. Biol. Macromol.* **50,** 69–76 (2012).
15. Nel, A. *Investigation of the effect of chitin nanowhiskers distribution on structural and physical properties of high impact polypropylene / chitin nanocomposites.* MSc Thesis, Stellenbosch University, South Africa, (2014
16. Nielsen, L. J., Eyley, S., Thielemans, W. & Aylott, J. W. Dual fluorescent labelling of cellulose nanocrystals for pH sensing. *Chem. Commun. (Camb).* **46,** 8929–8931 (2010).
17 Liu, P., Zhao, L., Wu, X., Huang, F., Wang, M. and Liu, X. Fluorescence enhancement of quercetin complexes by silver nanoparticles and its analytical application. *Spectrochimica Acta Part A: Molecular and Biomolecular Spectroscopy*. ***122,*** 238-245 (2014).
18. Suslov, A., Lama, P.T. and Dorsinville, R. Fluorescence enhancement of Rhodamine B by monodispersed silver nanoparticles. *Optics Communications*. ***345,*** 116-119 (2015).
19. Mondal, I. H., Islam, A. B. M. N. & Alam, J. Preparation of Chitosan-Silver Nanoparticles in Nonaqueous Medium under Heating. *Nano. Nanotech.* **5,** 64–69 (2015).
20. Twu, Y.-K., Chen, Y.-W. & Shih, C.-M. Preparation of silver nanoparticles using chitosan suspensions. *Powder Technol.* **185,** 251–257 (2008).
21. De Mesquita, J. P., Donnici, C. L. & Pereira, F. V. Biobased nanocomposites from layer-by-layer assembly of cellulose nanowhiskers with chitosan. *Biomacromolecules* **11,** 473–480 (2010).

Chapter 4: Preparation and characterization of individually incorporated organic and inorganic antimicrobial agents into EVOH

4.1 Introduction

Incorporation of different antimicrobial agents into a poly (ethylene-co-vinyl alcohol) matrix has been shown to improve certain polymer properties[1,2]. Cabedo et al.[2] reported an increase in the thermal stability, glass transition and oxygen barrier properties of EVOH with the addition of kaolinite concentrations less than 5%. Recently, EVOH nanocomposite films containing 2% TiO_2 nanoparticles were synthesized via a melt process and these nanocomposites showed excellent antimicrobial activity against *E. faecalis* and *P. aeruginosa*[3]. In this chapter the antimicrobial agents which were prepared in Chapter 3 were incorporated into an EVOH matrix in order to produce nanocomposite fibre mats and films. The morphological, chemical and thermal changes in the EVOH polymer upon addition of these agents were investigated. The results for both the nanocomposite films as well as electrospun nanocomposite fibre mats will be discussed in each section throughout this chapter.

4.2 Experimental

4.2.1 Materials

The poly (ethylene-co-vinyl alcohol) copolymer (EVOH) pellets used in this research was purchased from Sigma Aldrich and contained 44 mol% ethylene. Deionized water was produced in-house by an Elga Purelab instrument and the isopropanol used to dissolve the EVOH was supplied by Merck. Other chemicals and solvents used in this chapter were already reported in Section 3.2.1.

4.2.2 Preparation of EVOH nanocomposites

4.2.2.1 Dissolution of EVOH

Poly (ethylene-co-vinyl alcohol) (EVOH) copolymer pellets were dissolved in a deionized water/isopropanol solvent combination (30:70 vol/vol ratio) in the ratio 6:92 (w/w) at 100 °C under reflux with gentle stirring. EVOH was then used as a matrix to individually incorporate chitosan-based silver nanoparticles (CTSAgNPs), chitin nanowhiskers (ChNWs) and silver impregnated microcrystalline cellulose (AgMCC).

4.2.2.2 Incorporation of antimicrobial agents into EVOH

The antimicrobial agents were dispersed in an EVOH solution (10 g of EVOH in a 30:70 ratio of isopropanol water solvent) as 1 wt%, 3 wt%, 5 wt%, 8 wt% and 10 wt% with respect to the weight of the EVOH copolymer. The chitosan-reduced silver nanoparticles were dispersed in their aqueous state while both chitin nanowhiskers and silver impregnated microcrystalline cellulose were dispersed in their powder form in the EVOH solution. The procedure for the nanocomposite preparation was optimised by varying the reflux and sonication times to ensure the proper visual distribution of the agents. Sonication was varied between 2 min -15 min and refluxing was done between 1-2 hours. Reflux for 2 hours and 10 min of sonication were found to be the optimum conditions. The nanocomposite mixtures were either solvent cast into a film or electrospun to form a nanofibre mat. TEM, FESEM and CFM were used to investigate the morphology and dispersion of the antimicrobial agents in the EVOH matrix. The results discussed in Section 4.4 also show the chemical nature and thermal behavior of the EVOH nanocomposite films using established techniques[5, 7].

4.2.2.3 Solvent casting

The EVOH nanocomposites prepared above, which contained different loadings of antimicrobial agents, were cast into plastic petri dishes, left in the oven for 3 hours at 60 °C and further dried overnight at room temperature until all the solvent was evaporated. The prepared composite films were then subjected to further morphological, chemical and thermal analysis.

4.2.2.4 Electrospinning

Electrospinning of the EVOH nanocomposite mixtures was carried out on a horizontal electrospinning setup as shown in Figure 4.1. This device has a voltage supply unit with a range of 0-50 kV. A syringe pump and a spinneret connected to the positive terminal as well as a grounded collector plate connected to the negative terminal of the power supply unit. The voltage was varied between 10 kV and 20 kV, depending on the composite viscosity and dispersion, but for most composite mixtures 15 kV was used. The flow rate during electrospinning was also varied between 0.008 mL/min and 0.030 mL/min. The distance between the tip of the needle and the collector was varied between 10-20 cm for all the nanocomposite fibres.

Figure 4.1 Electrospinning setup used to fabricate nanocomposite fibre mats.

4.3 Characterization techniques

4.3.1 Field emission scanning electron microscopy (FESEM)

A Carl Zeiss MERLIN FESEM with a GEMINI II column was used to image all the composite films and fibres which were gold coated before images were taken. The films and fibres were placed on a stub using a double-sided carbon tape and gold coated to make the samples conductive. An in-lens detector was used to obtain the FESEM micrographs with a working distance of 3.8 mm, probe = 250 pA and EHT = 5.00 kV.

4.3.2 Scanning transmission electron microscopy (STEM)

The EVOH solvent cast nanocomposite samples as well as the EVOH nanocomposites fibres were embedded in AGAR 100 resin and the prepared capsule was ultra microtomed to study the nanoparticle and nanowhisker dispersion within the EVOH matrix by way of STEM analysis. A Carl Zeiss MERLIN FE SEM in STEM seg mode was used with images taken at dark fields. The solvent cast films and electrospun fibres were then embedded in the resin and left to harden overnight in the oven at 60 $^{\circ}$C. A Leica UC7 ultra microtome instrument was used to section sample slices which were between 70 nm and 100 nm in thickness. The microtomed samples were then placed in carbon coated grids and stained with 2% uranyl acetate twice and allowed to dry. The stained grids were then subjected to STEM analysis at a working distance of 9.5 mm and EHT target 20.0 kV.

4.3.3 Confocal fluorescence microscopy (CFM)

Confocal fluorescent microscopy was done on the nanocomposite films using a Carl Zeiss Laser Scanning Microscope (LSM) 780. The nanocomposite films and fibre mats were paper-punched into small pieces, mounted on a glass slide and covered with a cover slip. The instrument specifications are described in Section 3.6.5.

4.3.4 Attenuated total reflectance -Fourier transform infrared spectroscopy (ATR-FTIR)

FTIR data were recorded using a Thermo Fisher Nicolet iS10 instrument. The spectra were recorded at a minimum number of scans set at 32 taking background information before every sample scan and the resolution was 4 cm^{-1}. The synthesized nanocomposite films and fibres were analyzed as thin films or as fibre mats.

4.3.5 Thermal analysis

Differential scanning calorimetry (DSC) was used to investigate the crystallization and melting behaviours of the EVOH with response to the addition of different antimicrobial agents. The nanocomposite films and fibres were analyzed using a Q100 (TA Instrument) which was calibrated using Indium metal according to a standard procedure. Standard DSC pans were used to weigh about 4 mg of each sample and the pans were sealed was weighed off before analysis. The procedure consisted of three cycles and a heating/cooling ramp of 10 °C/min was used in a nitrogen atmosphere. Three repeats were done for analysis of each sample.

The thermal behaviour of all the nanocomposite films and fibres was investigated by measuring the weight loss of the nanocomposites as a function of temperature using a thermo gravimetric analyser (TGA), Q500, TA equipment. Approximately 10 mg of sample was heated at the rate of 20 °C per min from room temperature to 600 °C in a nitrogen atmosphere.

4.4 Results and Discussion

The EVOH nanocomposite films and fibre mats containing different antimicrobial agents (ChNWs, AgNPs and AgMCC) were subjected to field emission electron scanning microscopy (FESEM), scanning transmission electron microscopy (STEM) and confocal fluorescence microscopy (CFM) to investigate the arrangement and distribution of these agents in an EVOH matrix. Fourier transform infrared spectroscopy (FTIR) was used to evaluate the chemical changes that occur in the EVOH matrix with response to the addition of increasing

concentrations of the various antimicrobial agents. Possible changes in the thermal behaviour of the EVOH that might occur due to the incorporation of the antimicrobial agents were evaluated using differential scanning calorimetry (DSC) and thermogravimetric analysis (TGA).

4.4.1 Morphological analysis

Chitin nanowhiskers, silver nanoparticles and silver impregnated silver nanoparticles have shown a tendency to agglomerate in aqueous matrices as shown in Section 3.4. Not only is it important to investigate if this agglomeration also exists within an EVOH matrix, but it is also important to investigate the distribution of the antimicrobial agents in within the EVOH matrix. Proper distribution of the antimicrobial agents within the EVOH matrix is of great importance in order to ensure distribution of the envisioned antimicrobial properties within the matrix. Three different characterization techniques were utilized to investigate this distribution, namely, FESEM, STEM and CFM.

4.4.1.1 FESEM

Figure 4.2 below shows FESEM micrographs of neat 6 wt% EVOH solvent cast films. The films show two distinct areas. The surface is shown to be smooth and flat while the cross section of the film showed spherical structures with diameters of about 1 µm.

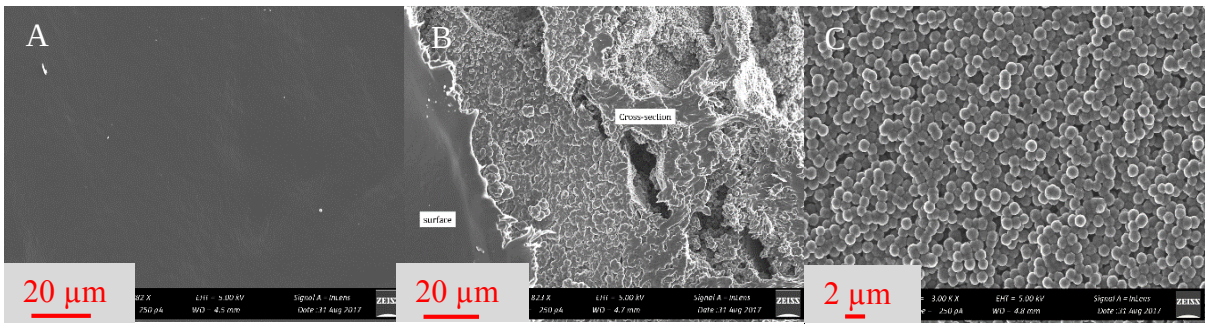

Figure 4.2 FESEM micrographs of neat 6 wt% EVOH films. (A) film surface, (B) film surfaces and cross sectional of the film and (C) zoomed-in image of the cross sectional area of the film.

Figure 4.3 shows FESEM micrographs of EVOH nanocomposite films (A and B) and fibres (C-F). The micrographs show the formation of spherical structures on the surface of the solvent cast EVOH films with the addition of ChNWs. The size of these spherical structures is shown to increase with an increase in the amount of nanowhiskers as shown Figure 4.3 (A) and (B). The cause for the formation of the spherical structures in both the neat and chitin nanowhisker

loaded films is not clear. The EVOH nanocomposite films prepared in this study had undergone some thermal treatment after solvent casting and this could maybe have an effect on the formation of these spherical structures. Unfortunately there is not clear evidence in literature available to explain the formation of these spherical structures.

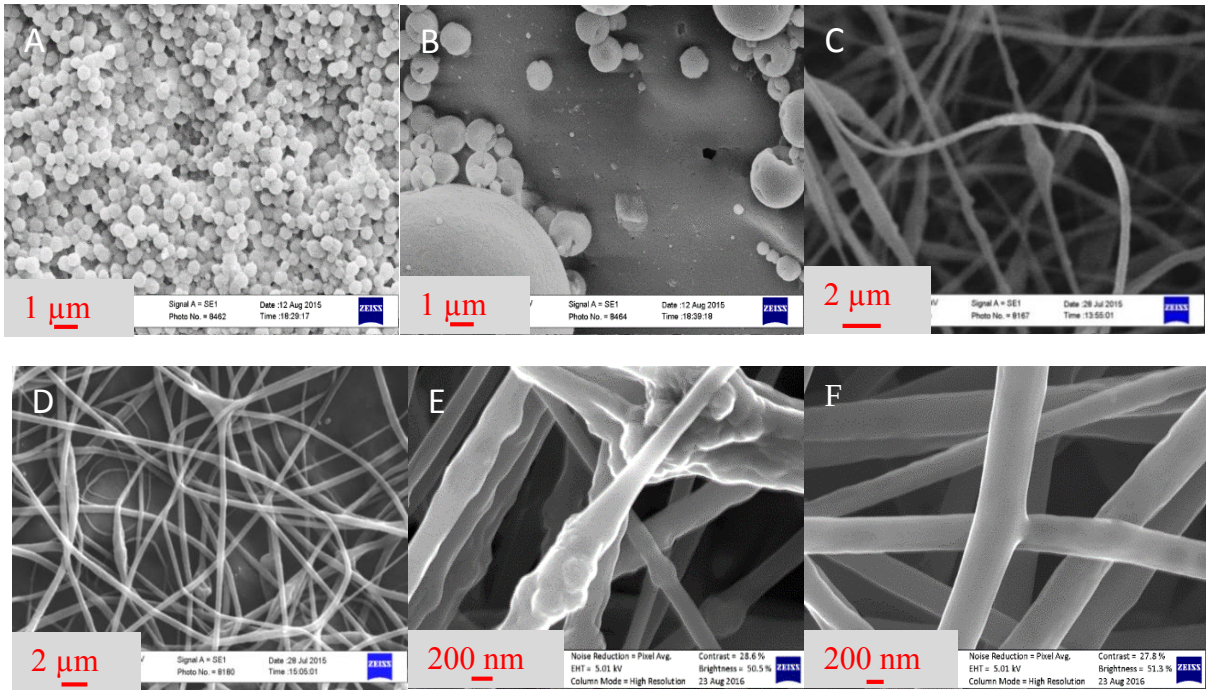

Figure 4.3 FESEM micrographs of chitin nanowhisker loaded EVOH films and nanofibre mats. (A) 1 wt% and (B) 3 wt% ChNW loadings in EVOH nanocomposite films. (C) 1 wt %, D) 3 wt%, (E) 5 wt% and (F) 10 wt% ChNW loadings in EVOH nanocomposite fibre mats.

According to the FESEM results, the ChNW loaded fibres appear to increase in diameter with the increase in chitin content. It was difficult to observe the dispersion of the whiskers within EVOH matrix with FESEM. The 1 wt%, and 5 wt% (Figure 4.3 C and E) loadings of ChNWs suggest that lower loadings of chitin nanowhiskers form fibres with slightly different diameters compared to one another and fibre beading is sometimes observed with the 5 wt% loading of chitin nanowhiskers. Higher chitin nanowhiskers loadings, such as in the case of 10 wt% (F) ChNWs show a formation of homogeneous nanofiber with no beading. Because of the insufficient evidence of the dispersion of ChNWs using FESEM, it was necessary to investigate other techniques to further explore the dispersion of the ChNWs within the EVOH matrix.

Figure 4.4 shows the FESEM micrographs of CTSAgNPs loaded EVOH nanocomposite films and fibre mats with increasing amounts of CTSAgNPs.

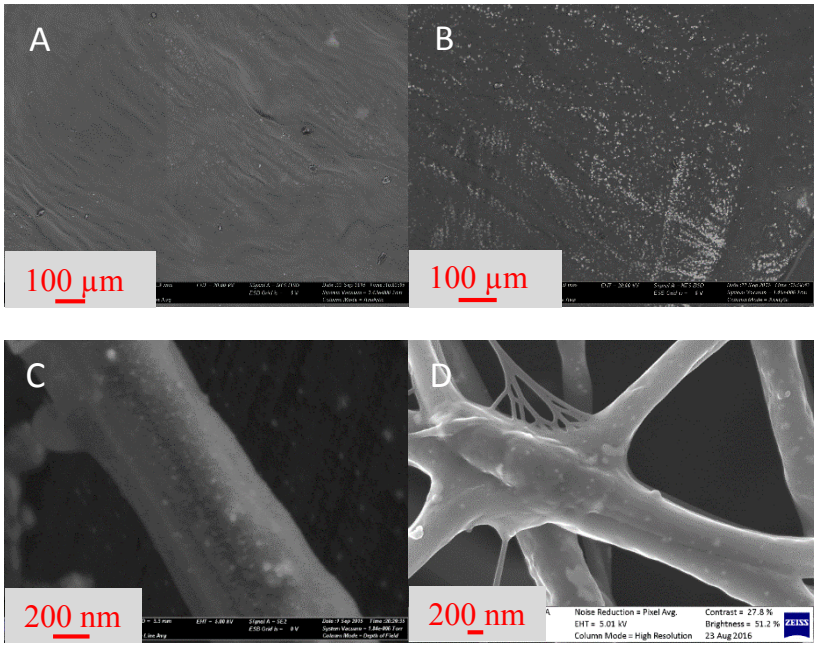

Figure 4.4 FESEM micrographs showing the distribution of silver nanoparticles in EVOH nanocomposites. (A) 3 wt% and (B) 10 wt% CTSAgNPs films. (C) 1 wt% and (D) 10 wt% CTSAgNPs nanofibres.

Figures 4.4 (A) and (B) show the homogeneous dispersion of the chitosan-reduced silver nanoparticles in EVOH nanocomposite films. The progressive increase in the amount of silver nanoparticles on the surface of the films is indicated by the increase in the bright fluorescing spots. This shows the increase in the amount of back scattered light as a backscattered detector was used for this analysis. Agglomeration is observed for the 10 wt % CTSAgNPs loaded sample in Figure 4.4 (B), which indicate the tendency of these silver nanoparticles to agglomerate and form clusters at higher concentrations. The silver nanoparticles are shown to have almost the same distribution throughout the nanocomposites in the cases of the films as seen in Figures 4.4 (A) and (B). Similar to the nanocomposite films, the fibres in Figures 4.4 (C) and (D) also show homogeneous dispersion of silver nanoparticles.

The electrospinning process appears not to have affected the size of the nanoparticles considering that the nanoparticles were loaded into the EVOH matrix before electrospinning which indicates some degree of stability of the silver nanoparticles. The slight agglomeration of silver nanoparticles within the EVOH nanocomposite fibres could be attributed to the viscous nature of the composite mixtures at higher concentrations, which therefore makes it difficult for the silver nanoparticles to homogeneously disperse in the EVOH. The composite mixtures with CTSAgNPs concentrations above 5 wt.% blocked the tip of the needle during the electrospinning process, which could be due to agglomeration of the silver nanoparticles.

The diameter of the electrospun nanofibres was observed to slightly decrease with an increase in the concentration of the CTSAgNPs in the EVOH matrix. This can be seen in Figure 4.4 (D) where 10 wt% loaded CTSAgNP fibres with an average diameter of 65 nm were observed compared to the fibres shown in Figure 4.4 (C) which had an average diameter of 390 nm. This effect is attributed to the increase in charge density and conductivity, which produces an increase in the stretching forces in the jet, consequently decreasing the fibre diameter.

Figure 4.5 shows FESEM micrographs of silver impregnated microcrystalline cellulose (AgMCC) dispersed in EVOH with (A) showing a nanocomposite film and (B) showing a nanocomposite fibre mat. The micrographs show homogeneous dispersion of the AgMCC in the EVOH nanocomposites. The fibres in Figure 4.5 (B) have an average diameter of about 250 nm and have dark bands on the inside of the individual fibres, indicating the presence of an element with a higher molecular weight or heavier metallic compounds, which is silver in this case. The increase in the AgMCC content in the fibres does not have a significant effect o nthe fibre diameter when compared to the neat EVOH fibres.

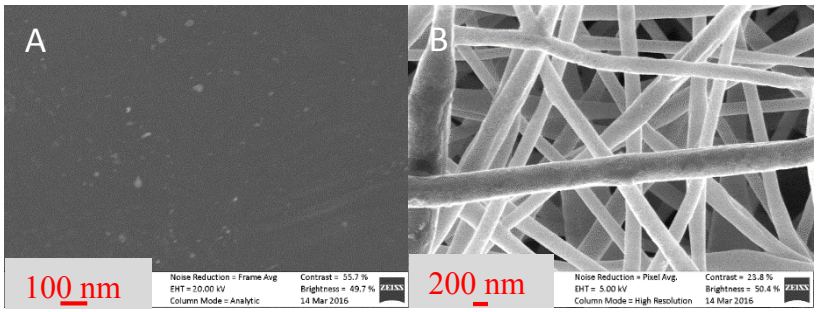

Figure 4.5 FESEM micrographs of AgMCC-EVOH nanocomposite films (A) and fibre (B) with 5 wt% loadings of AgMCC.

The nanoparticles were reduced in-situ in the microcrystalline cellulose matrix, which makes it difficult to visualize the sizes and shapes of the nanoparticles on the surface of the EVOH matrix, even with the use of a backscattered detector. This is due to the small amount of silver being successfully reduced to nanoparticles in the MCC matrix before addition of this AgMCC mixture to the EVOH polymer.

4.4.1.2 STEM

It was impossible to visualize the ChNWs within the EVOH matrix by using FESEM, even with a back scattered detector. This was the case for both films and fibre mats. The reason for this is the similar phases and chemical composition of the EVOH and the ChNWs. STEM was

therefore used to address this shortcoming. Figure 4.6 shows STEM micrographs of ChNW (A and B) and silver nanoparticle (C and D) loaded EVOH nanocomposites. The samples were microtomed to show the cross sectional area of the nanocomposite films (A, B and C) and nanocomposite fibre mat (D).

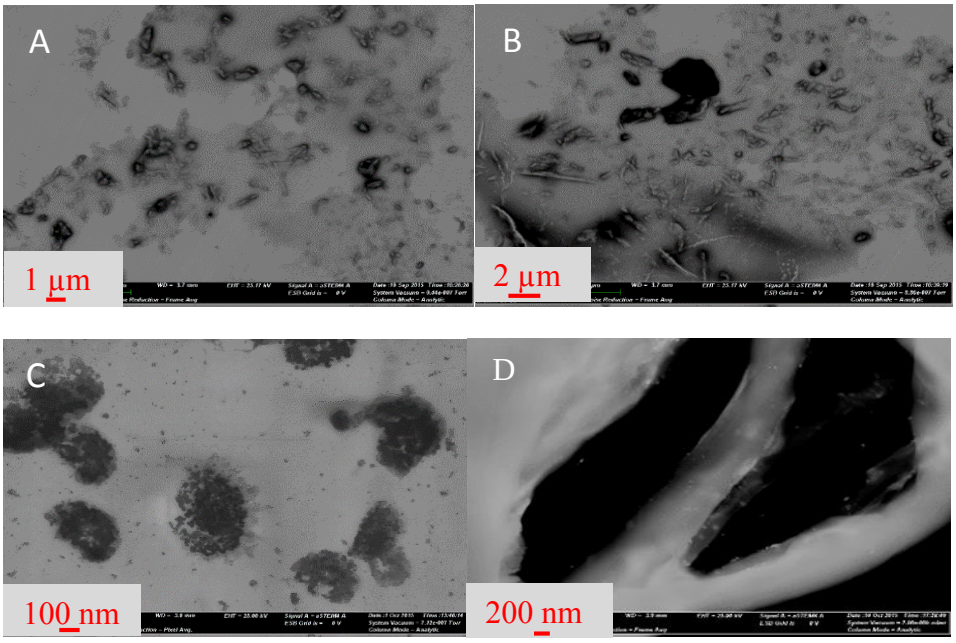

Figure 4.6 STEM micrographs of ChNW-EVOH and CTSAgNP-EVOH microtomed nanocomposites. (A) 3 wt% ChNW film and (B) 5 wt% ChNW film. (C) 10 wt% CTSAgNPs film and (D) 1 wt% CTSAgNPs fibres.

STEM micrographs of ChNW containing nanocomposite films were microtomed at 70 nm per slice. The slices were negatively stained with uranyl acetate to increase the contrast between chitin nanowhiskers and EVOH. This made it possible for the ChNWs to be easily observed within the EVOH matrix. The nanocomposite fibres containing 5 wt% ChNWs (B), appear to have uniformly distributed whiskers in some parts of the sample.

Though the micrographs show a uniform and homogenous dispersion of the nanoparticles, there are clusters or agglomerates that form within the EVOH matrix as shown in Figure 4.6 (C). It is very difficult to see the exact shape of the nanoparticles in the nanofibre mat shown in Figure 4.6 (D), because the microtomed fibre mat was too thick for the detector to penetrate through the sample.

4.4.1.3 CFM

Figure 4.7 shows CFM of Rhodamine B tagged ChNWs loaded nanocomposites.

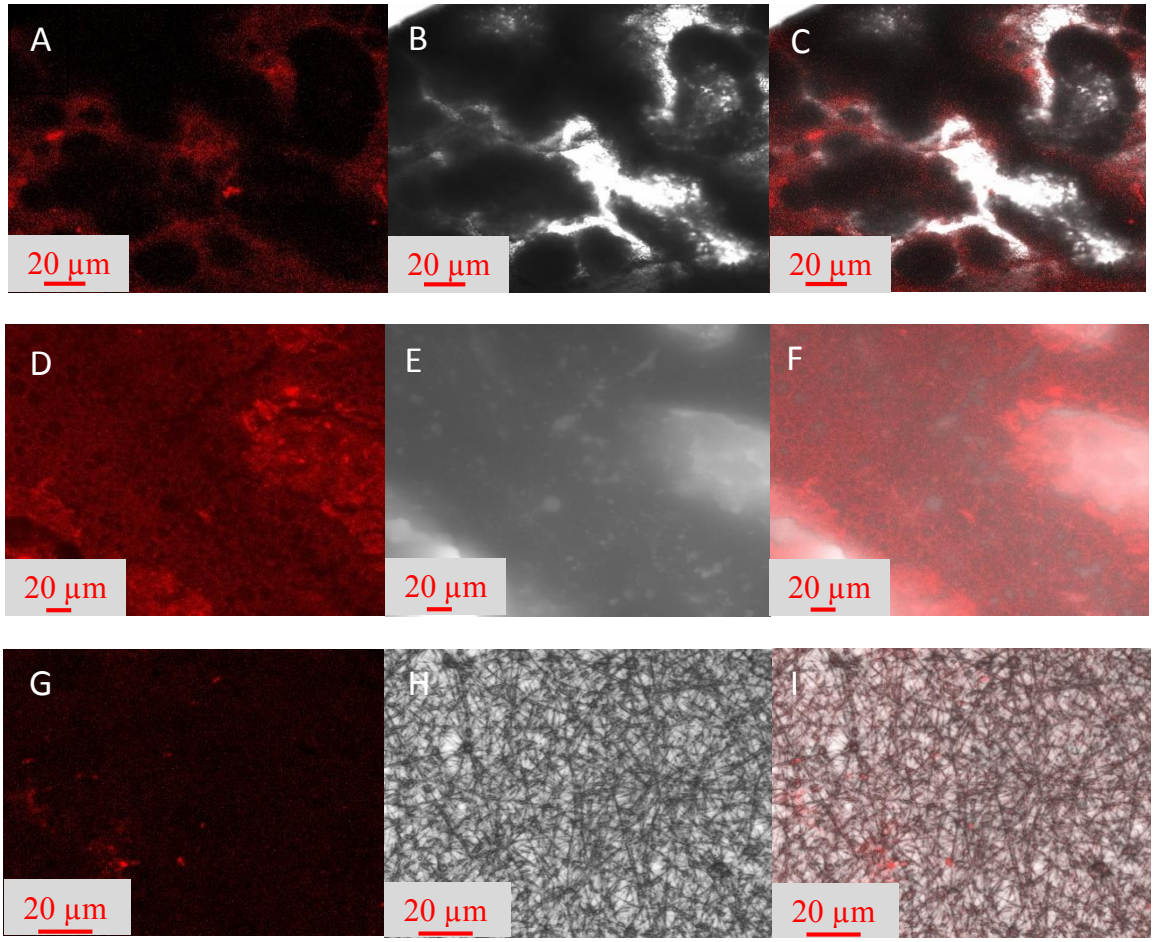

Figure 4.7 CFM micrographs of RhB-labelled ChNWs loaded in EVOH. (A) 3 wt% film, 561 nm laser, (B) 3 wt% film, TPMT filter, (C) 3 wt% film, overlay, (D) 10 wt% film, 561 nm laser, (E) 10 wt% film , TPMT filter, (F) 10 wt% film, overlay, (G) 10 wt% fibres, 561 nm laser, (H) 10 wt% fibers, TPMT filter and (I) 10 wt% fibres, overlay.

Fluorescent chitin nanowhiskers were prepared by tagging the ChNWs with Rhodamine B as explained in Section 3.2.3.5. These chitin whiskers were then dispersed in EVOH in concentrations varying from 1 wt% - 10 wt%, making use of proper sonication. This was done to investigate the dispersion and distribution of chitin whiskers within an EVOH matrix. The micrographs indicate heterogeneous dispersion of ChNWs at 3 wt% dispersion in films and the 10 wt% ChNWs is homogeneously dispersed within the EVOH fibres and films.

4.4.2 ATR-FTIR

Figure 4.8 shows the FTIR spectra of chitin nanowhiskers containing nanocomposite films (I) and fibre mats (II).

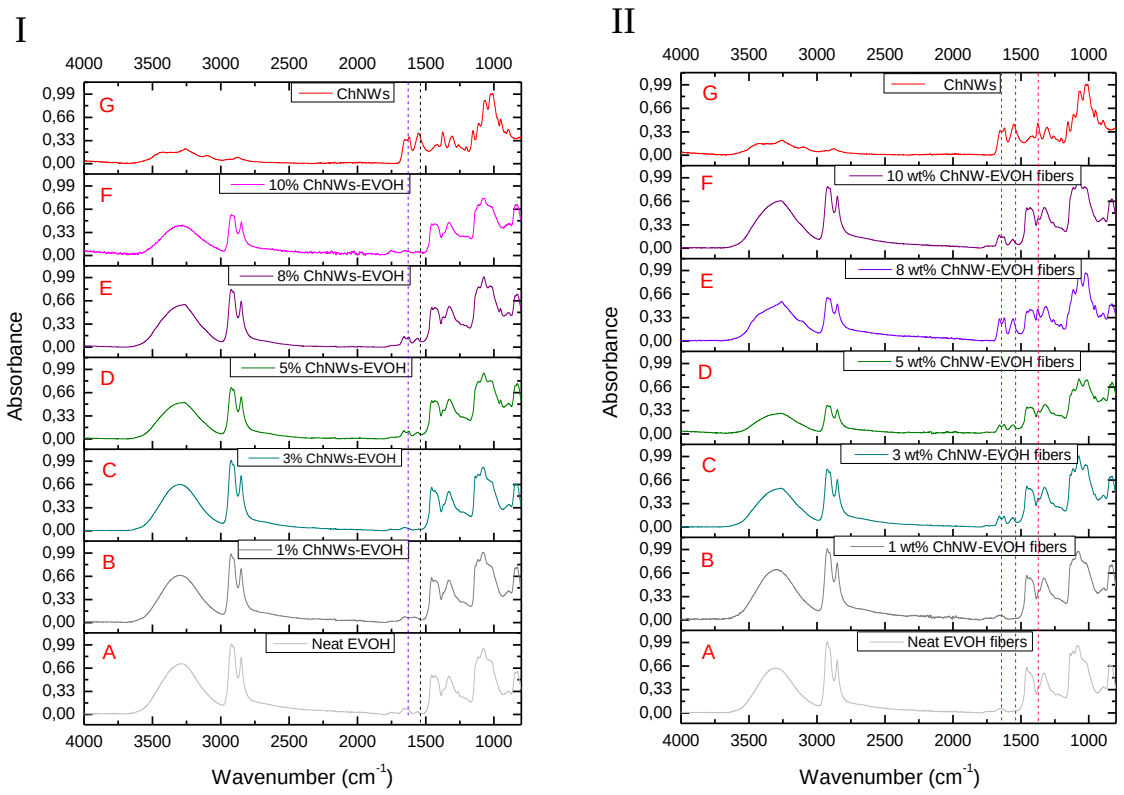

Figure 4.8 ATR-FTIR spectra of ChNWs-EVOH nanocomposites with increasing chitin nanowhisker loadings for EVOH nanocomposite (I) films and (II) fibres.

The FTIR analysis was carried out with the expectation of a gradual increase in the amide I, II and III peaks with the addition of increasing chitin nanowhiskers loadings into the EVOH matrix, seeing that this would indicate the successful incorporation and dispersion of an increasing amount of chitin nanowhiskers within the EVOH polymer matrix. The 5 wt% and the 8 wt% loadings of chitin nanowhiskers in the nanocomposite films illustrated in Figure 4.8 (I) showed a slight increase in the amide I, II and III peaks at 1559 cm^{-1}, 1629 cm^{-1} and 1657 cm^{-1}, respectively. These peaks present the characteristic absorption bands of α-chitin and corresponds to that reported for pure chitin[9]. The nanocomposite fibres showed a similar result in Figure 4.8 (II), with the 10 wt% loading showing the highest intensity of these peaks. This increase in the incorporation of ChNW with an increase in the nanowhisker loading during electrospinning is supported by an increase in the amount of hydrogen bonding between EVOH and the ChNW that forms in the interfacial area between the two polymers.

Figure 4.9 below shows the ATR-FTIR spectra of silver nanoparticle containing nanocomposites. Both CTSAgNPs and AgMCC spectra show no significant difference in absorbance peaks of the EVOH functional groups with the addition of increasing loadings of

silver nanoparticles in the EVOH matrix. This could be due to the similarities in the functional groups present in the EVOH, chitosan and cellulose matrices. The low concentrations of these antimicrobial agents in the nanocomposites make it difficult for the small changes that might occur to be clearly visible.

I

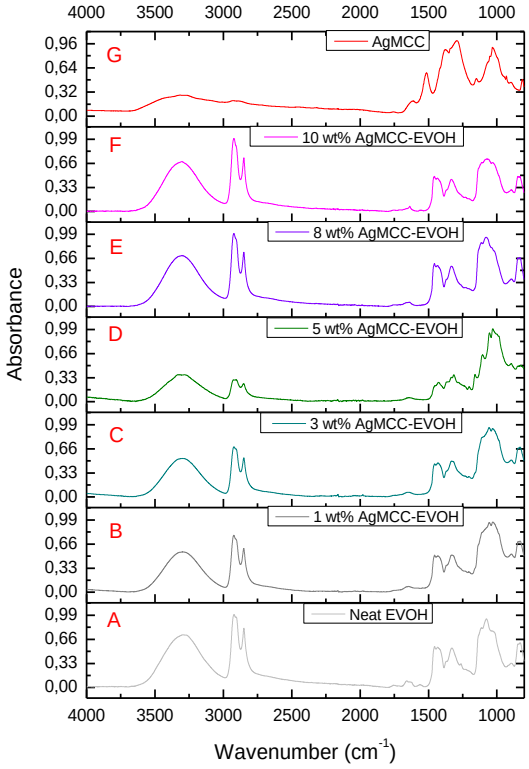

II

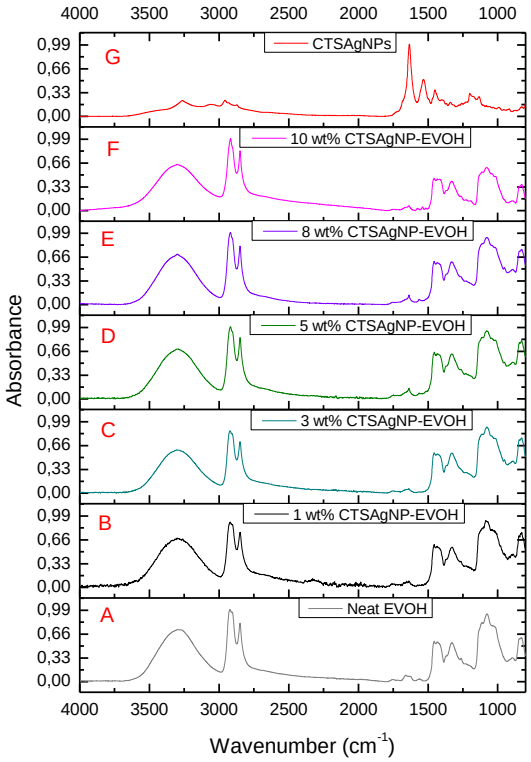

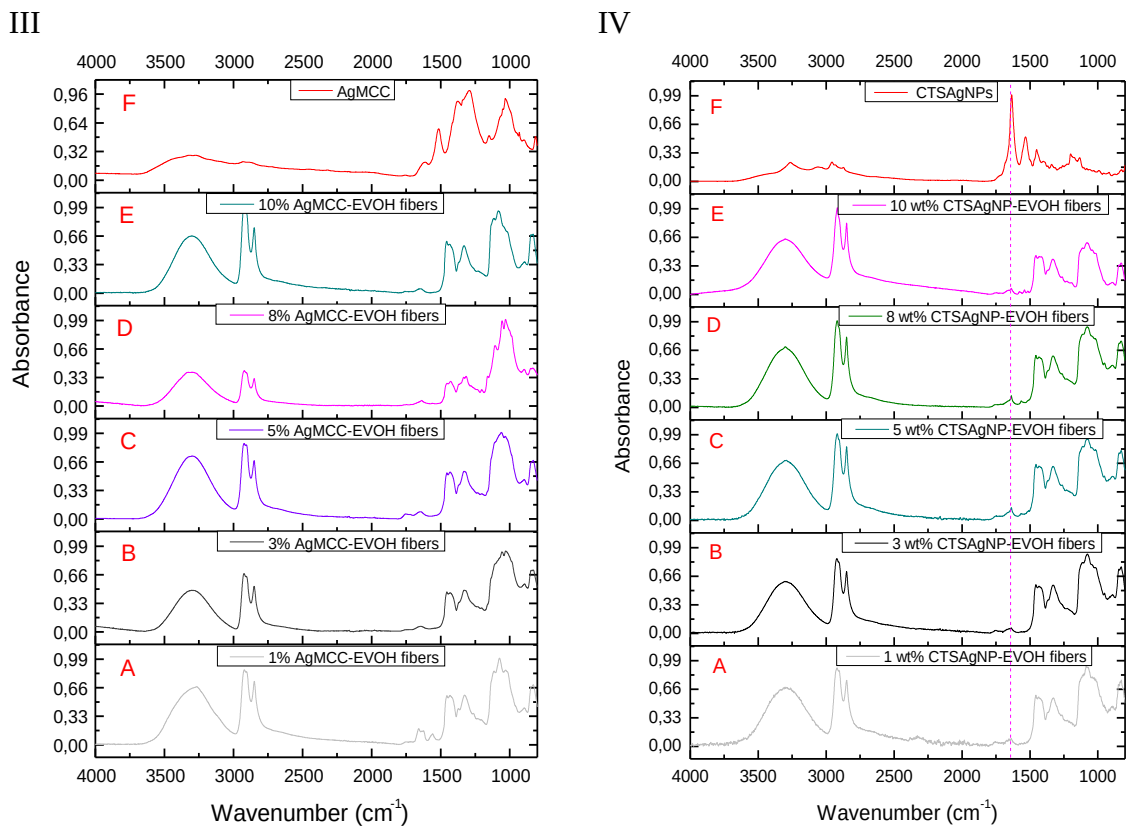

Figure 4.9 ATR-FTIR spectra of CTSAgNPs (I and II) and AgMCC (III and IV) in an EVOH matrix. (I) and (III) show nanocomposite films and (II) and (IV) show nanocomposite fibres.

In Figure 4.9 (IV), the intensity of the C-H peaks at around 2900 cm^{-1} differs only slightly for the 1 wt% and the 3 wt% loadings but this intensity increases for the 8 wt% and the 10 wt% loadings of AgMCC indicating an increase in the C-H bonds of the composites.

4.4.3 Thermal analysis

The DSC results shown in Figure 4.10 below revealed a slight increase (from 141°C to 144°C) in the crystallization temperature (T_c) of the EVOH nanocomposites films with the addition of 1 wt% chitin nanowhiskers. This increase is followed by a slight decrease in the crystallization temperature from 160 °C to 159 °C with the incorporation of higher loadings of chitin nanowhiskers. These changes are however very small when compared to the T_c of neat EVOH (141 °C). The changes in the melting temperature (T_m) with response to the addition of ChNWs in EVOH are, as in the case of the T_c, insignificant. This indicates that the presence of ChNWs within the EVOH matrix does not change these thermal properties of EVOH significantly.

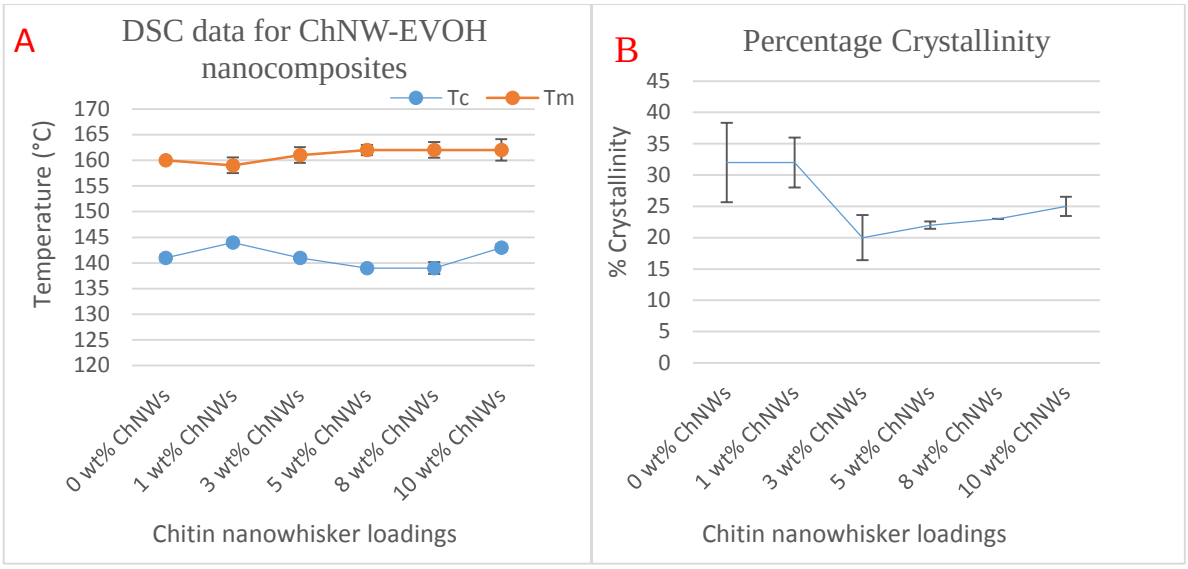

Figure 4.10 Thermal analysis (DSC) data of ChNW-EVOH nanocomposite films showing the melting and crystallization temperature (A) and percentage crystallization (B) of the nanocomposites with increasing loadings of ChNWs.

There is however a small decrease (from 30% for the neat EVOH sample to 20 % for the 3wt% loading) in the percentage crystallization of the nanocomposites with the increase in chitin nanowhiskers content, with the 3 wt% loaded nanocomposite showing the lowest crystallinity. This decrease in percentage crystallization of EVOH upon incorporation of ChNWs corresponds to the results found by Du Toit[7]. The nanocomposite fibres also showed no significant difference in T_c and T_m with an increase in the chitin nanowhisker content in the polymer matrix. The nanofibre results are presented in Addendum B, Figure B.1. The crystallinity of the nanocomposite fibre mats decreased a bit more than in the case of the films with an increase in the chitin nanowhisker content. Overall, it can however by concluded from the DSC results that the incorporation of up to 10 wt% nanowhiskers into an EVOH film or nanofibre matrix does not significantly influence the thermal properties of the EVOH matrix.

Figure 4.11 shows DSC results for the nanocomposite fibres loaded with increasing amounts of CTSAgNPs and AgMCC, respectively. According to Figure 4.11, the nanocomposite fibres show no significant difference in T_m and T_c upon loading of the EVOH matrix with 1 wt% to 10 wt% of CTSAgNPs, indicating that the silver nanoparticles do not change the thermal properties of the EVOH polymer. Only a slight increase in both T_m and T_c is visible for the nanocomposite fibres containing 10 wt% chitosan-reduced silver nanoparticles. In contrast with the ChNW containing EVOH nanocomposites a small increase in the percentage crystallinity was observed as the silver nanoparticle loadings increased from 1 wt% to 5 wt%

in the nanofibre mats when compared to neat EVOH. Thereafter the percentage of crystallinity showed to start decrease slightly for the 8 wt% and 10 wt% loaded samples but was still higher than that of the neat EVOH.

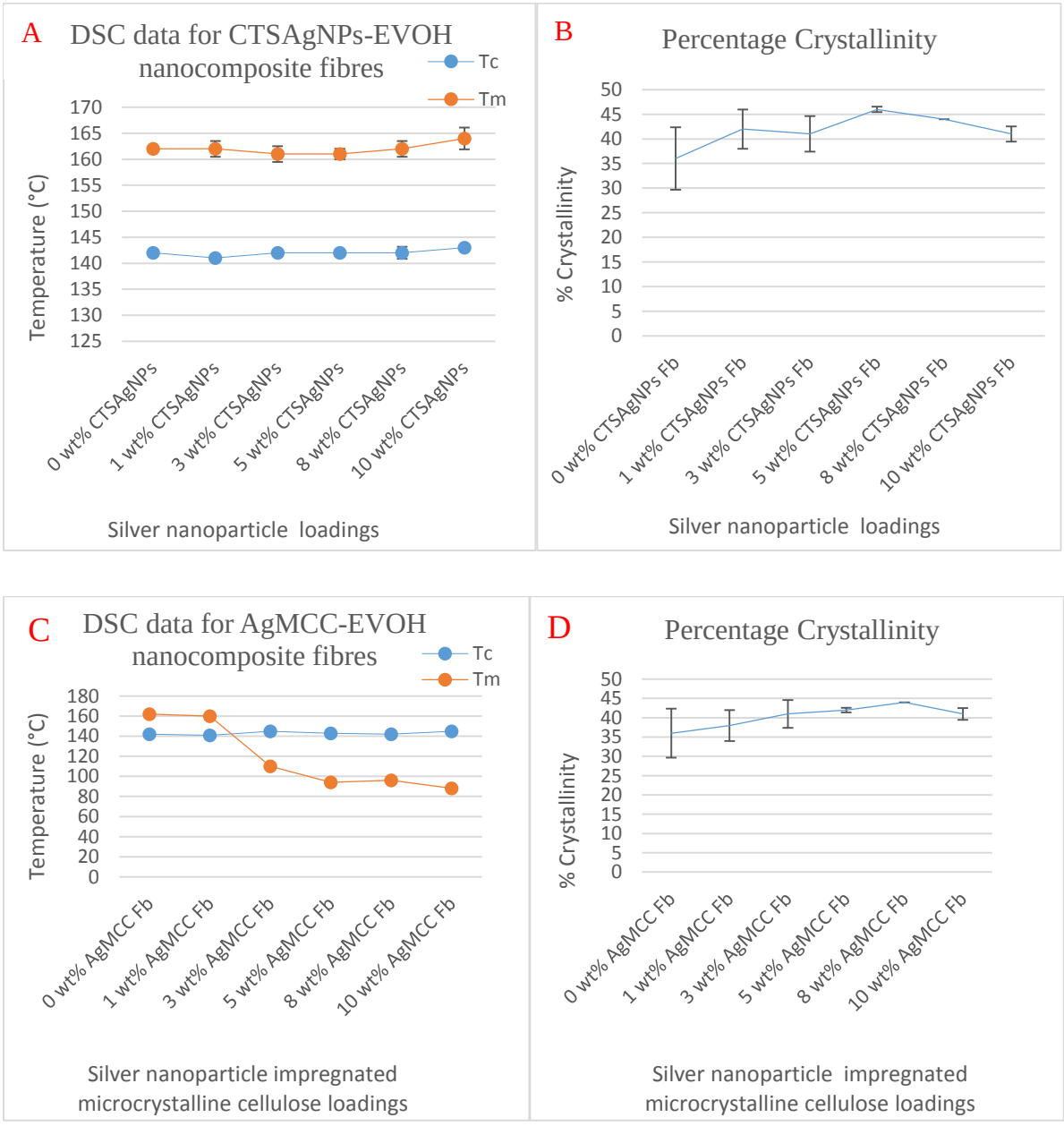

Figure 4.11 Thermal analysis (DSC) data of silver nanoparticle-EVOH nanocomposite films showing the melting and crystallization temperature (A and B) and percentage crystallization (C and D) of the nanocomposites with increasing loadings of CTSAgNPs and AgMCC in films and fibres, respectively.

The DSC results of the AgMCC-EVOH composites shown in Figure 4.11 are compared to that for neat EVOH samples in order to investigate the change in thermal properties of the

nanocomposites upon addition of different loadings of AgMCC. The DSC results of the AgMCC-EVOH composites show a significant change when compared to the neat EVOH results with regard to the melting temperature of the nanocomposites. There is a significant decrease in the melting temperature with an increase in the amount of AgMCC present in the composite films, from 161.9 ºC for the neat EVOH films to 88.2 ºC for the 10 wt% AgMCC loaded films. This decrease in melting temperature may possibly be due to a strong interaction between the MCC and the EVOH matrix, which can then destroy regular arrangement of molecular chains of the EVOH matrix. There is however no significant change in the crystallization temperature when EVOH films are loaded with AgMCC. A slight increase in the percentage crystallinity is observed upon addition of increasing amounts of AgMCC, but the 10 wt% loading shows a slight decrease again in percentage crystallinity. Similar results were observed in the case of the AgMCC loaded nanocomposite fibres.

The TGA results for the ChNW-EVOH films are presented in Table 4.1. According to these results there is a small decrease (from 367.2 ºC to 339.3 ºC) in the onset degradation temperature upon addition of 1 wt% of chitin nanowhiskers where after the onset degradation temperature increases (from 339.3 ℃ to 341.4℃) with the increasing amount of ChNWs. In the case of the 10 wt% loading, the sample onset degradation temperature is slightly lower again (365.1 ℃).

Table 4.1 Thermal behaviour of ChNW-EVOH films as analysed by TGA

ChNW-EVOH	Peak degradation (°C)	
	T Onset	T Max
0 wt%	367.2	429.3
1 wt%	339.3	392.4
3 wt%	341.4	402.6
5 wt%	365.8	424.4
8 wt%	369.3	427.9
10 wt%	365.1	425.8

The peak maximum degradation temperatures are however all slightly lower than that for neat EVOH. The incorporation of chitin nanowhiskers into the EVOH matrix as electrospun nanofibres gave similar TGA results than in the case of the EVOH films and can be seen in Table B.1 in Addendum B. The only difference that is notable is the fact that the onset of degradation temperatures are slightly higher for all the nanowhisker loaded nanofibre samples (except for the 1 wt% loaded nanocomposite) with the 8 wt% nanowhisker loaded nanocomposite having the highest onset of degradation temperature (386.9 ^{o}C). The incorporation of nanowhiskers into an EVOH matrix therefore does not affect the thermal stability of the matrix negatively, but can even improve the onset of degradation as seen in the case of the nanofibers. For all nanowhisker containing nanocomposite samples, an 8 wt% loading of chitin nanowhiskers gave the optimum thermal stability.

The TGA results of the EVOH nanocomposite fibres loaded with CTSAgNPs are presented in Table 4.2. These results indicate that addition of even as little as 1 wt% of the chitosan-reduced silver nanoparticles improves the thermal stability of the EVOH matrix.

Table 4.2 TGA data of chitosan-reduced silver nanoparticles loaded EVOH nanocomposite fibres.

CTSAgNPs-EVOH	Max Peak degradation (°C)	
	T Onset	T Max
0 wt%	367.2	429.3
1 wt%	376.2	457.9
3 wt%	385.4	456.9
5 wt%	403.5	452.6
8 wt%	411.4	477.9
10 wt%	393.5	451.7

Upon addition of 1 wt% of silver nanoparticles into the EVOH matrix via electrospinning the onset degradation temperature increases from 367.2 ^{o}C to 376.2 ^{o}C and reaches a maximum of 411.4 ^{o}C in the case of the 8 wt% loaded EVOH. In the case of the 10 wt% loaded EVOH nanofibre composite the onset of degradation seems to decrease again (393.5 ^{o}C). The peak maximum degradation temperatures presented a similar trend of increasing the thermal stability with an increase in the silver nanoparticle content. The 8 wt% loaded sample showed the best increase in the peak maximum degradation temperature 477.9 ^{o}C compared to 429.3 °C for neat EVOH where after the thermal stability seems to decrease. The 10 wt% silver nanoparticle loaded composite presented a peak maximum degradation temperature of 451.7 ^{o}C and even though this is lower than in the case of the 8 wt% loaded sample this is still about 20 °C higher than in the case of the neat EVOH (429.3 ^{o}C). The TGA results of the EVOH films of chitosan-reduced silver nanoparticles revealed similar results as in the case of the EVOH electrospun

nanocomposites.The AgMCC loaded EVOH nanocomposites showed similar TGA results as the CTSAgNPs containing nanocomposites.

4.5 Conclusions

FESEM, TEM and confocal fluorescence microscopy analysis of the nanocomposites showed the dispersion, arrangement and sizes of the antimicrobial agents within the EVOH nanocomposite films and fibres. All the antimicrobial agents appeared homogeneously dispersed throughout the EVOH matrix at concentrations lower than 5 wt%. The morphology of the antimicrobial agents within the nanocomposite matrices seems not to have been disturbed, which indicates the stability of the agents, even after chemical treatment. This agglomeration was also seen in the samples containing 10 wt% chitin nanaowhiskers using CFM. The nanocomposite fibres containing chitin nanowhiskers increased in diameter when the content of the whiskers increased in the composite. In the case of silver nanoparticle containing nanocomposites, a slight decrease in the fibre diameters was observed with the increase in the silver nanoparticle content. Agglomeration was more pronounced in the 10 wt% loadings of the all the silver nanoparticle containing nanocomposites (CTSAgNP and AgMCC). FESEM results illustrated that some of the silver nanoparticles were visible on the surface of the films, but it was difficult to see the dispersion of these nanoparticles within the EVOH matrix. This could be due to the agglomeration of the silver nanoparticles on the MCC as reported by Vivekanandhan et al[8]. This may be caused by neutralization of the surface charges present on the MCC by the silver, which can cause the aggregation. The silver nanoparticle containing nanofibres had uniform diameters and the inlens images of the 3 wt% and the 5 wt% loaded samples revealed dark bands on the inside of the fibres, indicating the presence of a heavy metal, which was silver in this case. The thermal stability of the chitin nanowhisker containing nanocomposites was shown to only slightly change with the addition of small concentrations of chitin nanowhiskers but these changes were not significant. These results correlate with the research done by Du Toit, during which different EVOH polymers (containing different percentage compositions of ethylene) were also loaded with chitin nanowhiskers, and no significant increase in thermal properties of the composites was observed with the addition of chitin nanowhiskers[7].

ATR-FTIR results showed no significant difference in the peaks with an increase in the content of each antimicrobial agent in the nanocomposites. This could be due to the small loadings of antimicrobial agents in the EVOH nanocomposite films and fibre mats. The thermal behaviour of the nanocomposite fibre mats was similar to that of the nanocomposite films. There were only slight differences in the T_m and T_c values when the EVOH matrix was loaded with CTSAgNPs and AgMCC. For certain nanocomposite samples, an increase in the crystallization

temperature was observed when the content of the silver nanoparticles was increased. TGA results for the nanocomposite fibres and the films showed a general increase in the thermal stability with an increase in the.

These results suggest that the incorporation of organic and inorganic agents in the EVOH matrix does not significantly alter or change the morphology or thermal properties of the thermoplastic. This indicates that these nanocomposite films and fibres could possibly be used in different applications where a polymer with antimicrobial release abilities is required.

4.6 References

1. Mokwena, K. K. & Tang, J. Ethylene vinyl alcohol: a review of barrier properties for packaging shelf stable foods. *Crit. Rev. Food Sci. Nutr.* **52,** 640–50 (2012).

2. Cabedo, L., Giménez, E., Lagaron, J. M., Gavara, R. & Saura, J. J. Development of EVOH-kaolinite nanocomposites. *Polymer (Guildf).* **45,** 5233–5238 (2004).

3. Munoz-Bonilla, A., Fernández-García, M. Polymeric Materials with Antimicrobial Activity. *Pro. Polym. Sci*. **37**, 281–339 (2016).

4. Nel, A. *Investigation of the effect of chitin nanowhiskers distribution on structural and physical properties of high impact polypropylene/chitin nanocomposites.* MSc Thesis, Stellenbosch University, South Africa. (2014).

5. Shang, M., Matsuyama, H., Maki, T., Teramoto, M. & Lloyd, D. R. Preparation and characterization of poly(ethylene-co-vinyl alcohol) membranes via thermally induced liquid-liquid phase separation. *J. Appl. Polym. Sci.* **87,** 853–860 (2002).

6. Zeng, J. B., He, Y. S., Li, S. L. & Wang, Y. Z. Chitin whiskers: An overview. *Biomacromolecules* **13,** 1–11 (2012).

7. Du Toit, M. L. *Incorporation of polysaccharide nanowhiskers into a poly(ethylene-co-vinyl alcohol) matrix.* MSc Thesis, Stellenbosch University, South Africa. (2013).

8. Vivekanandhan, S. Green Process for Impregnation of Silver Nanoparticles into Microcrystalline Cellulose and Their Antimicrobial Bionanocomposite Films. *J. Biomater. Nanobiotechnol.* **03,** 371–376 (2012).

9. Lu, Y., Weng, L., & Zhang l. Morphology and Properties of Soy Protein Isolate Thermoplastics Reinforced with Chitin Whiskers. *Biomacromolecules.* **5**,1046–1051 (2004).

Chapter 5: Investigation of the distribution of a combination of antimicrobial agents within an EVOH matrix using CLEM

5.1 Introduction

It has been established that a single antimicrobial agent does not have enough efficacy to work simultaneously as highly effective against the growth of Gram-positive bacteria, Gram-negative bacteria and a broad range of microbes. A single antimicrobial agent is usually highly effective against the growth of one kind of bacteria or microbe and less effective for the rest. The question is therefore if the simultaneous high efficacy against a variety of bacteria and microbes within a matrix can be increased and broadened by combining different antimicrobial agents within the relevant matrix. In a study by Ali et al., silver nanoparticles were used to enhance the antibacterial effects of chitosan nanoparticles to improve its bactericidal efficacy when applied on polyester fabrics[1,2]. The silver loaded chitosan composites showed antibacterial activity of 90% and above at very low concentrations while the composites containing only chitosan revealed a much lower activity of 58%. It is therefore important to explore the potential positive effects of different combinations of antimicrobial agents on the properties of a polymer matrix. One of the most important factors that plays a role in the improvement of polymer properties by incorporation of combinations of antimicrobial agents is however to achieve good dispersion of the agents throughout the matrix. One of the biggest challenges when investigating the dispersion of the antimicrobial agents is the ability to observe the distribution of more than one antimicrobial agent simultaneously within a specific matrix. This chapter reports on the preparation of nanocomposite materials that contain a combination of organic and inorganic antimicrobial agents (chitosan-reduced silver nanoparticles and chitin nanowhiskers) and addresses the challenging investigation of the arrangement or distribution of these antimicrobial agents simultaneously within the EVOH matrix. Chitin nanowhiskers and chitosan-reduced silver nanoparticles were both loaded, in increasing concentrations, in an EVOH matrix and the resultant nanocomposite mixture were either electrospun or solvent cast to form nanocomposite fibre mats or films, respectively.

This chapter presents results on the investigation of the distribution of combined antimicrobial agents within an EVOH matrix. Correlative light electron microscopy was used to investigate the distribution and dispersion of these agents within the same EVOH matrix. This technique has been used for imaging physiological samples containing different fluorophores using CFM and visualisation of subcellular structures by SEM and combining the techniques by superimposing the micrographs. The major disadvantage of this technique is that it images only

auto-fluorescent or fluorescent tagged structures[3,4]. Both antimicrobial agents used in this study are however able to either auto-fluoresce or be tagged with a fluorescing agent, which makes it possible to investigate their dispersion using CFM. SEM and SEM-EDX were furthermore used to investigate the elemental distribution of silver nanoparticles and chitin nanowhiskers as well as the morphological changes that occur on the EVOH surface as a result of the addition of the combined antimicrobial agents. The use of CLEM to investigate the dispersion of combinations of antimicrobial agents within nanocomposite polymer matrices is imperative for product functionality in the use of food packaging and medical industries.

5.2 Experimental

5.2.1 Preparation of CTSAgNP-ChNW-EVOH nanocomposites

Equal amounts of chitosan-reduced silver nanoparticles and chitin nanowhiskers were incorporated into an EVOH matrix in order to prepare nanocomposite mixtures containing 1 wt%, 3 wt%, 5 wt%, 8 % and 10 wt % concentrations of the combined antimicrobial agents with respect to the weight of the polymer. The nanocomposite mixtures were either electrospun or solvent cast to produced nanocomposite fibres and films, respectively.

5.3 Characterization techniques

5.3.1 Scanning electron microscopy and energy dispersive X-ray spectroscopy (SEM-EDX)

After analysis with the confocal microscope the samples were coated with a thin (~10 nm thick) layer of gold, using an Edwards S150A Gold Sputter Coater. Backscattered electron (BSE) micrographs and chemical quantification of samples were acquired using a Field Emission Gun Scanning Electron Microscope (FEG-SEM) (Zeiss MERLIN, Germany). The instrument is designed to perform qualitative analysis by taking high-resolution images and quantitative analysis, concurrently. Back scattered electron images were generated using a Zeiss 5-diode backscattered electron (BSE) detector (Zeiss NTS BSD) and Zeiss SmartSEM software. Chemical quantification of the surface of the sample was done using Energy Dispersive X-Ray Spectrometry (EDX) using an Oxford Instruments® X-Max 20 mm^2 detector and data analysis was done using an Oxford Aztec software and the software settings were as follows: a process time of 4, frame count of 3 and an EDX map resolution of 2 K. The counting time was 10 seconds live-time. Imaging and quantitate analysis was done using the following beam conditions:

Acceleration voltage: 20 kV

Probe current: 16 nA

Working distance: 9.5 mm

Beam current:11 nA

For fully quantitative un-normalized analyses the sample must be flat and have a high polish and be larger than the beam diameter which is approximately 1.5 micrometres and have a z-depth value more than the penetration depth of the electron beam (between 1-5 micrometres). The depth of penetration of the electron beam into a sample is dependent on the beam energy and the sample atomic mass. For all samples that do not meet these above-mentioned criteria, only semi-quantitative or qualitative analysis can be achieved.

5.3.2 CFM

Samples were mounted onto glass microscope slides using tape. A confocal microscope (Zeiss 780, Germany), equipped with a GaAsP detector and transmitting light detector, was used for fluorescence image acquisition. Samples were excited with a 405 nm diode laser for excitation of the silver nanoparticles and with the 561 nm laser for excitation of the Rhodamine B-tagged nanowhiskers. Emission was detected in the ranges 415-526 nm and 526-695 nm for silver nanoparticles and nanowhiskers respectively. Transmitted light was detected with the T-PMT detector.

Using the EC Plan-Neofluar 10x/0.3 M27 objective, tile scans of 5 x 5 were acquired of the area of interest for each sample. This was followed by the acquisition of sequential planes in Z-stacks with intervals of 12.454 μm when using the 10x/0.3 objective and 1.699 μm when using the LDPlan-Nuofluar 40x/0.6 Corr M27 objective.

5.3.3 Correlative light electron microscopy (CLEM)

To perform correlative microscopy, the glass microscope slides, onto which the samples were mounted, were marked with three gold and carbon L-shaped markers on three of the four corners of the one side of the rectangular slides using a custom-made stencil. The L-shaped marks were used to calibrate the coordinate system of the glass slides to enable correlation between the confocal and scanning electron microscopes. The coordinates of the three markers on each microscope slide were saved in the Shuttle and Find feature of ZEN 2012 software

(Zeiss, Germany) on the confocal microscope, thereafter coordinates of areas of interest were saved.

5.4 Results and discussion

5.4.1 SEM-EDX

Figure 5.1 shows the SEM results for the composite mixtures, containing both CTSAgNPs and ChNWs, where (A), (B) and (C) represent 3 wt%, 5 wt% and 10 wt% of combined loadings, respectively. The results are consistent with the results shown in Section 4.2.1, where the chitin nanowhiskers were shown to cause spherically shaped structures in the EVOH matrix. The bright particles in the composites represent chitosan-reduced silver nanoparticles and these show a tendency to agglomerate. Figure 5.1 (B) and (C) shows that higher concentrations of silver nanoparticles have a tendency to either agglomerate and disrupt the overall structure instead of forming a homogeneous dispersion on the surface of the chitin nanowhisker containing EVOH matrix.

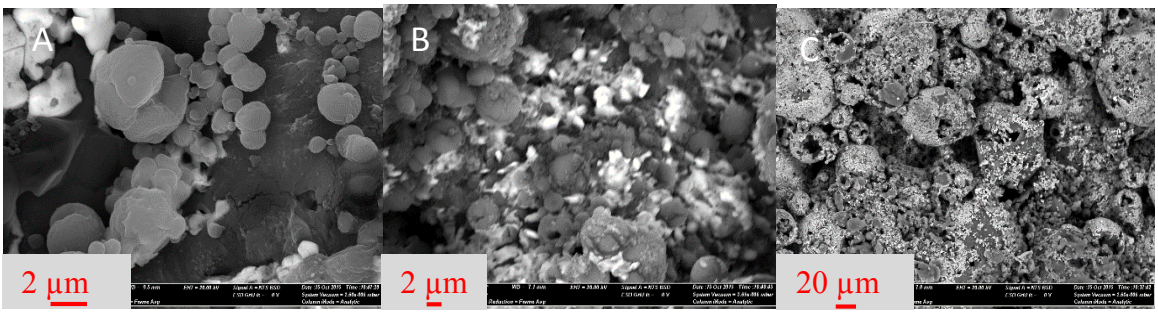

Figure 5.1 FESEM micrographs of CTSAgNPs-ChNWs-EVOH films with (A) 3 wt%, (B) 5 wt% and (C) 10 wt% combined loadings of CTSAgNPs and ChNWs.

It is evident that the dispersion of antimicrobial agents of organic and inorganic origin cannot be evaluated only by FESEM. This is because of the inability of this technique to show the presence and distribution of an antimicrobial agent of an organic nature such as chitin nanowhiskers, dispersed in an organic polymer matrix. Figure 5.2 shows secondary electron micrographs of EVOH nanocomposite films (A, B, C and D) and fibre mats (E and F). The secondary electron images were taken using a backscattered detector at bright field mode. These images show the dispersion of only the silver nanoparticles within the composites. The 3 wt% and 10 wt% loadings shown in (B and C) indicates a homogeneous dispersion of these nanoparticles on the surface of the films. There are spots on the surface that are shown to be slightly brighter than others, indicating possible agglomerates of silver in the nanocomposite matrix. The limitation of SEM here again is that the dispersion of the chitin nanowhiskers

cannot be observed using this technique because of the similar phases between the EVOH and the chitin nanowhiskers.

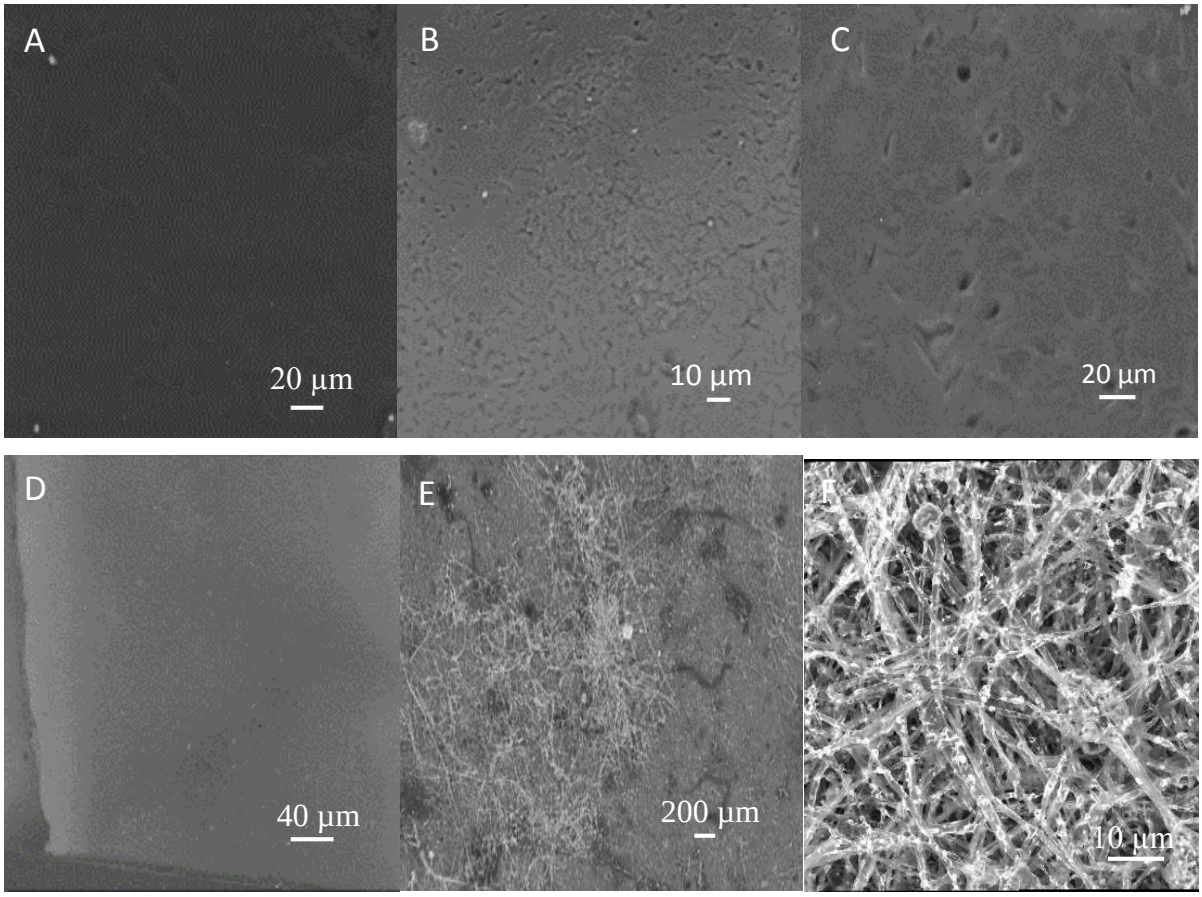

Figure 5.2 Backscattered electron micrographs illustrating homogeneous and heterogeneous spatial distribution of silver nanoparticles (AgNPs) within EVOH nanocomposite films (A-D) and fiber mats (E and F). (A) and (B) show films that contain 3 wt% and (C, D, E and F) contain 10 wt% dispersions of chitin nanowhiskers and silver nanoparticles.

Proper nanocomposite preparation and sonication is required in order to achieve a homogeneous dispersion of the antimicrobial agents in the nanocomposites. Figure 5.2 (D) shows a backscattered electron micrograph illustrating two distinct domains, which can be distinguished by varying contrast (brighter region in the lower left corner and the darker area in the upper right corner of the micrograph). This image illustrates a case of homogeneous and heterogeneous dispersion of agents in the same nanocomposite film.

In the case of nanocomposite fibres (Figure 5.2 E and F), the silver nanoparticles were well distributed throughout the fibres, with a few brighter spots that indicated agglomerated silver nanoparticles. The fibres containing combined antimicrobial agents tended to form beads and the fibres had larger diameters compared to the fibres containing individually incorporated

antimicrobial agents. The average diameter of the nanocomposite fibres containing both antimicrobial agents was about 2 µm (SD=0.5 µm), 649 nm (SD=121 nm) for the silver nanoparticles loaded fibres and 441 nm (SD=99 nm) for the chitin nanowhisker loaded fibres. Similar to nanocomposite films, it was not possible to investigate the dispersion of chitin nanowhiskers using only FESEM.

Qualitative EDX was used to investigate the distribution of the elements present in the nanocomposites. Figure 5.3 shows EDX maps of EVOH nanocomposites containing 3 wt% and 10 wt% loadings of ChNWs and CTSAgNPs. The maps show the distribution of carbon (A and E), oxygen (B and F) and silver (C and G) within the nanocomposite matrices.

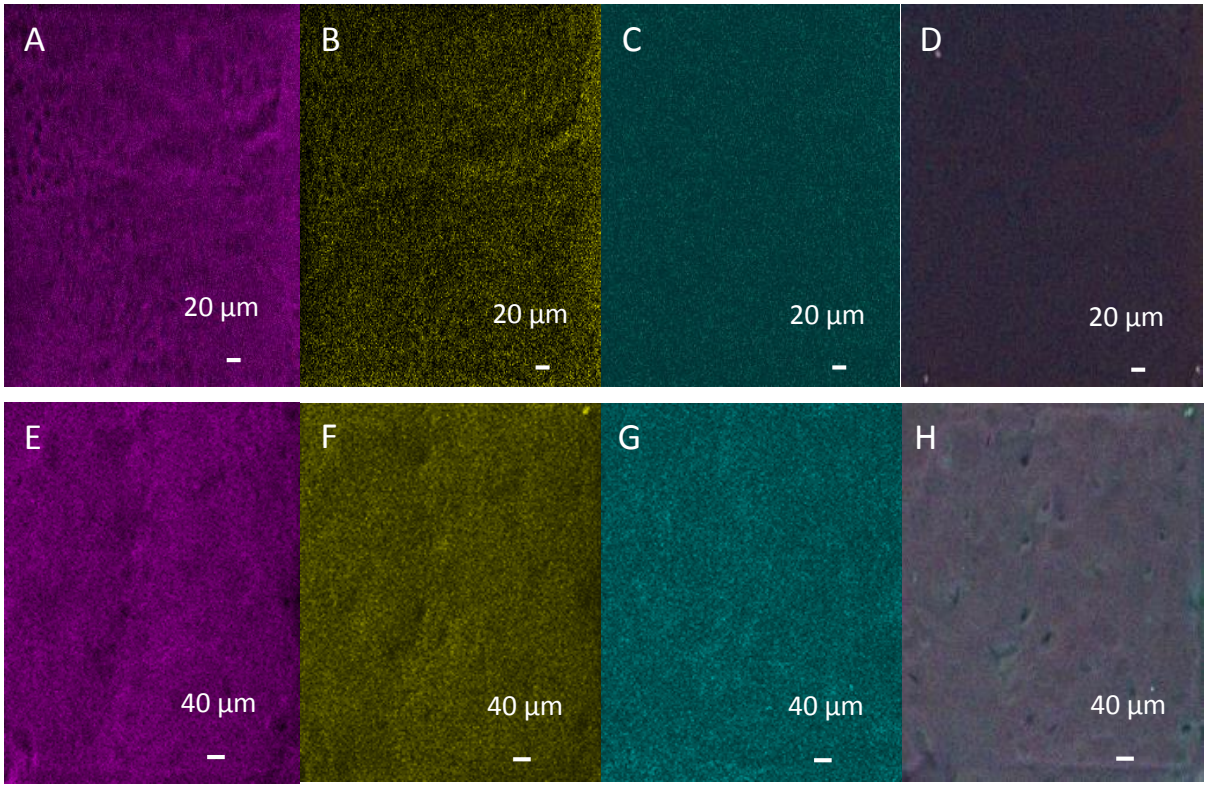

Table 5.3 SEM-EDX maps of EVOH nanocomposite films containing 3 wt% (A-D) and 10 wt% (E-H) loadings of chitin nanowhiskers and silver nanoparticles. Carbon maps (A and E), oxygen maps (B and F), silver maps (C and G) and an overlay of the elemental maps (D and H)

The elements were then analysed at the same time, forming the overlays presented in Figure 5.3 (D and H). According to these images the elements were dispersed homogeneously throughout the films with little to no agglomeration shown, however, silver is shown to have a few brighter spots, especially for the 10 wt% loading (G), indicating some agglomeration of silver particles.

5.4.2 CFM

Figure 5.4 shows the fluorescence of Rhodamine B labelled chitin nanowhiskers and the silver nanoparticle auto-fluorescence. The antimicrobial agents are dispersed in an EVOH polymer as 3 wt% and 10 wt% within the polymer. The micrographs showing the red fluorescent signals (A, D and G) represent the Rhodamine B labelled chitin nanowhiskers while the blue signals (B, E and H) show auto-fluorescence of the silver nanoparticles. According to these images, both antimicrobial agents were evenly distributed throughout the film surface and the dispersion of chitin was homogeneous.

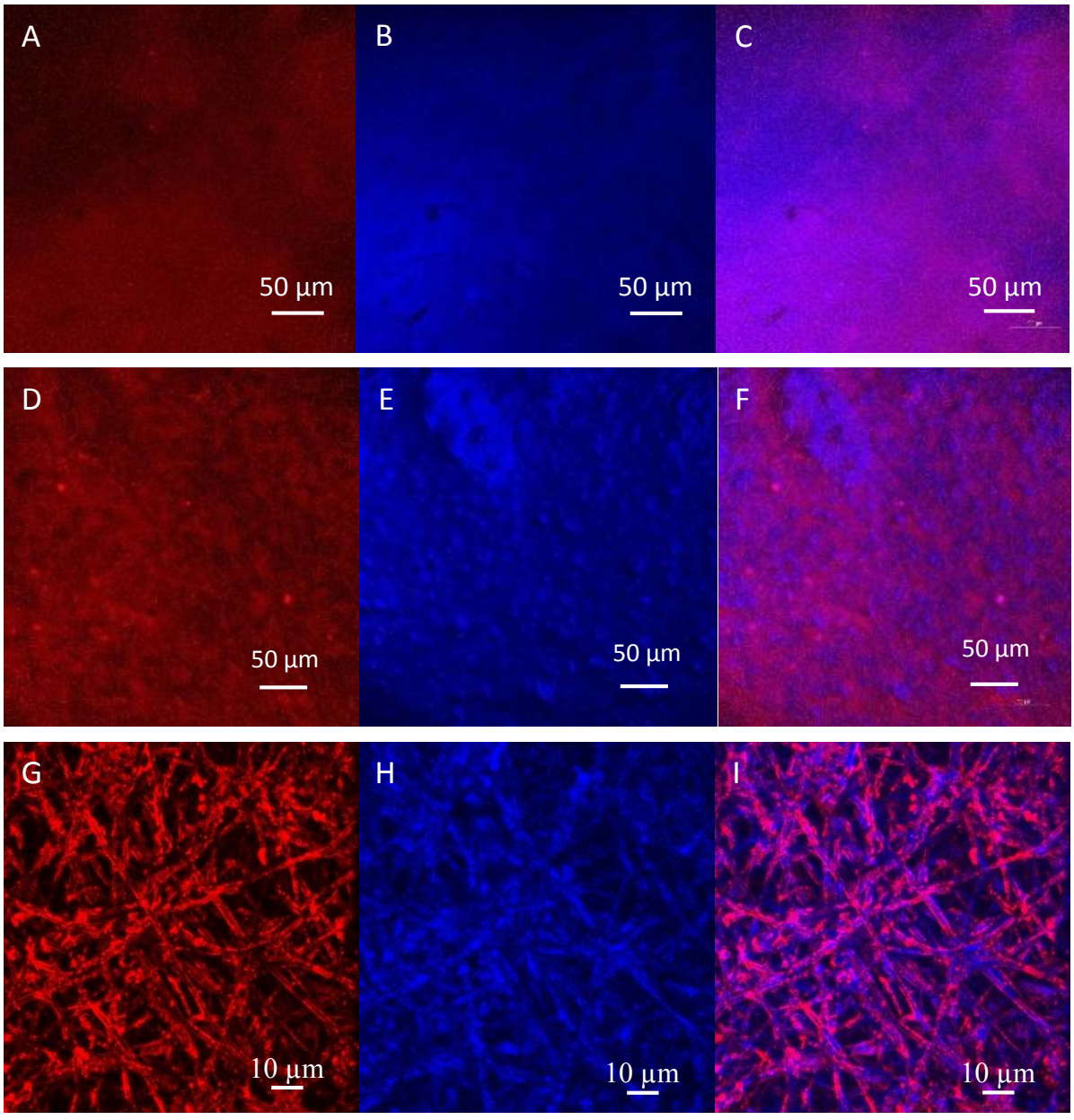

Figure 5.4 CFM images of EVOH nanocomposite films and fibres containing combined loadings of antimicrobial agents. A - F represent nanocomposite films and G - I represent

nanocomposite fibres. Rhodamine B labelled chitin nanowhiskers (A, D and G) shown by the red signals. Auto-fluorescent silver nanoparticles (B, E and H) shown by the blue fluorescent signals. The overlays (C, F and I) are taken with both red and blue lasers activated.

Figure 5.4 (I) shows an overlay of the two fluorescent signals showing G and H. This micrograph indicates regions where the silver nanoparticles and chitin nanowhiskers appeared to be slightly agglomerated. This tendency to agglomerate was even greater for the 10 wt% loading of the antimicrobial agents as can be seen in (D) and (E) where parts of the film showed bright red and blue spots for both fluorescent signals. These results provide a clear picture as to how both agents arrange and distribute themselves within the EVOH nanocomposite films. The dispersion of ChNWs within the EVOH nanocomposite fibres was successfully illustrated using confocal fluorescent microscopy. The dispersion and / or distribution of chitin nanowhiskers and silver nanoparticles in EVOH fibres has not been investigated using this technique before. The silver nanoparticles were found to be auto-fluorescent with a strong blue fluorescent signal and it was useful in order to get information about the location and distribution of both antimicrobial agents in an EVOH matrix. These results show that both ChNWs and CTSAgNPs were dispersed homogeneously within the EVOH fibres and it was interesting to note in Figure 5.4 (I) that the nanowhiskers were lying on the surface of the fibres while the silver nanoparticles were distributed on the inside of the fibres.

5.3.4 CLEM

Correlative light electron microscopy is a technique that combines scanning electron microscopy and confocal microscopy for which the images are then correlated to give clearer and more descriptive information about the location, arrangement and dispersion of the two antimicrobial agents within the EVOH matrix. Figure 5.5 shows SEM-EDX, CFM and CLEM images of nanocomposite fibres containing 10 wt% dispersion of CTSAgNPs and ChNWs.

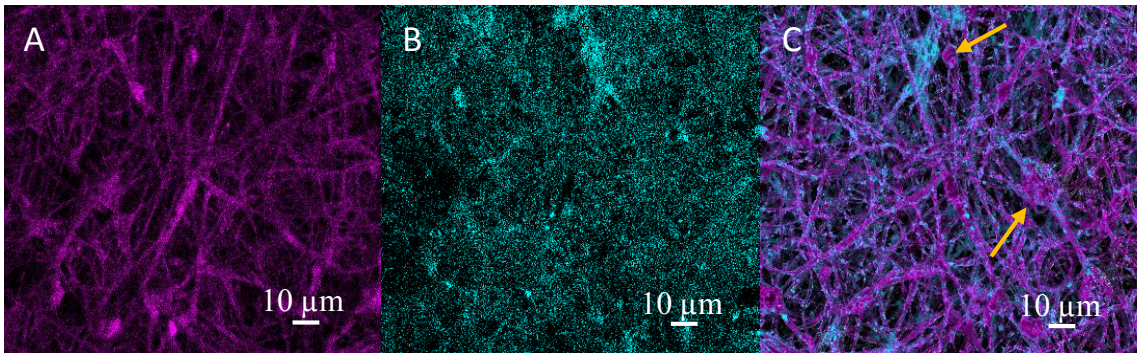

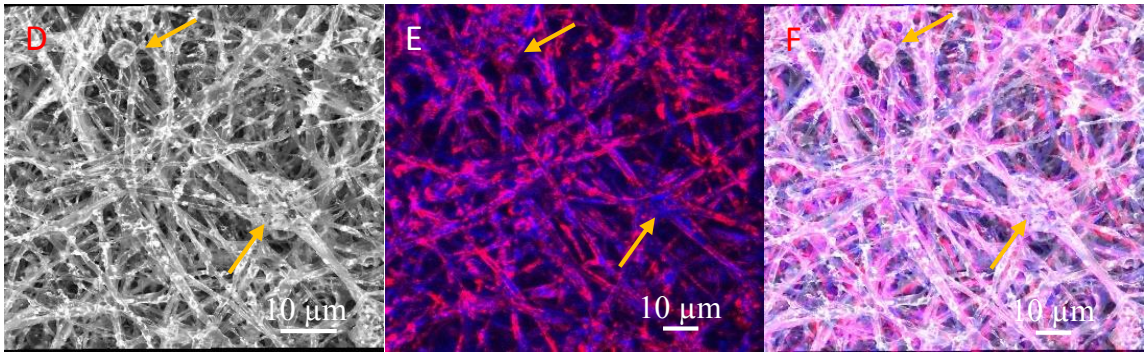

Figure 5.5 CLEM micrographs of 10 wt% loadings of combined antimicrobial agents (A) SEM-EDX carbon map, (B) SEM-EDX silver map, (C) Carbon and silver maps, superimposed. (D) Secondary electron, (E) CFM overlay and (F) CLEM micrograph.

One of the most significant advantages of the CLEM technique is the ability to take a secondary electron image, SEM-EDX map and CFM image of the same region or area of the sample. The micrographs presented in Figure 5.5 were taken from the same area of the sample for all techniques. Figure 5.5 (C) shows a CLEM image which is an overlay of the images from scanning electron microscopy and confocal microscopy, which illustrates the silver nanoparticle and chitin nanowhisker location within the fibres. The nanowhiskers were lying on the outside/surface of the fibres while the silver nanoparticles were distributed on the inside of the fibres. The fibres have larger fibre diameters when containing both antimicrobial agents as compared to when loaded with only one. Figure 5.6 shows three-dimensional scans of the nanocomposite films (A) and nanocomposite fibres mats (B).

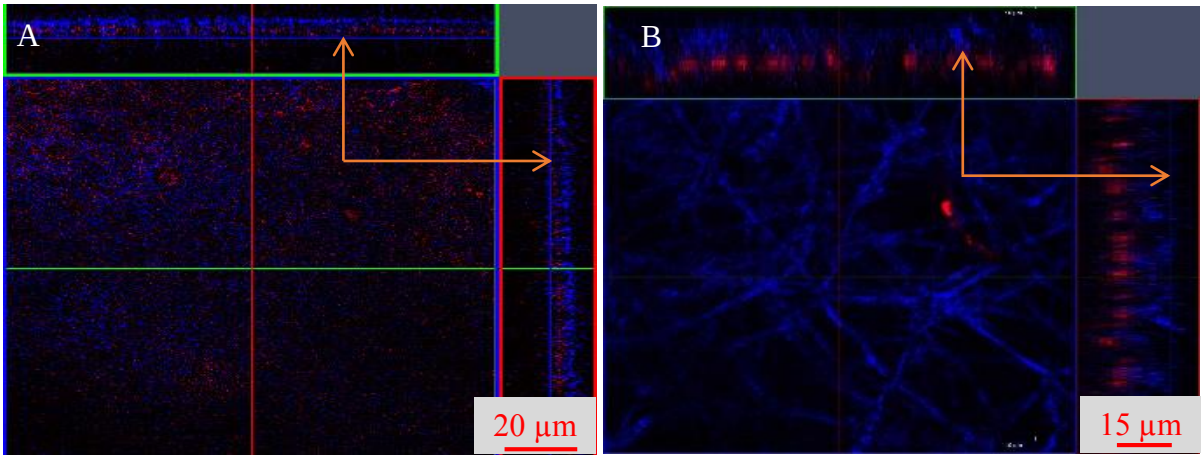

Figure 5.6 Three-dimensional scans of CFM micrographs of nanocomposites with RhB-induced fluorescence of chitin nanowhiskers and auto-fluorescent silver nanoparticles. (A) shows the nanocomposite films and (B) shows the nanocomposite fibres.

These micrographs indicate the arrangement of the agents on the surface and within the polymer matrix. These three-dimensional micrographs support the CLEM results shown in

Figure 5.5 which showed the dispersion of the chitin nanowhiskers on the surface of the films and the fibres, while the silver nanoparticles settle on the inside of the films and the fibres.

5.5 Conclusions

Polymer nanocomposite applications require proper dispersion and distribution of antimicrobial agents for the effectiveness of the antimicrobial activity of the final nanocomposite product. Scanning electron microscopy and confocal fluorescent microscopy (CFM) are examples of the techniques that are usually employed to investigate the distribution of some organic and inorganic antimicrobial agents dispersed in polymer matrices. Correlative light electron microscopy (CLEM) is a new technique that combines both SEM and CFM. This is a promising technique to investigate the presence, dispersion and distribution of multiple nanoparticle materials within polymer matrices. The use of SEM in combination with EDX can also give quantitative and qualitative information about the elemental contents and the distribution thereof in the nanocomposite films and fibre mats.

The dispersion of chitin nanowhiskers (ChNWs) and silver nanoparticles (AgNPs) dispersed in poly (ethylene co-vinyl alcohol) (EVOH) was investigated using correlative light electron microscopy (CLEM). Sonication was necessary to enhance the dispersion of both antimicrobial agents in the EVOH matrix. The results show the homogeneous dispersion of antimicrobial agents in the EVOH nanocomposite films and fiber mats, with only small amounts of agglomeration of silver nanoparticles observed. CLEM analysis revealed the tendency of the chitin nanowhiskers to align themselves on the outside of the fibers while the silver nanoparticles were localized on the inside of the fibers. In the case of the films, the silver nanoparticles were found settled on the inside of the film while the chitin was found closer to the surface of the films. There were cases where the silver nanoparticles would form large agglomerates or clusters of silver. This undesirable phenomenon can be attributed to insufficient sonication of the agents in the nanocomposite mixture before solvent casting or electrospinning. The diameter of the nanocomposite fibres containing combinations of antimicrobial agents slightly increased when compared to the diameter of the individually incorporated nanocomposite fibres. The EDX results also illustrated good distribution of elements like carbon, oxygen and silver in the nanocomposites. The results from this chapter furthermore show the significant value of CLEM to investigate the dispersion and distribution of multiple agents in a polymer matrix, especially in cases where the agents are organic and inorganic in nature. This technique outlines very important information about the dispersion

and distribution of the antimicrobial agents within a polymer matrix, which is something one would not be able to achieve when using the SEM and CFM, individually.

5.6 References

1. Ali, S. W., Rajendran, S. & Joshi, M. Synthesis and characterization of chitosan and silver loaded chitosan nanoparticles for bioactive polyester. *Carbohydr. Polym.* **83,** 438–446 (2011).

2. Aubert-Viard, F Aubert-Viard, Martin, A., Chai, F., Neut, C., Tabary, S., Martel, B & Blanchemain, N.Chitosan finishing nonwoven textiles loaded with silver and iodide for antibacterial wound dressing applications. *Biomed. Mater.* **10,** 015–023 (2015).

3. Brown, E. & Verkade, P. The use of markers for correlative light electron microscopy. *Protoplasma* **244,** 91–97 (2010).

4. Nakabayashi, M., Shoji, M., Yoshihara, M., Hisada, A. & Ominami, Y. Correlative Light and Electron Microscopy in Atmosphere. *Microsc. Microanal.* **22,** 230–231 (2016).

5. Perkovic, M., Kunz, M., Endesfelder, U., Bunse, S., Wigge, C., Yu, Z., Hodirnau, V.V., Scheffer, M.P., Seybert, A., Malkusch, S., Schuman, E.M., Heilemann, M., Frangakis, A.S., Correlative Light- and Electron Microscopy with chemical tags. *J. Struct. Biol.* **186,** 205–213 (2014).

Chapter 6: Peptide treatment and antimicrobial assay of EVOH nanocomposites

6.1 Introduction

In this chapter, all the nanocomposites were treated with an antimicrobial peptide (Gramicidin S) via a dip coating technique. This technique was performed post electrospinning and solvent casting. A review study by Rieger et al. described the use of chitosan to coat PVA electrospun fibres by submerging the fibres in a 1.0 wt% chitosan solution for one hour at 30 °C. Chemical modification of the functional groups at the surface of composite fibres and films enables the attachment of bio functional molecules or change the degree of hydrophobicity of the fibre mat or film[1]. A similar dip coating method was used whereby the nanocomposites were individually submerged in a peptide solution in order to attach or transfer desirable peptide properties to the fibre mats and films. The aim was to expand the antimicrobial efficacy of the EVOH nanocomposite matrix through combination of the different antimicrobial agents within the same matrix.

6.2 Experimental

6.2.1 Materials

Deionized water was produced in-house by an Elga Purelab instrument and the isopropanol used was supplied by Merck. MilliQ water, water from a reverse osmosis water purification plant and was further purified with a Millipore MilliQ water purification system from Milford, USA, was used for all the biological tests. Gram positive bacteria, Micrococcus luteus NCTC 8340 was obtained from National Collection of Type Cultures (Porton Down, Salisbury, United Kingdom). The Falcon® tubes were supplied by Becton Dickson Labware (Lincoln Park, USA), petri dishes - Greiner bio-one (Frickenhausen, Germany), tryptone - Merck (Darmstadt, Germany), yeast extract - Merck (Darmstadt, Germany), sodium chloride - Merck (Wadesville, Gauteng), agar - Merck (Darmstadt, Germany) and resazurin salt - Sigma-Aldrich (St. Louis, MA, USA) MTP - AEC Amersham (Johannesburg, South Africa).

6.2.2 Peptide treatment

Paper puncher sized pieces were cut from both solvent cast films and electrospun fibre mats for peptide treatment. Gramicidin S powder was used to treat all the EVOH composite samples containing different antimicrobial agents. A 50 µg/mL (975 µL water +25 µL peptide solution) Gramicidin S solution was diluted from a stock solution of 2 mg/mL in MilliQ water. All the

nanocomposite paper punched pieces were immersed in 200 µL of the Gramicidin S solution. The samples were then incubated for one hour at room temperature after which the excess peptide solution was decanted off and rinsed with MilliQ water followed by drying the samples overnight at 30 °C. The films and the fibres were sterilized by incubating the samples in a desiccator with a small amount of chloroform for one hour before the antimicrobial assay. To confirm the successful attachment of Gramicidin S to the surface of the fibres and the films, SEM and FTIR were employed to investigate the morphological and chemical changes that may occur on the surface of the fibres and the films when using the dip-coating process.

6.2.3 Antimicrobial tests

Alamar blue assay was used to quantitatively evaluate the antimicrobial effect of the EVOH nanocomposites against Gram-positive bacteria, *Micrococcus luteus* as described by Hamid et al and Pettit et al [2, 3]. *M luteus* bacteria was grown by streaking out freezer stocks and plates were incubated at 37 °C for 48 hours for the organism to grow. Three to five colonies were selected and grown overnight for 16 hours in 20 ml Lysogeny broth (LB) media to an OD620 = 0.8-1.2, slanted at 150 rpm. The media was prepared by mixing 10 g Tryptone, 5 g Yeast Extract, 10 g NaCl and 20 g Agar for LB agar plates. Subculturering was done by pipetting 500 µL of cultures into 20 mL fresh media followed by incubation for 5-6 hours or to OD620 = 0.6, then cultures were diluted to OD620 = 0.2.

The assay was carried out using the following five steps:

1. Samples were placed in 96 black well plates, flaming between each type of sample.

2. 100 µL of either culture or media was pipetted into the plates, including wells with just culture or media, no sample, which were used as controls.

3. The plates were covered with foil and incubated overnight (16 hours) at 37 °C.

4. Alamar blue (10 µL) was pipetted into wells (0.3mg/mL Resazurin sodium salt in phosphate buffered saline) and covered with foil and incubated for 2 hours 37 °C.

6.3 Characterization techniques

6.3.1 FESEM

A Carl Zeiss MERLIN FESEM with a GEMINI II column was used to image all the nanocomposite films and fibres which were gold coated before images were taken. The films and fibres were placed on a stub using a double-sided carbon tape and gold coated to make the samples conductive. FESEM images at lower and higher magnifications were taken for each solvent cast film and electrospun nanocomposite fibre. An in-lens detector was used to obtain the FESEM micrographs with a working distance of 3.8 mm, probe = 250 pA and EHT = 5.00 Kv.

6.3.2 Alamar Blue assay

The Alamar Blue dye was aliquoted and stored at -80°C and only brought to room temperature before each experiment. The dye content was covered by foil to minimise its exposure to light. The absorbance was measured using a Perkin-Elmer microplate reader. The results were analyzed and the growth inhibition was determined using the following equation:

$$\%\ Growth\ inhibition\ = 100 - \frac{100(F\ of\ well - Mean\ F\ of\ no\ growth)}{Mean\ F\ of\ growth - Mean\ F\ of\ no\ growth}$$

6.3.3 ATR-FTIR

FTIR data were recorded using a Thermo Fisher Nicolet iS10 instrument. The spectra were recorded at a minimum number of scans set at 32 taking background information before every sample scan and the resolution was 4 cm-1. The synthesized nanocomposite films and fibres were analyzed as thin films or as fibre mats.

6.4 Results and discussion

6.4.1 FESEM characterization of Gramicidin S attached nanocomposites

Figure 6.1 shows FESEM images of the neat EVOH electrospun fibres (electrospun from 6 wt% solution of EVOH polymer) and solvent cast films that were individually exposed to a 50 µg/mL Gramicidin S solution via dip-coating.

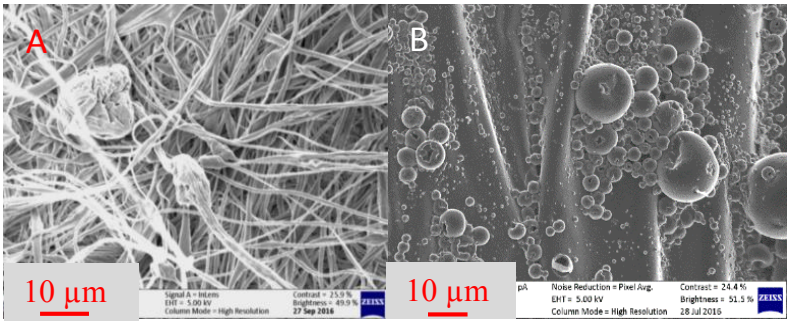

Figure 6.2 FESEM micrographs of (A) 6 wt% EVOH composites electrospun fibres and (B) solvent cast film. Both micrographs were taken after peptide treatment.

There is an appearance of beads with variable sizes and shapes on the surface of the fibres. After dip-coating, the fibres seem to stick together forming bead-like structures on the surface of the fibres. A similar result was observed for the solvent cast films where beads were dispersed on the surface of the films, but in this case the beads were smaller and they appeared to only stick to the surface of the films without disrupting the structure of the films at all.

Figures 6.2 illustrates FESEM micrographs of chitin containing EVOH nanocomposite films. The films were loaded with increasing concentrations of ChNWs. The micrographs show morphological changes that occurred on the surface of the nanocomposite films in response to the addition or attachment of the peptide to chitin containing nanocomposites. The 10 wt% loading of chitin nanowhiskers in EVOH nanocomposites seem to have the highest interaction with the peptide.

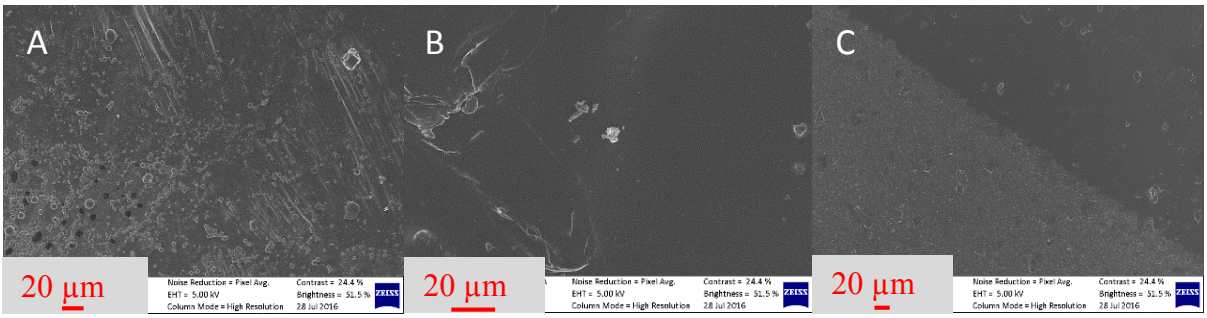

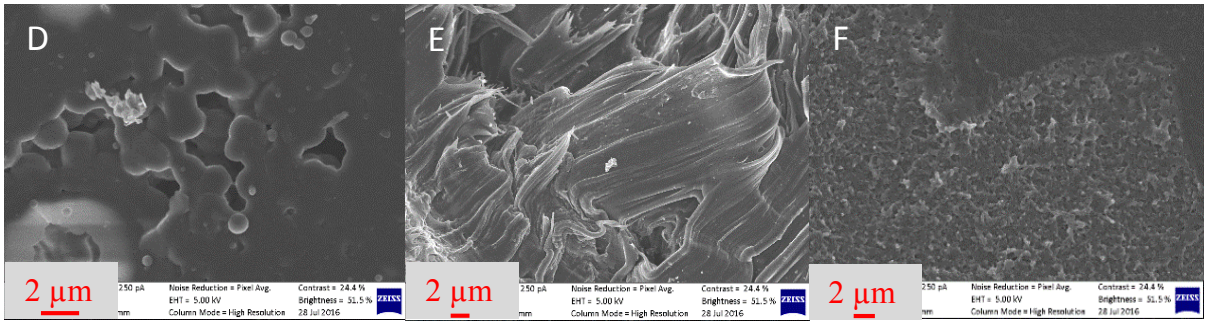

Figure 6.2 FESEM micrographs of Gramicidin S attached to chitin nanowhiskers-EVOH nanocomposite films. The nanocomposites show (A and D) 3 wt %, (B and E) 5 wt% and (C and F) 10 wt%, chitin nanowhisker content.

Figure 6.3 shows FESEM images of Gramicidin S attached nanocomposite fibres containing increasing amounts of chitin nanowhiskers. These micrographs show the attachment of the peptide on the surface of the fibres

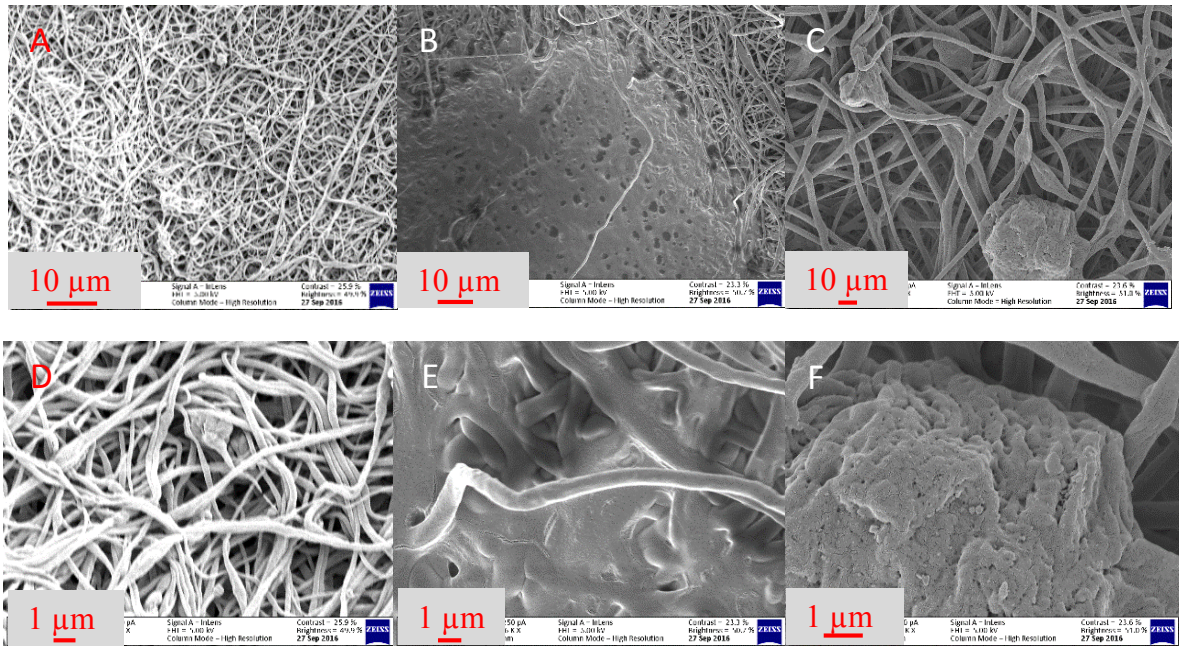

Figure 6.3 FESEM micrographs of Gramicidin S attached to chitin nanowhiskers-EVOH nanocomposite fibres. The nanocomposites show (A) 3 wt %, (B) 8 wt% and (C) 10 wt%, (D) 3 wt %, (E) 8 wt % and (F) 10 wt % chitin nanowhisker content.

This attachment seemed to have increased with an increase in the content of chitin nanowhiskers in the composite fibres. This increase in peptide attachment may have been possibly caused by the increase in chitin nanowhiskers or due to an increase in weight of the fibre mats. The characterized samples were “paper punched” and could unfortunately not be weighed because of the static nature of the nanofibres. The samples with the 8 wt% and 10

wt% loadings of chitin nanowhiskers showed a complete change in the morphology of the surface or structure of the fibres, with lumps of peptide sticking to the surface of the fibres, causing the fibres to stick together and form a mesh as illustrated in Figures 6.3 (B) and (C).

Figure 6.4 shows the FESEM micrographs of silver nanoparticle containing EVOH nanocomposite films. The peptide seems to be well dispersed throughout the silver nanoparticles containing films compared to the chitin nanowhisker containing nanocomposites. The peptide forms a web-like network on the surface of the films instead of forming lumps or beads a in the case of the nanocomposite fiber mats in Figure 6.3.

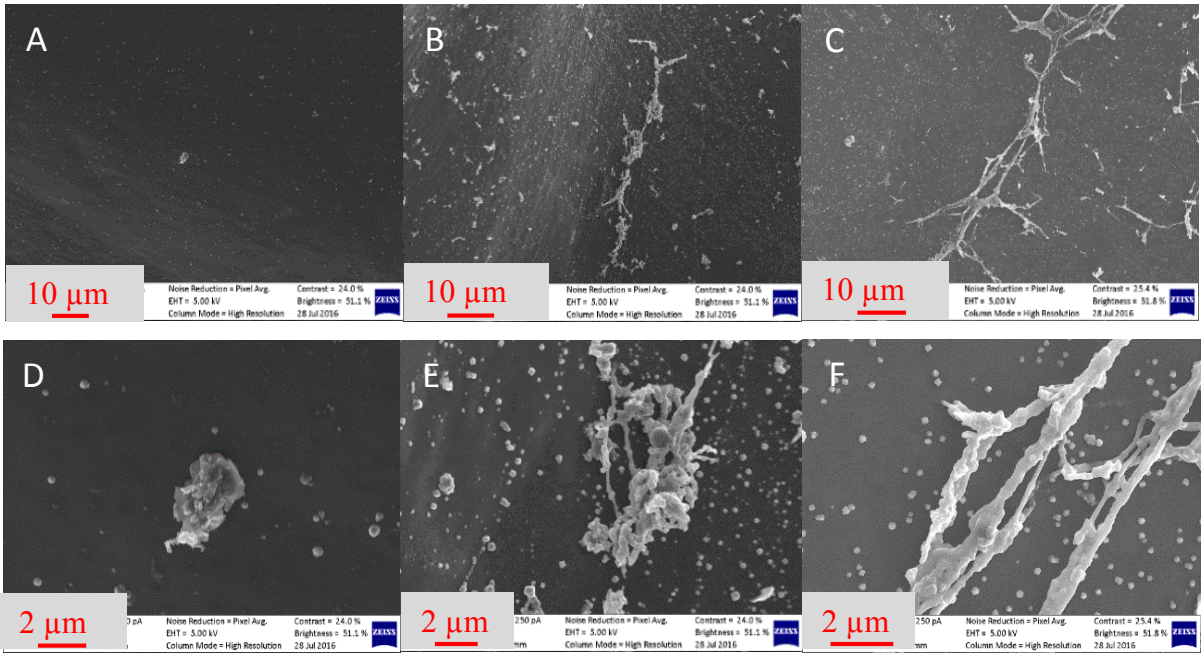

Figure 6.4 FESEM micrographs of Gramicidin S attached to chitosan-reduced silver nanoparticle-EVOH nanocomposite films containing (A and D) 1 wt %, (B and E) 5 wt%, (C and F) 10 wt% silver nanoparticle content.

The 1 wt% chitosan-reduced silver nanoparticle containing composite film (A and D) is shown to have only a few of these webs on its surface whereas the 5 wt% (B and E) and the 10 wt% (C and F) containing composite films have more web-like structures on their surface. The increase in the attachment of the web-like structures on the surface of the films is in response to the increasing chitosan-reduced silver nanoparticle content in the nanocomposites. This suggest that there is an interaction between the peptide and the silver nanoparticles in the EVOH nanocomposites.

The FESEM images of the chitosan-reduced silver nanoparticles that were not treated with the peptide (Chapter 4, Figure 4.3) were used as a comparison to these results to further confirm the attachment of the Gramicidin S to the surface of the chitosan-reduced silver nanoparticle nanocomposite films on the EVOH matrix. These FESEM results furthermore illustrated that the peptides prefer to attach to one another forming a continuous web-like network.

Figure 6.5 shows the FESEM micrographs of silver nanoparticles containing fibres treated with Gramicidin S. This micrographs show the attachment of Gramicidin S on the surface of the nanocomposite films and fibres.

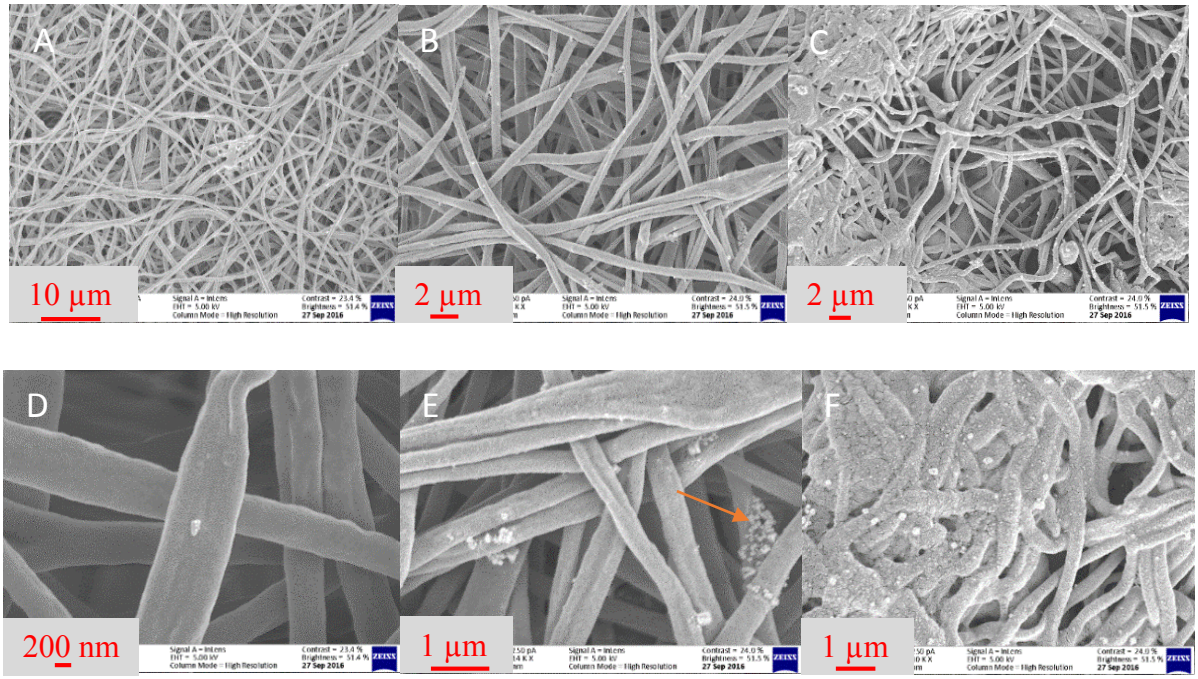

Figure 6.5 FESEM micrographs of Gramicidin S attached to chitosan-reduced silver nanoparticle-EVOH nanocomposite fibres containing (A) 1 wt %, (B) 5 wt%, (C) 10 wt%, (D) 1 wt %, (E) 5 wt % and (F) 10 wt %, silver nanoparticle content.

The 1 wt% silver nanoparticle containing fibre mat showed a similar result to the composite film shown in Figure 6.4 above. Only a few of the peptide structures were found attached to the surface of these 1wt % silver containing fibres. The 5 wt% silver nanoparticles containing nanocomposite fibre mats presented in Figure 6.5 (B) and (E) revealed a larger content of the peptide on the fibre surface and these peptide particles seemed to be homogeneously dispersed on the surface of these fibres. The peptides also showed a tendency to agglomerate forming clusters of peptide on the surface of the fibres as shown in (E). A complete disruption of the surface of the fibres was observed in the fibres containing 10 wt% of chitosan-reduced silver

nanoparticles, as shown in Figures 6.5 (C) and (F). The fibres showed a tendency to stick together forming a mesh. From these results it is clear that the peptide prefer to adhere to the surface of the composites containing higher contents of silver nanoparticles, which increases the chance of having peptide agglomeration and makes the fibres stick together forming a mesh-like structure.

Figure 6.6 illustrates FESEM micrographs showing the attachment and dispersion of the Gramicidin S on the surface of the AgMCC-EVOH nanocomposite films and fibres, respectively.

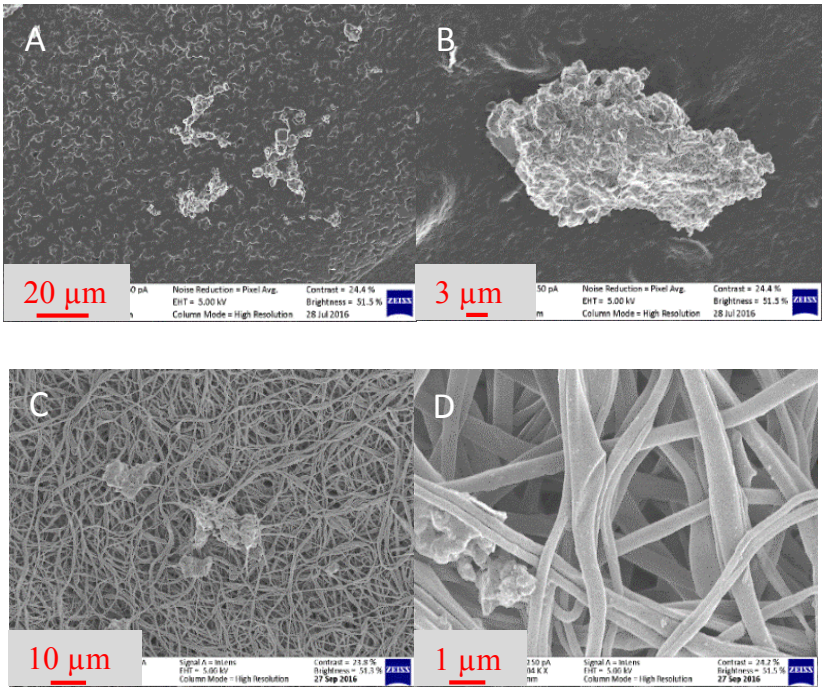

Figure 6.6 FESEM micrographs of Gramicidin S attached to nanocomposites containing 3 wt% AgMCC. (A) and (B) are nanocomposite films while (C) and (D) are nanocomposite fibre mats.

Images (A) and (B) presents the attachment of Gramicidin S to the surface of the 3 wt% AgMCC-EVOH films at different magnifications. The Gramicidin S was heterogeneously dispersed. It formed either lumps or a small continuous network. A similar effect was observed for the 3 wt% AgMCC containing fibres in (C) and (D). Small lumps of Gramicidin S were found on the surface of the fibres. Figure 6.7 shows FESEM micrographs of the EVOH nanocomposites containing silver nanoparticles and chitin nanowhiskers. Gramicidin S showed a tendency to adhere to surfaces of EVOH nanocomposite films containing both chitosan-reduced silver nanoparticles and chitin nanowhiskers. These nanocomposite films have a much

higher affinity towards Gramicidin S compared to the nanocomposites with individually incorporated antimicrobial agents.

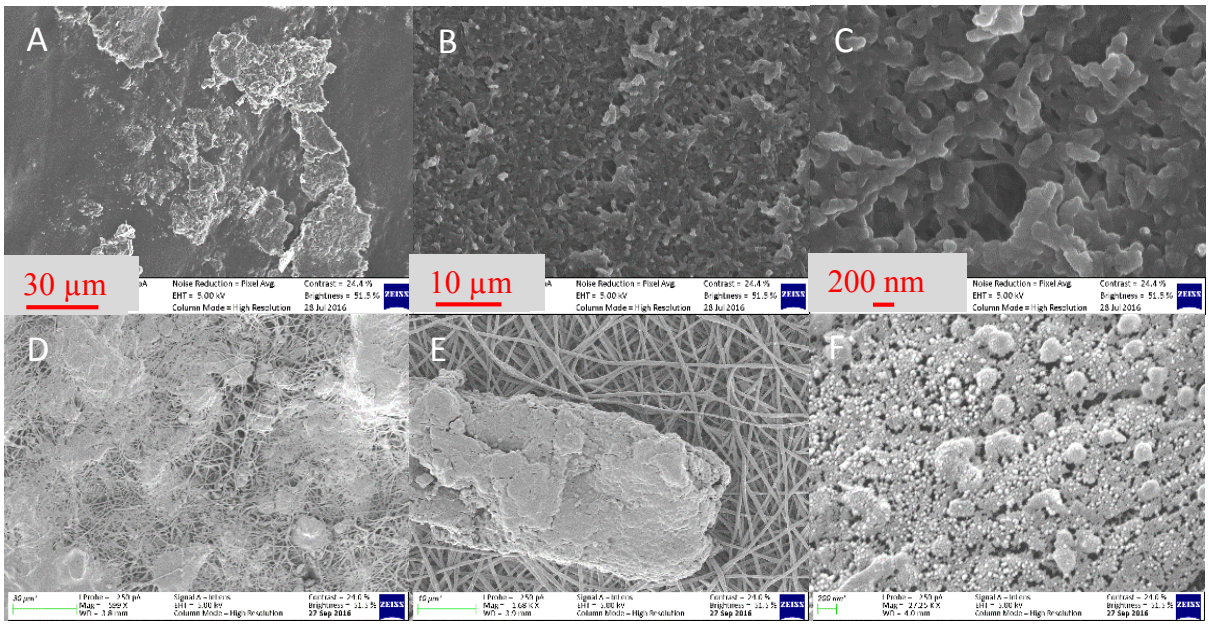

Figure 6.7 FESEM micrographs of Gramicidin S treated EVOH nanocomposites. (A) 5 wt %, (B) 8 wt% and (C) 10 wt% films. (D) 5 wt %, (E) 8 wt % and (F) 10 wt % fibres. These nanocomposites are loaded with silver nanoparticle and chitin nanowhisker.

This is shown by the wide spread Gramicidin S network on the surface of the films from as little at 5 wt% combined antimicrobial agents. This tendency indicates the presence of a much stronger bond between the nanocomposite films and fibre mats on the one hand and the Gramicidin S matrix on the other hand. In this case the peptide is shown to not only adhere to the surface of the films but to also penetrate deeper into the film, exposing more regions for peptide bonding. The fibre mats also showed a similar result where the Gramicidin S structure formed a mesh like surface at concentrations as low as 5 wt% of the antimicrobial agents. The change in the surface morphology of the fibres was observed to be more for the 10 wt% loaded sample than all of the other loadings, as shown in Figure 6.7, indicating a higher bonding tendency for the fibres containing more antimicrobial agents to the Gramicidin S peptide

6.4.2 ATR-FTIR

FTIR was used to investigate the chemical changes that may occur on the surface of the films and the fibres after peptide treatment, as shown in the spectra in Figure 6.8. The most noticeable difference in the FTIR spectra of the neat films compared to the chitin nanowhisker containing nanocomposites was the increase in the carbonyl moieties of the films which became more defined with an increase in the Gramicidin S attachments on the surface of the films. There was also a slight decrease in the intensity of the OH and C-H peaks at 3180 cm $^{-1}$ and 2920 cm $^{-1}$. This may be attributed to the attachment or bonding of the peptide to the backbone of the EVOH utilizing the exposed OH groups thereby decreasing the number of these groups on the surface of the EVOH composites. There are some peaks showing an increase in intensity with an increase in the chitin content and therefore also with the increase in Gramicidin attachment. The most noticeable increase in the peaks at about 1600 cm^{-1} and 1700 cm^{-1} is observed with the 10 wt% loading of chitin nanowhiskers which shows the highest absorbance peaks. These increases were also observed in the FTIR spectrum of the films and fibre mats not treated with Gramicidin S shown in Section 4.1.2.4 above. It is therefore difficult to decide whether this attachment is due to of the peptide or the increase in the chitin nanowhisker content.

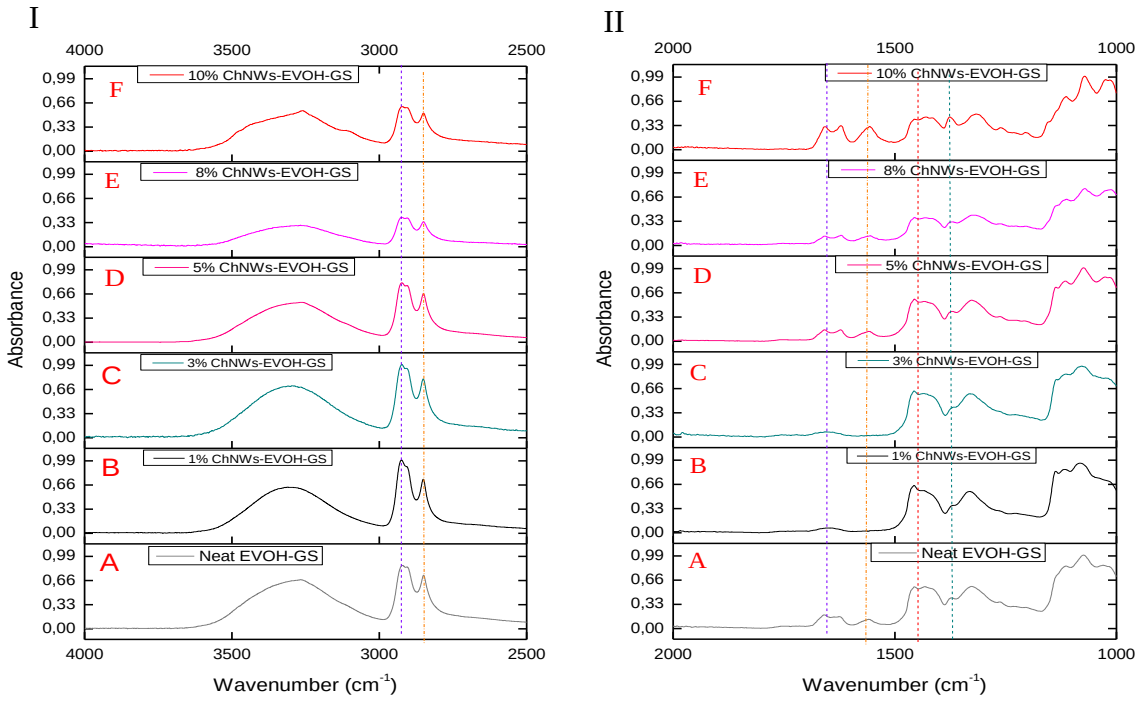

Figure 6.8 FTIR spectra of Gramicidin S attached chitin nanowhisker containing EVOH nanocomposite films (I) and fiber mats (II).

Figure 6.9 shows the FTIR spectra of gramicidin S treated EVOH nanocomposites containing increasing amounts of chitosan-reduced silver nanoparticles. No significant difference in the FTIR spectra of the peptide treated nanocomposites compared to the untreated was observed, which suggests that there is no notable change in the chemistry of the surface of the films or fibres with the incorporation of the peptide.

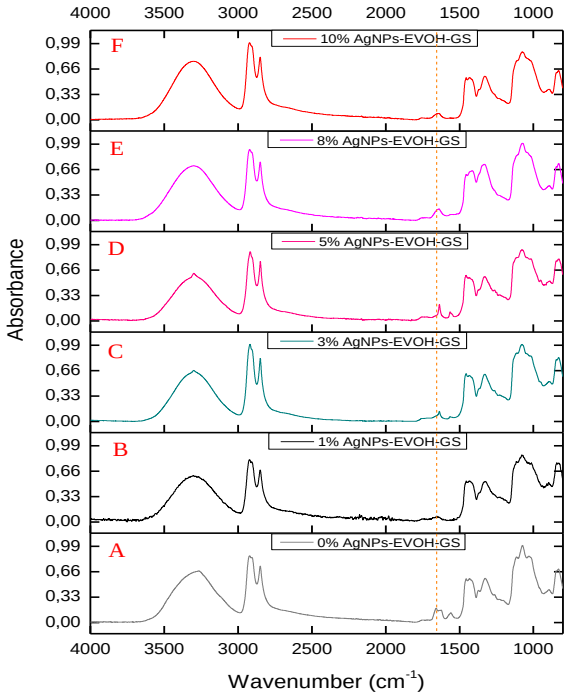

Figure 6.9 FTIR spectra of Gramicidin S attached silver nanoparticle containing nanocomposite films.

These small changes observed in the FTIR spectrum could be attributed to the fact that all functional groups present in the Gramicidin S peptides are similar to the functional groups in the chitosan and EVOH backbone. The composite fibres and films contain only up to only 10 wt% of the total composites, which are loading that could be very small to make a significant chang in the EVOH matrix. There is an appearance of a peak in the carbonyl region around at 1650 cm^{-1} which indicates the presence of the C=C bonds of the two benzene rings attached to the D-Phenylalanine found in the backbone of the Gramicidin S. The 10 wt% silver nanoparticle containing composite shows a slight increase in the intensity of the OH and the C-H peaks which can be attributed to the increase in these functional groups due to the incorporation of the cyclic peptide to the composite films as the backbone of the peptide is stabilized by four intramolecular hydrogen bonds. A similar result was observed for the fibres

where the combined FTIR spectra showed no significant changes between the different silver loadings.

6.4.3 Alamar Blue assay

The graph in Figure 6.10 illustrates the activity of the ChNW-EVOH nanocomposite films represented by the percentage growth inhibition against *M. Luteus* bacteria. The growth inhibition increased from 46% to 70% for the untreated films while the fibres increased from 52% to 72% with the incorporation of the 1 wt% ChNWs to the EVOH matrix with the peptide treated composites showing the highest activity.

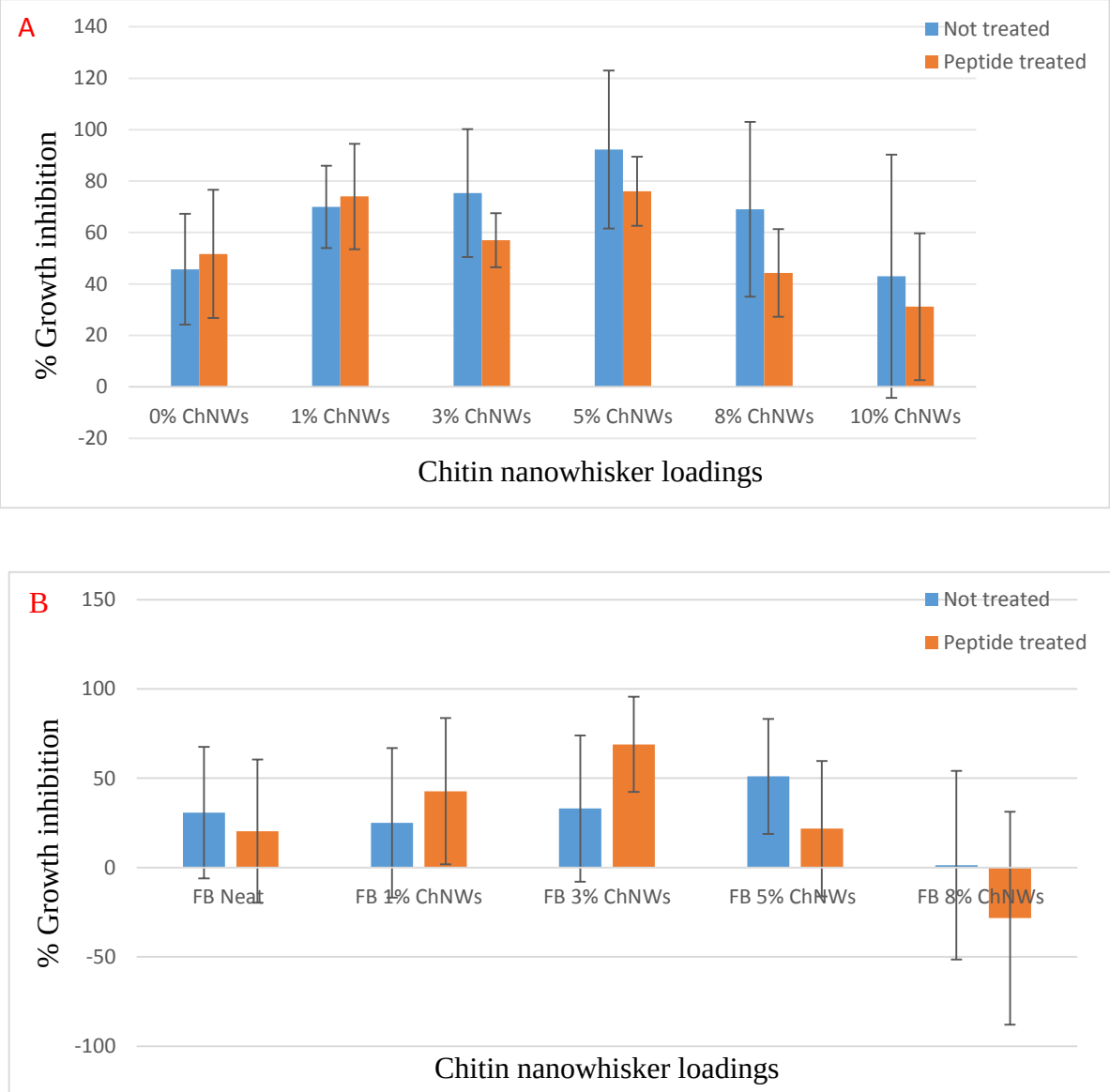

Figure 6.10 The percentage growth inhibition of Gramicidin S treated and untreated chitin nanowhiskers containing EVOH films (A) and fibres (B).

The growth inhibition was observed to increase again for the 3 wt% and 5 wt% loadings of ChNWs. The 5 wt% loaded sample had more than a 50% increase in activity compared to the neat EVOH film. The sample with 8 wt% and the 10 wt% loadings of ChNWs had a decrease in the percentage growth inhibition, which suggests that for these composite films, the 5 wt% loading is the optimum concentration for maximum antimicrobial activity. The incorporation of ChNWs in the EVOH was also shown to slightly improve the bacterial growth inhibition in the case of the 5 wt% loaded fibres showing up to 68% growth inhibition. Again, the 5 wt% loading proved to be optimum concentration, as shown in the nanocomposite films. Furthermore, the 10 wt% loaded sample revealed a wide distribution in activity, with some of the runs showing a growth inhibition that is less than that for the neat EVOH. This could be attributed to a strong interaction between the peptide and the nanowhiskers resulting in the hindrance of the active sites of either the peptide or the ChNW-EVOH composites. All the these composite films showed a higher percentage growth inhibition for the untreated films compared to the Gramicidin S treated samples, except for in the case of the 1 wt% loaded sample. The nanocomposite films containing chitin nanowhiskers showed a higher percentage growth inhibition compared to the nanocomposite fibre mats.

The graph in Figure 6.11 shows a comparison between the percentage growth inhibition of the treated and untreated EVOH composite films and fibre mats containing chitosan-reduced silver nanoparticles. The graphs show this behavior in response to an increase in the content of the chitosan-reduced silver nanoparticles in the composite films and fibres.

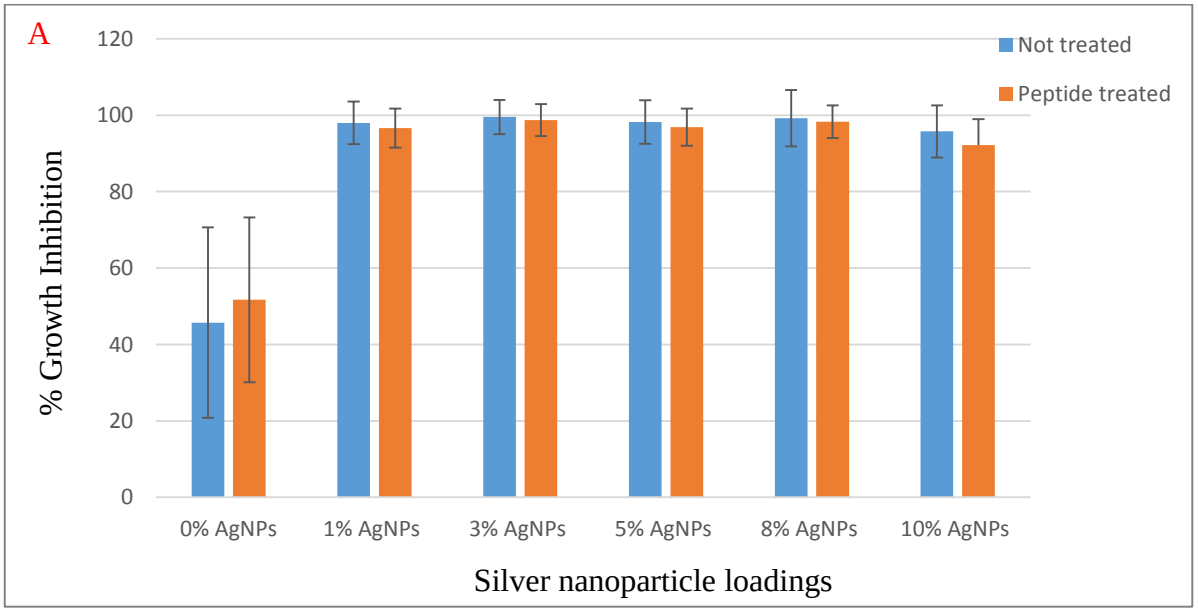

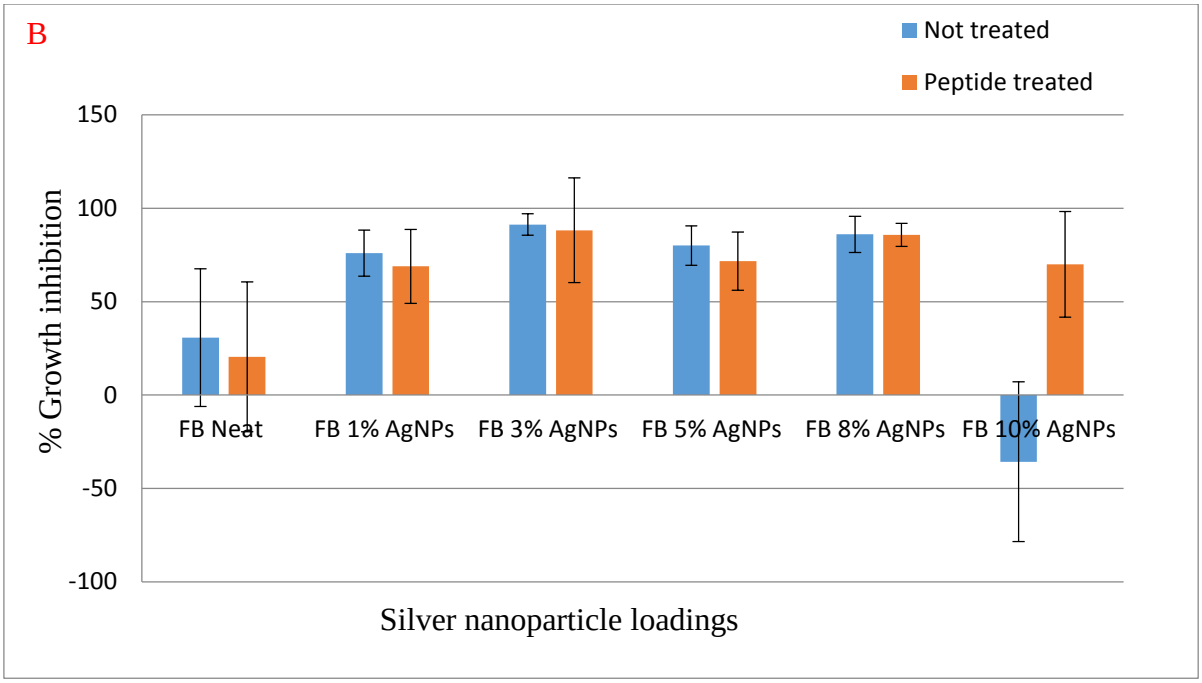

Figure 6.11 The percentage growth inhibition of Gramicidin S treated and untreated EVOH films with different loadings of chitosan-reduced silver nanoparticles. (A) films and (B) fibres.

The presence of 1 wt% silver nanoparticles in the nanocomposite films caused a dramatic increase in the percentage growth inhibition when compared to the neat EVOH films. The bacterial growth of all the Gramicidin S treated and untreated silver containing composite films was higher than that of the neat EVOH films with up to 70 % difference. Due to a very low standard deviation in the case of all the silver containing films the results can be considered as repeatable and reproducible. The overall inhibition of all the nanocomposites was almost the same for the 3 wt% and 8 wt% loadings but a slight decrease was observed for the 10 wt% silver nanoparticles loaded films. The treated 10 wt% silver nanoparticle containing fibres show a decrease in the bacterial growth inhibition for the 10 wt% loaded sample, which may be due to the fibre-disruption effect at this silver concentration shown by FESEM. The results however showed an unexpected higher growth inhibition for the untreated films compared to the Gramicidin S treated films for all silver loadings. This suggests that the peptide attachment hinders some of the silver nanoparticle activity, but this difference is not significant. The silver loaded nanocomposite films show a higher antimicrobial activity for all the silver loadings compared to the nanocomposite fibres. This could be due to a number of reasons, which include the freeze-drying step in the peptide attachment process that may have a negative effect on the quality of the peptide efficacy in the case of the nanofibres.

Figure 6.12 shows the graph illustrating a comparison between the percentage growth inhibition of the Gramicidin S treated and untreated EVOH composite films and fibre mats containing AgMCC. The nanocomposite films and mats are loaded with increasing amounts of AgMCC.

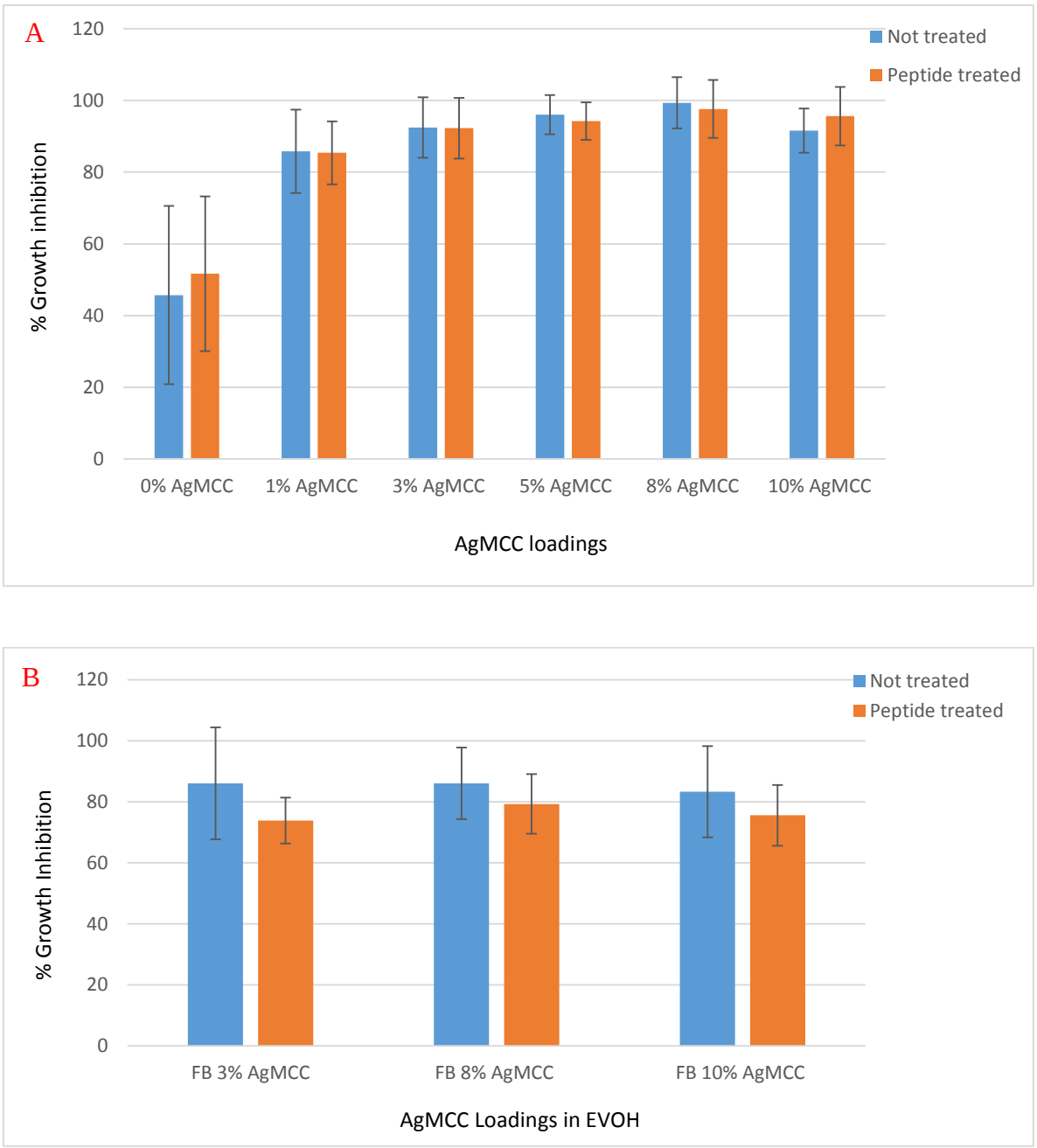

Figure 6.12 The percentage growth inhibition of Gramicidin S treated and untreated EVOH nanocomposites containing AgMCC. (A) films and (B) fibres.

The nanocomposite films containing AgMCC exhibited high antimicrobial activity, as shown by the high percentage of growth inhibition. The addition of 1wt% of AgMCC to neat EVOH films resulted in an increase from 46% to 86% for the untreated films. There was a gradual increase in the growth inhibition for the different increasing AgMCC concentrations but a slight decrease in the activity was seen for the sample containing the 10 wt% loadings. The untreated films had slightly higher growth inhibition compared to the Gramicidin S treated films except in the case of the 10 wt% loading, where the peptide treated films revealed a higher percentage growth inhibition compared to the untreated films. The AgMCC loaded nanocomposite fibres showed a small decreasing trend in the growth inhibition with the increase in the content of the AgMCC in the nanocomposites. The activity of the untreated fibres was higher than that of the peptide treated fibres. This could be attributed to the unfavorable interaction between the peptide and the AgMCC as also indicated by the FESEM results.

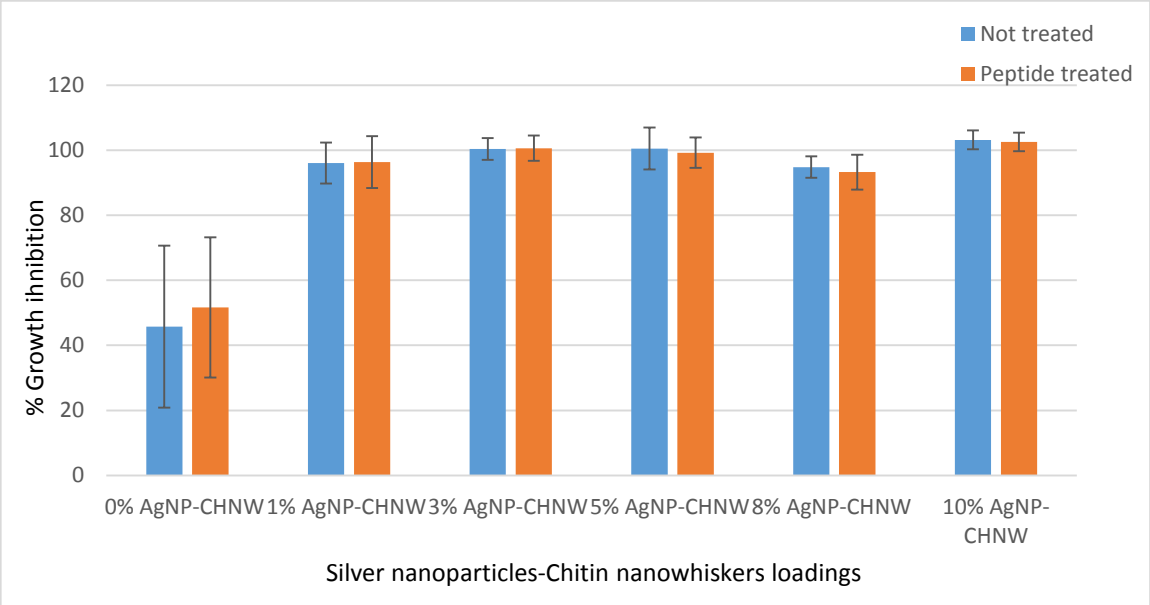

Figure 6.13 The percentage growth inhibition of Gramicidin S treated and untreated nanocomposite films containing chitosan-reduced silver nanoparticles and chitin nanowhiskers combined in an EVOH matrix.

The antimicrobial activity of the composite films and fibres that contain chitosan-reduced silver nanoparticles and chitin nanowhiskers was evaluated and the results are presented by the graph shown in Figure 6.13. The bacterial growth inhibition for the nanocomposite films containing 1 wt% of combined antimicrobial agents was shown to be the highest compared to the nanocomposites containing 1 wt% of the agents loaded individually. These composites inhibited up to 96% of the bacterial growth and this value was the same for both Gramicidin S

treated and untreated films. In the case of the 3 wt% loaded composites the films revealed 100% growth inhibition for both treated and untreated composite films. A slight increase in the growth inhibition was observed with an increase in the concentration but this increase was so small that it can be ignored. Only in the case of 8 wt% loading there was a decrease in the activity with only a 6 % decrease when compared to the 5 wt% and the 10 wt% loaded samples. Overall, the results showed a high antimicrobial activity for the nanocomposite films that contained more than two antimicrobial agents.

6.5 Conclusions

EVOH nanocomposite electrospun fibres and solvent cast films were subjected to peptide treatment via a dip coating technique and the successful attachment of the peptide to the surface of the fibres and the films was confirmed by FESEM. The results show an increase in the peptide attachment with an increase in the content of the antimicrobial agent in the nanocomposite. The increase in the presence of the Gramicidin S network on the surface of the films and fibre mats was more pronounced in the silver containing nanocomposites (CTSAgNPs and AgMCC). The attachment of spherically structured Gramicidin S was observed on the surface of the film and fibres but at high chitin concentration the Gramicidin S agglomerates forming lumps on the surface of the composites and causing the fibres to form mesh-like structures. FTIR results did not show significant changes in the spectra due to the peptide treatment, however, a slight increase in the O-H and C-H peaks were observed, especially for the 10 wt% composite films and fibres which could be attributed to the four hydrogen bonds in the Gramicidin S backbone. The appearance of a peak at 1650 cm^{-1} was observed and this peak is due to the C=C bonds of the two benzene rings of the Gramicidin S D-phen moiety.

The antimicrobial activity of the nanocomposites was evaluated by measuring the bacterial growth inhibition of the nanocomposite films and fibres using an Alamar Blue Assay. Alamar Blue assay results showed a general increase in the percentage growth inhibition for both the films and the fibres with the addition of antimicrobial agents. This indicates an increase in the antimicrobial activity of the nanocomposites with an increase in the content of the silver nanoparticles. The activity of the untreated films and fibres was higher than that of the treated composites and this could be attributed to the inhibition or hindrance of the silver activity due to the attachment of the peptide on the surface of the fibres and the films as shown by FESEM. For both nanocomposite films and fibres loaded with ChNWs, concentrations greater than 5

wt% showed little to no activity and sometimes negative activity indicating a growth of bacteria. According to Malmsten, AMPs affect bacteria in numerous ways, but their main mode of action is the disruption of bacterial membranes. Peptide length, charge, secondary structure, and hydrophobicity all influence AMP–membrane interactions[4]. The negative growth inhibition of these concentrations could be attributed to a bond formed between the peptide and the composites. At high chitin concentrations, there is a high amount of exposed OH groups on the surface of the composites which are used to bind the peptide and thereby hiding the peptide active sites[5,6,7].

These results show that these nanocomposites have high antimicrobial activity against Gram-positive bacteria. They also indicate a slight improvement in the activity when evaluating combined antimicrobial agents in the EVOH matrix. These nanocomposites could therefore probably be used in nanocomposite applications such as food packaging.

6.6 References

1. Rieger, K. A., Birch, N. P. & Schi, J. D. wound healing – a review. *Mater. Chem. B.* **1**, 4531–4541 (2013).

2. Hamid, R., Rotshteyn, Y., Rabadi, L., Parikh, R. & Bullock, P. Comparison of alamar blue and MTT assays for high through-put screening. *Toxicol. Vitr.* **18,** 703–710 (2004).

3. Pettit, R. K., Weber, A. C., Kean, M. J., Hoffmann, H., Pettit, G. R., Tan, R., Franks, K. S & Horton, M. L. Microplate Alamar Blue Assay for Staphylococcus epidermidis Biofilm Susceptibility Testing Microplate Alamar Blue Assay for Staphylococcus epidermidis Biofilm Susceptibility Testing. *Antimicrob. Agents Chemother.* **49,** 2612–2617 (2005).

4. Malmsten, M. Antimicrobial peptides. *Ups. J. Med. Sci.* **119,** 199–204 (2014).

5. Semrau, S. Monster, M. W. L., van der Knaap, M., Florea, B. I., Schmidt, T & Overhand, M. Membrane lysis by gramicidin S visualized in red blood cells and giant vesicles. *Biochim. Biophys. Acta - Biomembr.* **1798,** 2033–2039 (2010).

6. Izadpanah, A. & Gallo, R. L. Antimicrobial peptides. *Dermatology J. Am. Acad.* **52,** 381–390 (2005).

7. Shrivas, K. & Wu, H. Modified Silver Nanoparticle as a Hydrophobic Affinity Probe for Analysis of Peptides and Proteins in Biological Samples by Using Liquid-Liquid Microextraction Coupled to AP-MALDI-Ion Trap and MALDI-TOF Mass Spectrometry (AgNPs) in toluene as hydrophobi. *Direct* **80,** 2583–2589 (2008).

Chapter 7: Conclusions and Recommendations

7.1 Conclusions

7.1.1 Antimicrobial agents

The successful preparation and isolation of chitosan-reduced silver nanoparticles, chitin nanowhiskers and silver impregnated microcrystalline cellulose was confirmed by evaluating the morphological and chemical properties of these antimicrobial agents. TEM and confocal microscopy showed the presence and dispersion of these nano-sized antimicrobial agents, while FTIR revealed the presence of the individual functional groups in the antimicrobial agents. This confirmed the successful isolation of chitin nanowhiskers, reduction of silver nitrate to silver nanoparticles and attachment of silver nanoparticles to the surface of microcrystalline cellulose.

Chitosan-reduced silver nanoparticles formed for Sample 2 (22 mM silver nitrate solution) of these silver nanoparticles had variable shapes and sizes but most of the nanoparticles were spherically shaped with an average diameter of 4 nm. Because of the small diameters of the nanoparticles formed for Sample 2, the silver nanoparticles formed in this sample were used further for nanocomposite preparation in this study. The isolated chitin nanofibrils were whisker-like rods with sharp points and had average sizes of 160 nm in length and 27 nm in diameter. MCC was successfully impregnated with silver nanoparticles and these nanoparticles were shown to have diameters of about 40 nm and lied on the surface of the MCC and as well as within the MCC matrix. The properties of the prepared antimicrobial agents were similar to recently published research as discussed in previous chapters, which confirmed the successful formation of these antimicrobial agents.

7.1.2 EVOH nanocomposite films and fibres

Various antimicrobial agents were individually incorporated into an EVOH matrix to obtain EVOH nanocomposite films and nanofibres via solvent casting and electrospinning, respectively. The effect of the concentration of the antimicrobial agents on these EVOH nanocomposites was evaluated by loading different amounts of these agents into the EVOH matrix. Loadings of 1 wt%, 3 wt%, 5 wt%, 8 wt% and 10 wt% were used for this purpose and these concentrations were varied with respect to the amount of the polymer used. Combinations of the antimicrobial agents were also loaded in different combinations into the same polymer matrix. These EVOH nanocomposite films and fibres were characterized using different

techniques to evaluate the distribution, dispersion, chemical orientation and thermal behavior of these antimicrobial agents within the EVOH matrix. FESEM, STEM, CLEM, confocal microscopy, FTIR, TGA and DSC were the techniques used to characterize these nanocomposite films and fibres.

The microscopy techniques used in this study showed that lower concentrations of these antimicrobial agents have better distribution and dispersion within the EVOH matrix while higher concentrations tend to form agglomerates. The sizes and shapes of these antimicrobial agents were not altered by the incorporation into EVOH, though some cases revealed larger clusters of antimicrobial agents agglomerated together within the polymer. The nanofibres tended to increase in diameter with an increase in the content of antimicrobial agents in the polymer. This is attributed to the increase in viscosity of the nanocomposite solution which also lead to difficulties in electrospinning. CLEM was successfully used to show the orientation, distribution and dispersion of silver nanoparticles and chitin nanowhiskers within the same EVOH matrix. This technique showed the tendency of chitin nanowhiskers to align themselves on the surface of the films and fibres while the silver prefers to settle on the inside of the nanocomposites. The diameter of the nanocomposite fibres increased with the increase in both antimicrobial agents, making it difficult to obtain nano-sized fibres at higher concentrations. This was the first time that CLEM was successfully used to investigate the distribution of both chitin nanowhiskers and silver nanoparticles simultaneously when used as an antimicrobial combination within a polymer matrix. Without the use of CLEM these two antimicrobial agents could only be investigated individually using confocal microscopy in order to view the chitin nanowhiskers distribution and SEM in the case of the silver nanoparticles. This is a very significant part of the research, which may now open doors to investigate similar combinations of antimicrobial agents within other polymer matrices.

The FTIR results showed the successful incorporation of these agents into the EVOH polymer matrix. Because low concentrations or loadings of antimicrobial agents were used in this study and due to overlapping of some of the FTIR peaks in the antimicrobial agents with some of those from the EVOH matrix, it was however difficult in some cases to confirm the incorporation of the antimicrobial agents through FTIR.

7.1.3 Peptide attachment and antimicrobial assay

The EVOH nanocomposites synthesized in this study containing chitosan-reduced silver nanoparticles, chitin nanowhiskers and silver impregnated microcrystalline cellulose were dip-

coated in a Gramicidin S solution. This was done to monitor the attachment or bonding of this peptide to the surface of these nanocomposite films and fibres and evaluate the antimicrobial activity of these agents individually and in different combinations within the EVOH matrix. FESEM revealed the distribution of Gramicidin S on the surface of the nanocomposites. This technique showed an increase in the attachment of the peptide with an increase in the amount of the antimicrobial agents present in the nanocomposite films and fibres. The interaction between the Gramicidin S and the antimicrobial agent containing films and fibres also indicate the interaction between the peptide and the antimicrobial agents. Silver nanoparticles and the silver containing MCC revealed better interaction with the peptide as compared to the chitin nanowhiskers. The antimicrobial activity evaluated by measuring the bacterial growth inhibition of the nanocomposite films and fibres revealed a higher growth inhibition for the nanocomposites compared to the neat EVOH films and fibres. The percentage growth inhibition in the nanocomposites however showed to decrease again at a loading higher than 8 wt% of antimicrobial agents.. The overall activity of the films and fibres was very high, with growth inhibition increasing up to 99 wt% for the 5 wt% and the 8 wt%. The nanocomposite films showed higher antimicrobial activity when compared to the fibres and all the silver containing nanocomposites had the highest antimicrobial activity when compared to the nanocomposite films containing the chitin nanowhiskers.

These results indicate that out of the three antimicrobial agents, silver nanoparticles have the highest antimicrobial efficacy against gram-positive bacteria, *Micrococcus luteus*. This is also shown in the nanocomposites containing both silver nanoparticles and chitin nanowhiskers, which indicates that that silver nanoparticles are mostly responsible for the antimicrobial activity of these nanocomposites. One of the advantages of silver nanoparticles shown by this work is that it works very well at low concentrations as much as it does for higher concentrations, which indicates that only small amounts of silver nanoparticles are needed for maximum antimicrobial efficacy. Nanocomposite films show a higher activity than the nanocomposite fibres, which may be attributed to the nature of the nanofibres, the electrospinning conditions and the distribution in the nanocomposite fibre mats.

7.2 Recommendations

1. The antimicrobial activity of these nanocomposite films and fibre mats can additionally be tested against Gram-negative bacteria.

2. Different polymers with different properties could be used to incorporate these antimicrobial agents individually as well as in different combinations to evaluate the antimicrobial activity of these polymers to widen the uses of these nanocomposites.
3. Cold stage cryo-ultra microtome and cryo-STEM could be used to investigate the dispersion of the antimicrobial agents within the same polymer matrix. CLEM could be used to further investigate the dispersion of the antimicrobial agent containing microtomed slices in order to investigate similar regions or slices of the sample with STEM and confocal microscopy.
4. A series of different peptides that are stable at different temperatures could be used to investigate the activity of these nanocomposite films and fibres against a wider range of bacteria.

Addenda

Addendum A

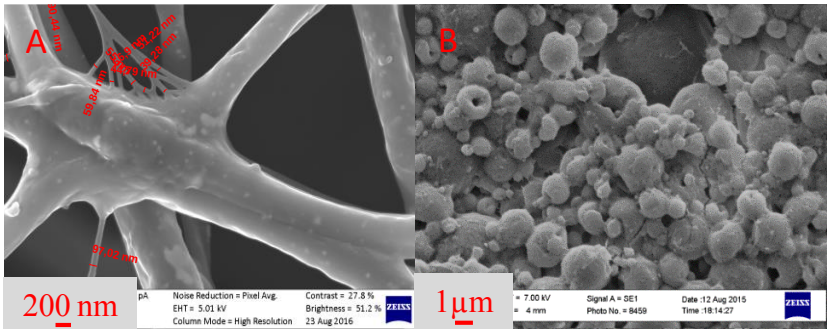

Figure A.1 FESEM micrographs of EVOH nanocomposites containing (A) 10 wt% chitosan-reduced silver nanoparticles and (B) 5 wt% chitin nanowhiskers.

Addendum B

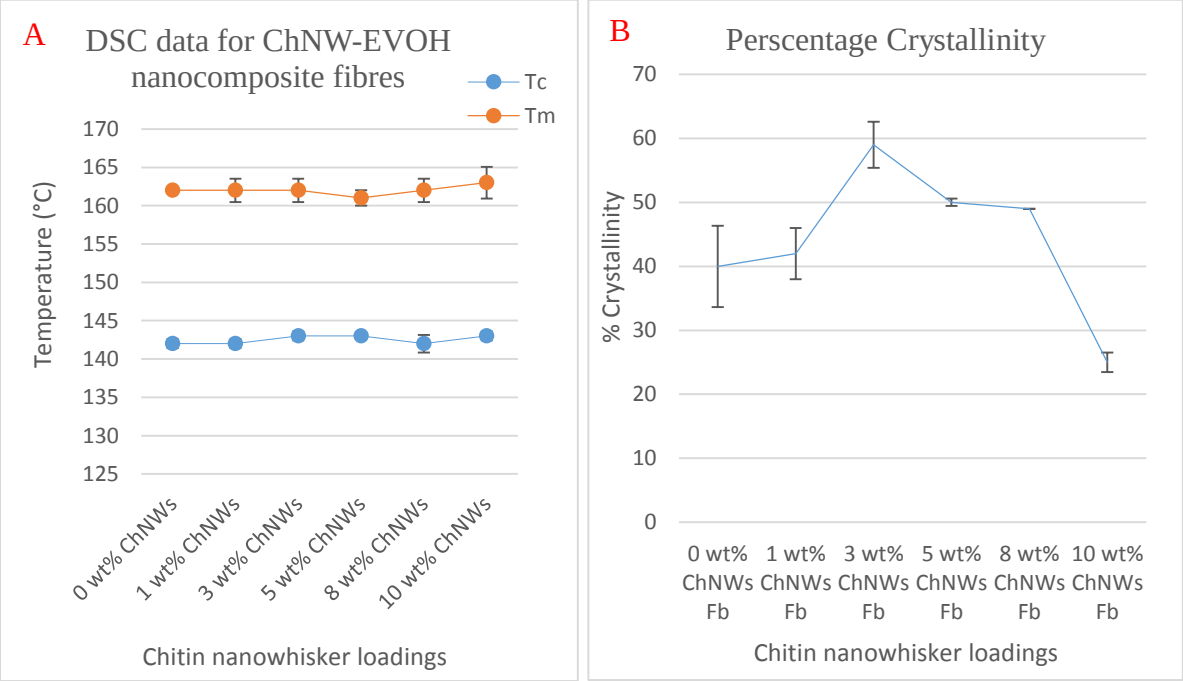

Figure B.1 Thermal analysis (DSC) data of ChNW-EVOH nanocomposite fibres showing the melting (A), crystallization temperature (A) and percentage crystallization (B) of the nanocomposites with increasing loadings ChNWs.

Table B.1 Thermal behaviour of ChNW-EVOH nanofibres as analysed by TGA

ChNW-EVOH	Peak degradation (^{0}C)	
	T Onset	T Max
0 wt%	367.2	429.3
1 wt%	362.5	388.9
3 wt%	370.8	408.2
5 wt%	383.0	417.9
8 wt%	386.9	428.3
10 wt%	377.1	407.4

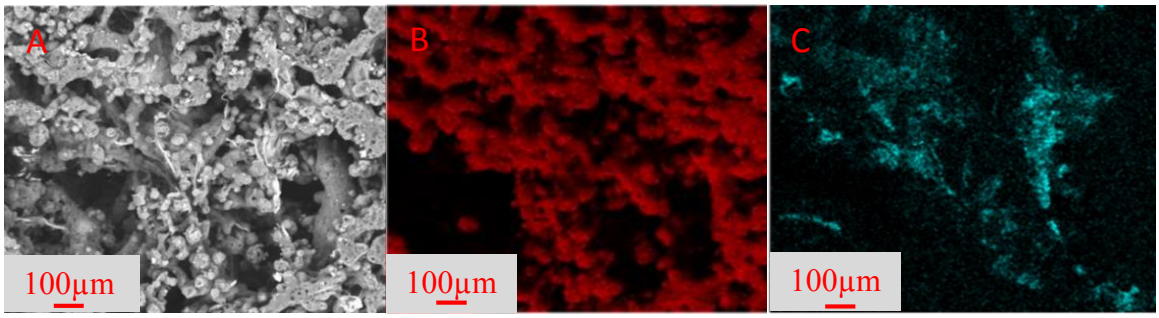

Figure B.2 SEM-EDX micrographs highlighting a case of silver nanoparticle agglomeration in the EVOH matrix. (A) SEM image, (B) Carbon map and (C) Silver nanoparticle map.

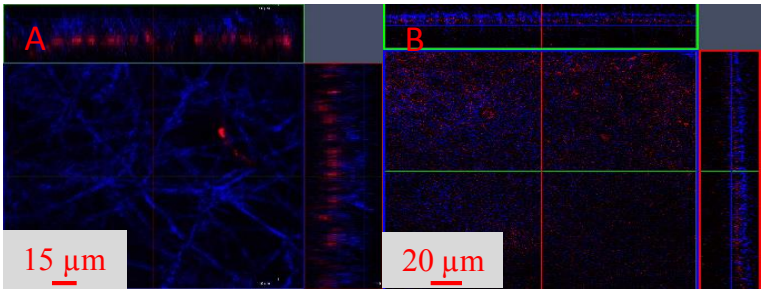

Figure B.2 CLEM micrographs of EVOH nanocomposites fibres (A) and films (B) containing both silver nanoparticles and chitin nanowhiskers in orthogonal view.

Addendum C

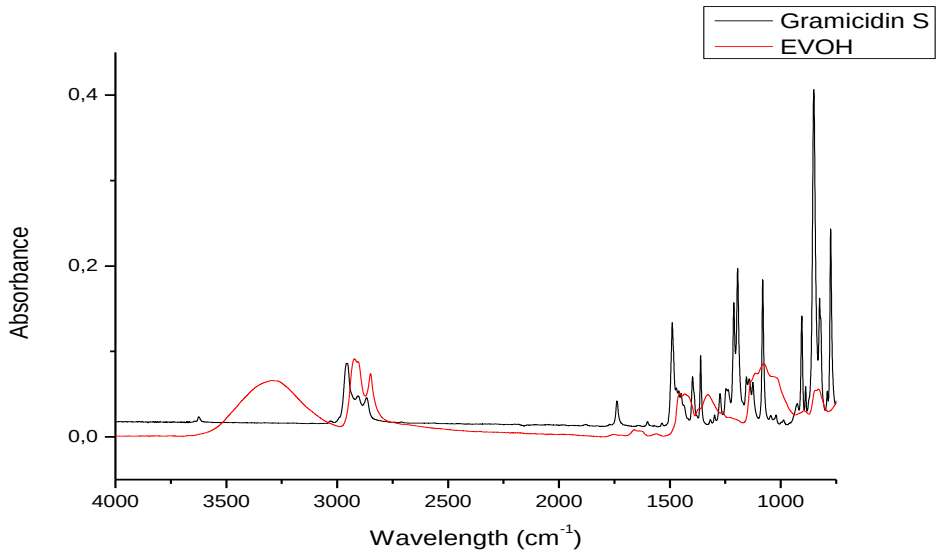

Figure C.1 FTIR spectra showing the overlap between Gramicidin S (Black spectrum) and EVOH (Red spectrum).